

HIGOR LUIS SILVA

**CONTRIBUTIONS TO CONCEPTUAL DESIGN OF
ELECTRIC AND HYBRID-ELECTRIC AIRCRAFT**



UNIVERSIDADE FEDERAL DE UBERLÂNDIA
FACULDADE DE ENGENHARIA MECÂNICA

2019

HIGOR LUIS SILVA

**CONTRIBUTIONS TO CONCEPTUAL DESIGN OF
ELECTRIC AND HYBRID-ELECTRIC AIRCRAFT**

Master dissertation submitted to the Department of
Mechanical Engineering – FEMEC-UFU, in partial
fulfillment of the requirements for the master degree of
the Master Program in Mechanical Engineering. *FINAL
VERSION*

Concentration Area: Solid Mechanics and Vibrations

Advisor: Prof. Dr. Thiago A. M. Guimarães

Co-advisor: Prof. Dr. Leonardo Sanches

Uberlândia - MG

2019

Dados Internacionais de Catalogação na Publicação (CIP)
Sistema de Bibliotecas da UFU, MG, Brasil.

S586c
2019 Silva, Higor Luis, 1993-
Contributions to conceptual design of electric and hybrid-electric
aircraft [recurso eletrônico] / Higor Luis Silva. - 2019.

Orientador: Thiago Augusto Machado Guimarães.
Dissertação (mestrado) - Universidade Federal de Uberlândia,
Programa de Pós-Graduação em Engenharia Mecânica.
Modo de acesso: Internet.
Disponível em: <http://dx.doi.org/10.14393/ufu.di.2019.26>
Inclui bibliografia.
Inclui ilustrações.

1. Engenharia mecânica. 2. Aeronaves - Projeto. 3. Aerodinâmica. 4.
Energia - Dimensionamento. I. Guimarães, Thiago Augusto Machado,
1985-, (Orient.). II. Universidade Federal de Uberlândia. Programa de
Pós-Graduação em Engenharia Mecânica. III. Título.

CDU: 621

**UNIVERSIDADE FEDERAL DE UBERLÂNDIA**

Coordenação do Programa de Pós-Graduação em Engenharia Mecânica
Av. João Naves de Ávila, nº 2121, Bloco 1M, Sala 212 - Bairro Santa Mônica, Uberlândia-MG, CEP 38400-902
Telefone: (34) 3239-4282 - www.posgrad.mecanica.ufu.br - secposmec@mecanica.ufu.br

**ATA**

Ata da defesa de Dissertação junto ao Programa de Pós-graduação em Engenharia Mecânica da Faculdade de Engenharia Mecânica da Universidade Federal de Uberlândia.

Defesa de Dissertação, nº 540, COPEM

Data: 09 de abril de 2019

Hora início: 09:00 h

Hora encerramento: 11:30 h

Discente: Higor Luis Silva - 11812EMC010

Título do Trabalho: **"Contributions to Conceptual Design of Electric and Hybrid-Electric Aircraft"**

Área de concentração: Mecânica dos Sólidos e Vibrações

Linha de pesquisa: Dinâmica de Sistemas Mecânicos

Projeto de Pesquisa de vinculação:

Reuni-se no Auditório do Laboratório de Mecânica dos Fluidos do Bloco 5P - Campus Santa Mônica da Universidade Federal de Uberlândia, a Banca Examinadora, designada pelo Colegiado do Programa de Pós-graduação em Engenharia Mecânica, assim composta: Professores Doutores: Francisco José de Souza - FEMEC/UFU; Gustavo Luiz Trapp - EMBRAER e Thiago Augusto Machado Guimarães - FEMEC/UFU, orientador do candidato. Ressalta-se que o Prof. Dr. Leonardo Sanches (coorientador) - FEMEC/UFU participou da defesa por meio de vídeo conferência desde a cidade de Lyon/França e os demais membros da banca e o aluno participaram *in loco*.

Iniciando os trabalhos o presidente da mesa Dr. Thiago Augusto Machado Guimarães apresentou a Comissão Examinadora e o candidato, agradeceu a presença do público, e concedeu ao Discente a palavra para a exposição do seu trabalho. A duração da apresentação do Discente e o tempo de argüição e resposta foram conforme as normas do Programa.

A seguir o senhor presidente concedeu a palavra, pela ordem sucessivamente, aos examinadores, que passaram a argüir o candidato. Ultimada a argüição, que se desenvolveu dentro dos termos regimentais, a Banca, em sessão secreta, atribuiu os conceitos finais.

Em face do resultado obtido, a Banca Examinadora considerou o candidato:

() Aprovado(a)

(X) Aprovado(a) com modificações a serem submetidas para a aprovação do orientador

() Aprovado(a) com modificações a serem submetidas para a aprovação da banca

() Reprovado(a)

Esta defesa de Dissertação de Mestrado é parte dos requisitos necessários à obtenção do título de Mestre. O competente diploma será expedido após cumprimento dos demais requisitos, conforme as normas do Programa, a legislação pertinente e a regulamentação interna da UFU.

Nada mais havendo a tratar foram encerrados os trabalhos. Foi lavrada a presente ata que após lida e achada conforme foi assinada pela Banca Examinadora.

Assinaturas dos membros da banca via SEI



Documento assinado eletronicamente por **Thiago Augusto Machado Guimarães, Professor(a) do Magistério Superior**, em 09/04/2019, às 11:47, conforme horário oficial de Brasília, com fundamento no art. 6º, § 1º, do [Decreto nº 8.539, de 8 de outubro de 2015](#).



Documento assinado eletronicamente por **Francisco José de Souza, Professor(a) do Magistério Superior**, em 09/04/2019, às 11:49, conforme horário oficial de Brasília, com fundamento no art. 6º, § 1º, do [Decreto nº 8.539, de 8 de outubro de 2015](#).



Documento assinado eletronicamente por **Luis Gustavo Trapp, Usuário Externo**, em 09/04/2019, às 11:55, conforme horário oficial de Brasília, com fundamento no art. 6º, § 1º, do [Decreto nº 8.539, de 8 de outubro de 2015](#).



Documento assinado eletronicamente por **Leonardo Sanches, Professor(a) do Magistério Superior**, em 09/04/2019, às 11:59, conforme horário oficial de Brasília, com fundamento no art. 6º, § 1º, do [Decreto nº 8.539, de 8 de outubro de 2015](#).



A autenticidade deste documento pode ser conferida no site https://www.sei.ufu.br/sei/controlador_externo.php?acao=documento_conferir&id_orgao_acesso_externo=0, informando o código verificador **1153027** e o código CRC **D7451F68**.

HIGOR LUIS SILVA

**CONTRIBUIÇÕES AO PROJETO CONCEITUAL DE
AERONAVES ELÉTRICAS E HÍBRIDAS**

Dissertação apresentada à Faculdade de Engenharia
Mecânica – FEMEC-UFU, como parte dos requisitos para
obtenção do título de Mestre em Engenharia Mecânica.

VERSÃO REVISADA

Área de Concentração: Mecânica dos Sólidos e Vibrações

Orientador: Prof. Dr. Thiago A. M. Guimarães

Coorientador: Prof. Dr. Leonardo Sanches

Uberlândia - MG

2019

To my family for their unconditional love and support.

ACKNOWLEDGEMENTS

I would like to firstly thank my mom and dad, Dalmi and Gaspar, for being my first school, teaching me the essential values in life: humility and unconditional love. They always believed and inspired my goals, being directly responsible for everything I achieved and still intend to do. Especially to my brothers, Denes and Rubens, for the encouragement, examples, advices, and for being the backbone that kept me up and ready to face the challenges.

I would like to thank the full support and advices given by Prof. Dr. Thiago A. M. Guimarães, my advisor and friend, throughout this project development. Without his motivation and encouragement, I would not have carried out this work with confidence. He has been a great source of inspiration and knowledge to me, putting my happiness in first place and teaching how to think out of the box.

I would like to acknowledge the Federal University of Uberlândia, the Faculty of Mechanical Engineering and all professors that guided my undergraduate and graduate life, specially my co-advisor Prof. Dr. Leonardo Sanches, for being my example of humility, positivity, and resilience.

I would like to thank the Graduate Program in Mechanical Engineering for the coordination of the course, and the Brazilian research agencies CAPES, CNPq and FAPEMIG for the financial support.

I would also like to acknowledge the examination board for their patience reading this work and constructive critical approaches.

Thank God for blessing and comforting all this journey.

*“As invenções são, sobretudo,
o resultado de um trabalho de teimoso.”
(Santos Dumont)*

*“Inventions are, above all,
the result of a stubborn work.”
(Santos Dumont)*

RESUMO

SILVA, H. L. **Contribuições ao Projeto Conceitual de Aeronaves Elétricas e Híbridas**. 2019. 128 p. Dissertação (Mestrado em Engenharia Mecânica) – Faculdade de Engenharia Mecânica, Universidade Federal de Uberlândia, Uberlândia – MG, 2019.

O trabalho de pesquisa realizado busca estudar como a definição de um sistema propulsivo híbrido impacta no projeto conceitual de aeronaves elétricas e híbridas. Em virtude das metas de redução de poluentes, ruídos e outras questões ambientais que são definidas por organizações internacionais, este tema de pesquisa tem se tornado muito relevante atualmente, sendo foco de trabalhos recentes em todo o mundo. Neste contexto, foram apresentadas as principais arquiteturas que formam os sistemas propulsivos híbridos, destacando suas vantagens e limitações, e foram listados exemplos de protótipos de aeronaves que já realizaram o primeiro voo, além de projetos que ainda estão em desenvolvimento. Em seguida, foram retratados os conceitos relativos a sistemas de propulsão distribuída (DP) e como seus efeitos aero-propulsivos podem influenciar no projeto conceitual final. Um método para construção de diagrama de restrições foi descrito e uma aeronave do tipo *thin haul* foi escolhida para ser o exemplo de aplicação. Os resultados mostraram uma melhora aerodinâmica devido ao DP, o que resultou em um aumento do espaço viável de projeto, permitindo asas e conjuntos propulsivo menores. Além disso, foi proposta uma abordagem de dimensionamento por energia de fase de missão típica para estimar os pesos dos componentes da aeronave. A análise paramétrica mostrou que a missão exigida e a tecnologia de baterias atual é crucial para dimensionar a aeronave. Não obstante, foram apresentados os principais efeitos da eletrificação no projeto de aeronaves, juntamente com os desafios atuais e necessidades tecnológicas esperadas.

Palavras-chave: Projeto de aeronaves, Aeronaves híbridas, Diagrama de restrições, Dimensionamento por energia, Otimização .

ABSTRACT

SILVA, H. L. **Contributions to Conceptual Design of Electric and Hybrid-Electric Aircraft.** 2019. 128 p. Dissertação (Mestrado em Engenharia Mecânica) – Faculdade de Engenharia Mecânica, Universidade Federal de Uberlândia, Uberlândia – MG, 2019.

The developed research work seeks to study how the definition of a hybrid propulsion system impacts on the conceptual design of full-electric and hybrid-electric aircraft. Due to the targets of reducing pollutants and other environmental issues defined by international organizations, this research theme has become very relevant recently, being the focus on current works around the world. In this context, the main architectures that form the hybrid propulsive systems were presented, highlighting their advantages and limitations, and examples of prototypes of aircraft that have already performed the first flight were listed, as well as projects that are still under development. Then, concepts related to distributed propulsion systems (DP) were presented and how their aerodynamic effects can influence the final conceptual design. A method for constructing a constraint diagram has been described and a thin haul aircraft has been chosen to be the application example. The results showed an aerodynamic improvement due to the DP, which increased the design feasible space, allowing smaller wings and powertrain. Furthermore, an energy sizing approach was proposed to estimate the weight breakdown of the aircraft, whereas a parametric analysis showed that the required mission and the current battery technology is crucial to size the aircraft. Moreover, the main effects of electrification on aircraft design were presented, along with the current challenges and expected technology needs.

Keywords: Aircraft design, Hybrid-electric aircraft, Constraints diagram, Energy sizing, Optimization.

LIST OF FIGURES

Figure 1 – Targets recommended by NASA in the Environmentally Responsible Aviation document.	32
Figure 2 – Normalized energy cost of Northwest U.S. wholesale electricity versus U.S. Jet A-1.	33
Figure 3 – Ragone diagram displaying available technologies in 2008.	39
Figure 4 – Available and predicted specific power (left) and energy (right) trends for Li-ion based cells for HEVs and EVs.	40
Figure 5 – Electric motor SP260D (left) and Extra 330LE (right).	43
Figure 6 – Example of a Degree-of-Hybridization trade-study conducted for a hypothetical Dual-Energy Storage-Propulsion-Power System (YEIS 2035).	45
Figure 7 – Electric aircraft propulsion architectures.	46
Figure 8 – Conventional and more electric aircraft, from	47
Figure 9 – Summary of flyable, manned electric aircraft.	52
Figure 10 – Summary of electric fixed-wing aircraft concepts and studies.	53
Figure 11 – Progression of manned electric aircraft demonstrators. (Data from Table 9).	54
Figure 12 – Airbus E-Fan X.	55
Figure 13 – Boeing SUGAR Volt.	56
Figure 14 – NASA X-57 Maxwell.	57
Figure 15 – The three phases or levels of aircraft design.	60
Figure 16 – Design phases integrated into the entire government program.	61
Figure 17 – Conceptual design flowchart.	61
Figure 18 – Propulsion integration.	64
Figure 19 – Simplified models of the different powertrain architectures considered, including the power paths (indicated with lower-case subscripts), and powertrain components and energy sources (indicated with upper-case letters). Lines with two arrow heads indicate paths where the power can flow in both directions, with the positive direction shown by the filled arrowhead. Legend:“F” = fuel, “GT” = gas turbine, “GB” = gearbox, “P” = propulsor, “BAT” = batteries, “EM” = electrical machine (i.e. electric omotor or generator), “PM” = power management and distribution system.	65
Figure 20 – Representation of two HEDP aircraft: one featuring leading-edge distributed propellers powered by two thermal engines in a serial configuration (a), and one featuring over-the-wing DP combined with a propulsive empennage (b).	68

Figure 21 – Lift and thrust produced by the propulsive system.	68
Figure 22 – Simplified DP-system representation, indicating the main geometrical parameters.	70
Figure 23 – Simplified DP-system representation, indicating the main geometrical parameters.	74
Figure 24 – Wing-loading versus thrust-to-weight-ratio diagram indicating the curves obtained from the equilibrium of forces along the X' axis (Eq. 3.37) and Z' axis (Eq. 3.38) for a given velocity and airframe lift coefficient.	77
Figure 25 – Wing-loading versus thrust-to-weight-ratio diagram (a) and wing-loading power-loading diagram (b), indicating the constraint curve obtained by evaluating the equilibrium flight points for different airframe lift-coefficient values at constant flight speed.	77
Figure 26 – Takeoff distance estimation.	79
Figure 27 – Cruise constraint construction.	83
Figure 28 – Gas turbine power loading diagrams for aircraft with conventional powertrain architecture.	84
Figure 29 – Optimum design points and feasible design space in constraint diagram.	84
Figure 30 – Construction of the four constraint curves for the serial configuration.	87
Figure 31 – Total power loading diagrams for aircraft with conventional and serial powertrain architecture.	87
Figure 32 – Component power-loading diagrams for the thin-haul aircraft with conventional and serial powertrain architecture.	88
Figure 33 – Typical mission profile.	92
Figure 34 – Sketch of aircraft with N propulsors distributed along each semi-wing.	99
Figure 35 – Pareto-front that represents the solution for the optimization problem.	103
Figure 36 – Variation of some parameters during the mission for the selected point P_2	105
Figure 37 – Visual representation of the powertrain architecture for each mission phase.	106
Figure 38 – Weight breakdown of the aircraft.	106
Figure 39 – Parametric analysis for the mission regarding e_b and R	107
Figure 40 – Weight breakdown for conventional configuration and different ranges.	107
Figure 41 – Weight breakdown for full-electric configuration and different ranges and specific energy of the batteries.	108
Figure 42 – Nova aircraft developed by Onera designers.	110
Figure 43 – Bauhaus Luftfahrt’s propulsive fuselage hybrid-electric concept.	111

LIST OF TABLES

Table 1 – Expected characteristics for batteries in 2035.	41
Table 2 – Classification of architectures for a hybrid-electric propulsion system.	45
Table 3 – Summary of advantages and disadvantages of hybrid-electric architectures.	51
Table 5 – Top-level aircraft requirements.	82
Table 6 – Design and technology parameters assumed.	82
Table 7 – Aerodynamic properties assumed.	82
Table 8 – Requirements and constraints of the thin haul aircraft.	85
Table 9 – Requirements and constraints of the thin haul aircraft.	85
Table 10 – Selected design parameters for the thin haul aircraft.	86
Table 11 – Aerodynamic assumptions for the thin haul aircraft.	86
Table 12 – Statistical regression values relating empty weight to takeoff weight.	93
Table 13 – Correlation coefficients for parasite area.	95
Table 14 – Statistical regression values relating wetted surface to takeoff weight.	95
Table 15 – Electric motors examples.	101
Table 16 – Requirements for the general aviation aircraft of example.	102
Table 17 – Assumptions for the general aviation aircraft of example.	102
Table 18 – Results of the optimization.	104

LIST OF ABBREVIATIONS AND ACRONYMS

AIAA	American Institute of Aeronautics and Astronautics
BLI	Boundary layer ingestion
BPF	Blade pass frequency
CAEP	Committee on Aviation Environmental Protection
DESPPS	Dual-energy storage-propulsion-power system
DoD	Depth of discharge
DoH	Degree-of-Hybridization
DP	Distributed propulsion
e-VTOL	Electric vertical takeoff and landing
EAS	Essential Air Service
EPNdB	Effective perceived noise in decibels
EV	Electric vehicle
FAA	Federal Aviation Administration
HALE	High-altitude long-endurance
HEP	Hybrid-Electric Powertrain
HEV	Hybrid-electric vehicle
HTS	High Temperature Superconducting
HWB	Hybrid-wing-body
ICAO	International Civil Aviation Organization
LCC	Life-cycle cost
LEAPtech	Leading Edge Asynchronous Propellers Technology
MEA	More Electric Aircraft
MTOW	Maximum takeoff weight
MTOW	Maximum takeoff weight
NASA	National Aeronautics and Space Administration
OEI	One-engine-inoperative
PMAD	Power Management And Distribution
ROC	Rate of climb
SCEPTOR	Scalable Convergent Electric Propulsion Technology and Operations Research
SOC	State of charge
SOF	State of fuel

SPPH	Serial/parallel partial hybrid
SUGAR	Subsonic Ultra-Green Aircraft
TLR	Top Level Requirements
UAS	Unmanned aircraft systems
YEIS	Year entry-into-service

LIST OF SYMBOLS

\mathcal{R} — Aspect ratio

c — Rate of climb

C_D — Drag coefficient

c_f — Sectional skin friction coefficient

C_L — Lift coefficient

$C_{L_{\max}}$ — Maximum lift coefficient

D — Drag

D_p — Propulsor diameter

D_p^2/W — Disk loading

e — Oswald factor

e_b — Specific energy of battery

e_f — Specific fuel energy

f — Parasite area

H_E — Degree of hybridization for energy

H_P — Degree of hybridization for power

i_p — Angle between the propeller axis and the wing chord

L_{AB} — Airborne run

L_{airframe} — Lift due to airframe

L_{GR} — Ground run

L_{TO} — Takeoff run

m_{bat} — Battery mass

m_{empty} — Aircraft empty mass

m_{fuel} — Fuel mass

m_{PT} — Powertrain mass

m_{PL} — Payload mass

m_{TO} — Takeoff mass

M — Mach number

N — Number of propulsors

N_{crew} — Number of crew

N_{pax} — Number of passengers

P — Power

P_{bat} — Battery power

P_{e1} — Electric power

P_{e2} — Electric power

P_f — Fuel power

P_{gb} — Gearbox power

P_{gt} — Gas turbine power

$P_{GT,max,SL}$ — Installed sea-level static power of the gas turbine

P_{in} — Input power

P_{out} — Output power

P_p — Powerplant power

P_{p1} — Primary propulsor power

P_{p2} — Secondary propulsor power

P_{SL} — Sea-level power

P_{s1} — Primary powertrain power

P_{s2} — Secondary powertrain power

q — Dynamic pressure

Re_c — Reynolds number evaluated at cruise

S — Wing area

S_{wet} — Wet area

T — Total thrust

T_0 — Conventional thrust

T_{dp} — Thrust due to installed distributed propulsion

V_{md} — Speed of minimum drag

V_{mp} — Speed of minimum power

V_{ST} — Stall speed

W_{bat} — Battery weight

W_{em} — Electric motor weight

W_{empty} — Empty weight

W_{fuel} — Fuel weight

W_{gt} — Gas turbine weight

W_{PL} — Payload weight

W_{PT} — Powertrain weight

W_{TO} — Takeoff weight

α — Angle of attack

α_p — Propulsor angle

β — Finite-slipstream correction factor

γ — Climb gradient

$\delta_y/2$ — Lateral clearance

ΔE — Energy variation

Δt — Time variation

ΔV_p — Velocity increase at the propeller disk

$\Delta y/b$ — Wingspan occupied by the DP array

$\Delta \eta_{dp}$ — Increase in efficiency due to distributed propulsion

η_{dp} — Distributed propulsion efficiency

η_{EM1} — Electric motor efficiency

η_{EM2} — Electric motor efficiency

η_{GB} — Gearbox efficiency

η_{GT} — Gas turbine efficiency

η_i — Component efficiency

η_{PM} — Power management efficiency

η_{P_1} — Primary powertrain efficiency

$\Lambda_{c/2}$ — Wing half-chord sweep angle

μ — Friction coefficient

ξ_{GT} — Gas turbine throttle

ρ — Air density

ρ_{SL} — Air density at sea-level

σ — Air density ratio

φ — Shaft power ratio

Φ — Supplied power ratio

χ — Thrust-to-weight ratio

CONTENTS

1	INTRODUCTION	31
1.1	Research Objective and Approach	34
1.2	Document Structure	34
2	LITERATURE SURVEY AND THEORY	37
2.1	Batteries and Energy Storage Systems	37
2.1.1	<i>Li-ion and Li-poly Batteries</i>	38
2.1.2	<i>Li-air Batteries</i>	40
2.1.3	<i>Li-S Batteries</i>	41
2.1.4	<i>Battery Forecasts</i>	41
2.2	Electric Motors and Systems	42
2.3	Hybrid-Electric Aircraft Fundamentals	43
2.3.1	<i>All-Electric Configuration</i>	46
2.3.2	<i>Series and Turboelectric Configuration</i>	48
2.3.3	<i>Parallel Configuration</i>	49
2.3.4	<i>Series-Parallel Configuration</i>	49
2.3.5	<i>Partial Turboelectric Configuration</i>	50
2.3.6	<i>Summary of Hybrid-Electric Architectures</i>	50
2.4	Review of Hybrid-Electric Aircraft Projects	50
2.4.1	<i>Commercial Products and Prototypes</i>	54
2.4.2	<i>Recent Concepts and Studies</i>	55
3	SIZING APPROACHES IN ELECTRIC AND HYBRID-ELECTRIC AIRCRAFT DESIGN	59
3.1	Aircraft Development Phases	59
3.2	Aircraft Sizing Method - Conceptual Design Process	61
3.2.1	<i>Requirement Analysis</i>	61
3.2.1.1	<i>Payload</i>	62
3.2.1.2	<i>Range</i>	62
3.2.1.3	<i>Cruise Speed/Altitude Capability</i>	62
3.2.1.4	<i>Takeoff Distance</i>	62
3.2.1.5	<i>Climb Requirements</i>	62
3.2.1.6	<i>Airport Compatibility</i>	63

3.2.1.7	<i>Environmental Issues</i>	63
3.2.1.8	<i>Reliability and Durability</i>	63
3.2.2	<i>Configuration Selection</i>	63
3.2.2.1	<i>Definition of Power Control Parameters</i>	66
3.2.2.2	<i>Solving the Powertrain Equations</i>	66
3.2.3	<i>Power Constraints: Wing and Powertrain Sizing</i>	67
3.2.3.1	<i>Thrust, Lift and Drag Decomposition</i>	67
3.2.3.2	<i>Aero-Propulsive Interaction Model</i>	70
3.2.3.3	<i>Derivation of Performance Constraint Equations</i>	73
3.2.3.4	<i>Constructing the Performance Constraint Diagram</i>	76
4	ASSESSMENT OF ELECTRIFICATION ON CONCEPTUAL AIR-CRAFT DESIGN	81
4.1	Top-Level Requirements and Assumptions	81
4.2	Validation of the Constraint Diagram	82
4.3	Application Example	84
5	ENERGY SIZING APPROACH AND OPERATIONAL ANALYSES	91
5.1	Typical Mission of an Aircraft	91
5.2	Energy Sizing	93
5.2.1	<i>Aerodynamic Data Estimation</i>	94
5.2.2	<i>Performance Estimation</i>	95
5.2.2.1	<i>Takeoff</i>	96
5.2.2.2	<i>Climb</i>	96
5.2.2.3	<i>Descent</i>	97
5.2.2.4	<i>Cruise</i>	97
5.2.2.5	<i>Loiter</i>	98
5.2.3	<i>Mission Evaluation</i>	98
5.3	Example of Energy Sizing Optimization	101
6	EFFECTS OF ELECTRIFICATION AND NEW CHALLENGES	109
6.1	Direct Electrification Effects	109
6.2	Propulsion Effects	110
6.3	Aerodynamic Effects	111
6.4	Sizing Effects	112
6.5	Weight Effects	112
6.6	System Safety Effects	113
6.7	Noise and Heat Signature Effects	114
6.8	Current Challenges and Future Research and Technology Needs	114
7	CONCLUSIONS AND PERSPECTIVES	117

BIBLIOGRAPHY 121

INTRODUCTION

Over the last few years, engineers and researchers all over the world have spent their time studying and developing a new design concept in aviation: fully or partially electric aircraft. The need to develop even more efficient and “greener” aircraft leads to the motivation to innovate and go beyond what currently exists in terms of engineering, creating disruptive technologies.

A lot of new start-up ventures has engaged in this proposal, seeking a way to enter this market and make profit. At the same time, the academic community has become more involved with this trend, which is corroborated by the increase of published papers recently. From 2006 to 2009, there was about one paper per year on electric and hybrid electric aircraft design and analysis. From 2015 to present, the volume of similar papers has increased to nearly 20 per year (BRELJE; MARTINS, 2018).

The main factor that aroused public interest in electrification is the growing concern with global emissions and the rapidly expanding air-transport, which brought many governmental and international authorities and agencies to settle bold emissions and noise reduction targets for the next decades. NASA’s Subsonic Fixed Wing program established aggressive goals for energy consumption, nitrogen oxides (NO_x), and noise for three generations of airplanes extending out to the 2030s (GUYNN *et al.*, 2013; FOLLEN *et al.*, 2011).

In Europe, the objective of Flightpath 2050 (BUSQUIN *et al.*, 2001) is a reduction of 75% in CO₂-emissions per passenger kilometer, a 90% in NO_x-emissions and a 65% in perceived noise relative to aircraft of the year 2000. On the other hand, there are also aggressive performance targets for the “N+3” generation with projected entry-into-service dates in the mid-2030s: -52 dB noise at the airport boundary, -80% NO_x, and -60% fuel burn relative to 2006-era technology. Some of these NASA N+3 targets are displayed in Fig. 1. The International Civil Aviation Organization (ICAO) has established certification standards for noise and NO_x in the 2020s¹ and a voluntary carbon offset scheme aiming to hold overall sector carbon emissions

¹ Available at: <www.icao.int/environmental-protection/Pages/technology-standards.aspx>.

at 2020 levels (ERLING, 2017).

Figure 1 – Targets recommended by NASA in the Environmentally Responsible Aviation document.

TECHNOLOGY BENEFITS*	TECHNOLOGY GENERATIONS (Technology Readiness Level = 4-6)		
	N+1 (2015)	N+2 (2020**)	N+3 (2025)
Noise (cum margin rel. to Stage 4)	-32 dB	-42 dB	-52 dB
LTO NOx Emissions (rel. to CAEP 6)	-60%	-75%	-80%
Cruise NOx Emissions (rel. to 2005 best in class)	-55%	-70%	-80%
Aircraft Fuel/Energy Consumption† (rel. to 2005 best in class)	-33%	-50%	-60%

* Projected benefits once technologies are matured and implemented by industry. Benefits vary by vehicle size and mission. N+1 and N+3 values are referenced to a 737-800 with CFM56-7B engines, N+2 values are referenced to a 777-200 with GE90 engines

** ERA's time-phased approach includes advancing "long-pole" technologies to TRL 6 by 2015

† CO2 emission benefits dependent on life-cycle CO2e per MJ for fuel and/or energy source used

Source: Aviation (2012).

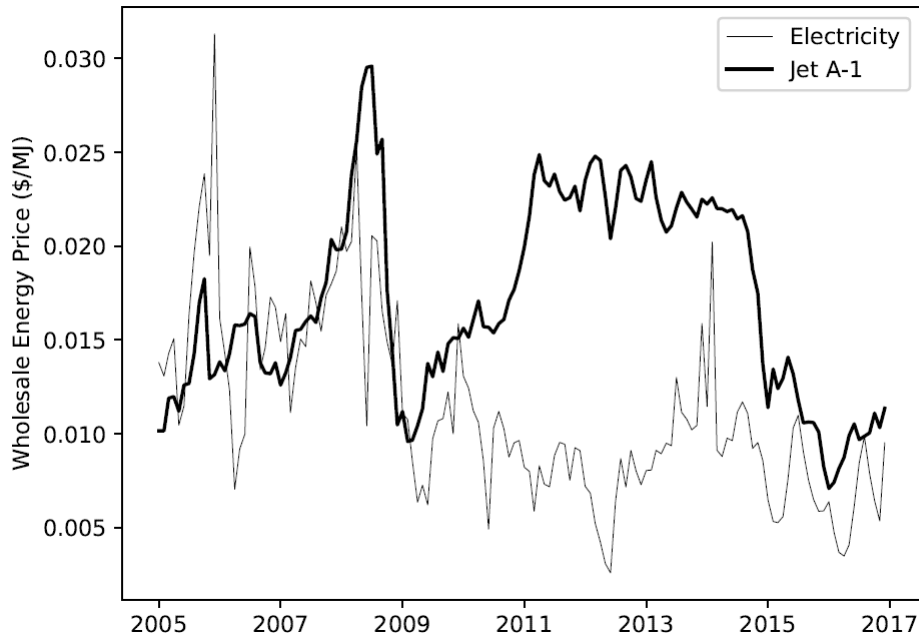
Thereby, the scientific community has been rethinking alternative ways to meet those targets. Thus, the introduction of electric propulsion systems can be a great option, where batteries can be used as a power source instead of conventional fuels. However, a fully electric aircraft is not yet seen as feasible for the civil aviation segment, since the use of batteries itself brings challenges such as the weight on board. Therefore, a synergy between conventional and electric propulsive technologies is proposed, giving rise to hybrid systems. The expected benefits of using a Hybrid-Electric Powertrain (HEP) in flight vehicles are summarized in reference (MADAVAN; ROSARIO; JANKOVSKY, 2015) and reported below:

- Fewer emissions by reducing fuel burn;
- Less atmospheric heat release;
- Smaller noise impact for communities and quieter flight for passenger comfort;
- Better energy conservation and less dependence on fossil fuels;
- Better reliability by substitution of turbo-machinery with electric motors as means of propulsive power producers.

From the economic point of view, the electrification allows a great reduction of operational costs, when compared to the conventional aircraft, and a range of possibilities that can make feasible the entrance in new and profitable markets. The reduction of operating costs can be obtained directly by replacing fossil fuel with electricity from batteries, in addition to the inherent reduction in total energy consumption or by reducing maintenance costs such as oil

change and mechanical components. The variation in the price of aviation fuel in the United States can be observed in Fig. 2. The value of electricity has become lower in the last ten years. However, it would be interesting not to depend on the fluctuations in fossil fuel prices that are directly related to uncertain Middle East policies.

Figure 2 – Normalized energy cost of Northwest U.S. wholesale electricity versus U.S. Jet A-1.



Source: U.S. Energy Information Administration (2017).

Moreover, it may also enable new concepts of operations that are not currently feasible with conventional aircraft propulsion architectures. Electric vertical takeoff and landing (e-VTOL) concepts have been studied by many companies around the world, including VoloCopter, Ehang, Zee Aero, Joby Aviation, and Airbus. In this context, Uber Technologies Inc. released the “Elevate” white paper in 2016, arguing that a potential market exists for point-to-point urban air mobility, catalyzing activity in this field (THOMSON *et al.*, 2017). This topic was widely discussed in the AIAA SciTech Forum 2019, where members from different companies and countries debated on how this new trend of urban air mobility has impacted science, technologies, and policies that are shaping the future of aviation and space.

Regarding fixed-wing aircraft with electric propulsion systems, many papers have been published recently. Thomson *et al.* (2017) provide a non-technical summary of aviation electrification from a business perspective. Schäfer *et al.* (2018) discuss a first-order assessment of the energy, economic and environmental implications of all-electric aircraft. Hepperle (2012) presents an overview of electric propulsion architectures and some basic sensitivity analyses based on the Breguet range equation. Pornet (2010) addresses practical conceptual design considerations of hybrid-electric passenger aircraft using lower-order sizing methods and graphical methods, but is missing coverage of higher fidelity optimization tools. Later, Pornet *et al.* (2014) proposes a sizing and performance methodology for hybrid-energy aircraft, which includes a

design study of a battery and fuel hybrid-energy single-aisle retrofit in order to demonstrate the methodology and to analyze the implications of the associated new design variables on the sizing and performance. Finger, Braun and Bil (2018) describe the methodology and the benefits of an initial sizing algorithm that is able to consider aircraft with hybrid-electric propulsion systems by using an innovative point and mission performance analysis, where the central element is the use of the matching diagram (power-to-weight ratio P/W vs. wing-loading W/S). Furthermore, Vries, Brown and Vos (2018) present a generic sizing method suitable for the first stages of the design process of hybrid-electric aircraft, taking into account the power train architecture and associated propulsion–airframe integration effects.

1.1 Research Objective and Approach

The need to develop methodologies for conceptual design of electric and hybrid-electric aircraft has been very apparent recently. So much so that it was subject of the last competitions of aeronautical project realized by The American Institute of Aeronautics and Astronautics (AIAA). Thus, the main objectives of this work include:

- (i) To make a literature review of the most pertinent fundamentals and concepts involving full-electric and hybrid-electric aircraft designs, including architectures and definitions;
- (ii) To present a generic sizing method for the initial phases of conceptual design of hybrid-electric aircraft, taking into account the influences of the architectures and the effects of aero-propulsive interactions;
- (iii) To propose a methodology for aircraft dimensioning by energy per mission phase, and to perform an optimization study of degree-of-hybridization in each flight phase, where the objective functions are to minimize fuel consumption and minimize the maximum takeoff weight;
- (iv) To discuss the effects of electrification in aircraft design and to address the current challenges and future research and technology needs.

1.2 Document Structure

This document is structured, as follows:

- Chapter 2: it is presented the main concepts related to hybrid-electric aircraft, which include the types of batteries and energy storage systems, electric motors, fundamentals of degree-of-hybridization and architectures, highlighting the main advantages and disadvantages of each one of them. Furthermore, it is listed some prototypes of aircraft that have already flown, and other studies under development;

- Chapter 3: it is discussed the main classification of aircraft design phases. Moreover, the conceptual design phase is addressed deeper, where top-level requirements are defined. Next, a generic sizing method is proposed, considering the concept of constraint diagrams (power loading vs. wing loading);
- Chapter 4: it is performed the assessment of electrification on conceptual aircraft design. A thin-haul aircraft proposal is selected to be the example of method application. Constraint diagrams are plotted and discussed, highlighting the aero-propulsive interactions due to the distributed propulsive system installed. Furthermore, it is evaluated how the optimum design point affects the final aircraft design;
- Chapter 5: it is proposed a methodology for aircraft dimensioning based on the required power and energy in each phase of the mission. Also, it is sized the weight of powertrain (engines and electric motors), batteries and fuel, and a mission optimization is performed to evaluate the optimum degrees-of-hybridization in each flight phase that reduces fuel consumption or maximum takeoff weight;
- Chapter 6: it is presented the effects of electrification and how they affect the aircraft design in terms of propulsion, aerodynamics, sizing, weight, system safety, noise, and heat signature. Moreover, the main challenges and future research and technology needs are addressed;
- Chapter 7: this chapter summarizes the main aspects covered by this work and discuss the main conclusions regarding the methods and approaches presented, and what are the next proposals for future works.

LITERATURE SURVEY AND THEORY

In the following chapter, it is presented the main concepts related to hybrid-electric aircraft. The propulsive architectures are introduced, highlighting their aspects, advantages and disadvantages. The available technologies in terms of batteries, electric motors and generator are discussed, with focus on forecasts for the next two-three decades. At the end of the chapter, a review of existing aircraft examples is presented as well as the projects and prototypes under development by the industry.

2.1 Batteries and Energy Storage Systems

An electric flight is directly dependent and related to the energy storage technology available in the market. The lighter, safer and more compact, the better. Within this design philosophy, the most common technologies: electro-chemical batteries, ultra-capacitors, and fuel cells.

Ultra-capacitors are usually used in high specific power applications, but for projects that require specific high energy, they are not appropriate. Even in the best estimates for the next decade, ultra-capacitors will only reach specific energy levels compared to advanced Li-Ion cells, but, even so, below the more advanced batteries such as Li-S (Lithium Sulphur) and Li-Air (LithiumAir) (FARHADI; MOHAMMED, 2015; TODD *et al.*, 2010).

On the other hand, fuel cells have similar performances when compared to batteries (SHIN; LEE; CHANG, 2016), but they bring issues related to fuel storage. The high specific energy of hydrogen is severely limited by its low energy density. Hydrogen-based aircraft need either a large storage tank for gaseous hydrogen or a cryogenic high-pressure tank for carrying hydrogen in liquid form (SCIENCES; MEDICINE, 2016).

Therefore, a more viable source of energy for aircraft electrification and, consequently, use in hybrid-electric aircraft is the battery. Batteries and other systems hence must be able to

meet both power density and energy density requirements, as well as they must be able to show high convenience from an economical and ecological point of view (KUHN; SIZMANN, 2012).

Some concepts and terminologies regarding batteries are important to come up with, as follows:

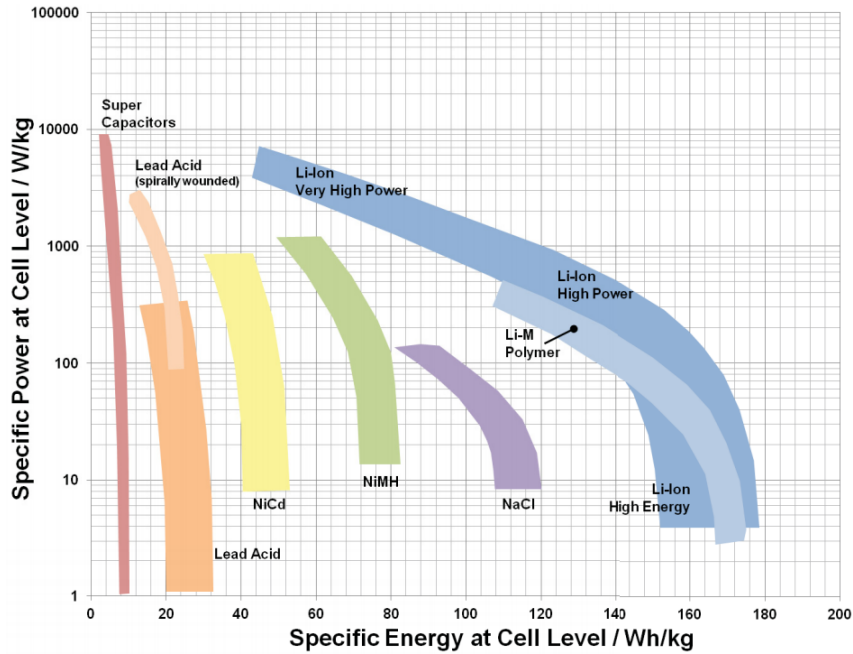
- *Specific Energy* [Wh/kg]: it is also known as gravimetric energy density, and it is defined as the amount of electrical energy stored for unit battery mass. Thus, it is dependent on battery chemistry and packaging;
- *Specific Capacity* [Ah/kg]: it represents the Amp-hours available when the battery discharges at a certain current, per unit of mass. Similar to the specific energy, limits to the discharge current are given by the cell chemistry and its weight is influenced both by the materials necessary in the electrochemical process as well as the packaging of the cells;
- *Specific Power* [W/kg]: dependant on chemistry and packaging, it determines the weight required to reach a given performance. There is a strong trade-off between specific energy and specific power for high discharge rates during high power demands, in which the battery capacity drops very fast, significantly reducing the specific energy (CINAR *et al.*, 2017);
- *Energy Density* [Wh/m³] or [Wh/l]: along with the energy consumption of the vehicle, it determines the volume occupied by the battery, being a function of packaging and chemistry;
- *Stored Energy* [Wh] or [J]: the energy stored is equal to the product of the battery voltage V and the capacity Q [Ah]. The stored energy is a function of how quickly a battery is charged or discharged as with increasing currents the internal losses grow;
- *State of Charge (SOC)* [%]: it is defined as the ratio between the remaining capacity and the nominal capacity. It goes from 100% (fully charged) to 0% (fully discharged), but batteries usually have a practical lower SOC limit under which the cells are permanently damaged. This limit is usually around $SOC = 20-30\%$ for modern Li-Ion batteries;
- *Depth of Discharge (DoD)* [%]: it is the rate of discharged capacity over the nominal capacity. It is also defined as $DoD = 1-SOC$.
- *Cost* [\$/Wh]: depending on the cost of raw materials and industrial processes required to manufacture the battery.

2.1.1 Li-ion and Li-poly Batteries

Lithium-ion and Lithium-polymer batteries are the most common batteries due to very high performance compared to other technologies available on the market. Figure 3 shows that

Li-ion batteries grant the highest flexibility to be either used as capacitors, with a high power (low energy setting), and as batteries, with high energy and high to medium power. Li-poly technology shares the same kind of performance in this latter case.

Figure 3 – Ragone diagram displaying available technologies in 2008.



Source: Kuhn and Sizmman (2012).

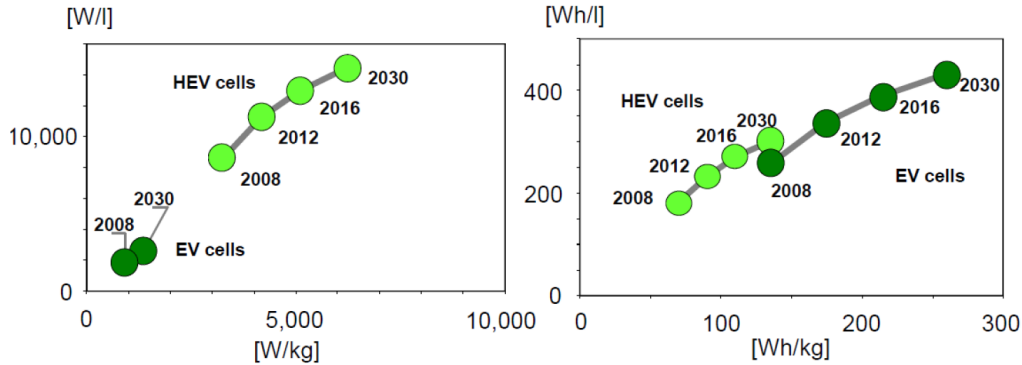
A regular Li-ion cell has a graphite anode, a cathode made of lithium metal oxide, an electrolyte made of an organic solvent and lithium salts in solution. The maximum theoretical specific energy can be calculated based on the mass of the electrodes and their chemistry. The most commonly used cell chemistry is:



This reaction is characterized by a specific energy of 584 Wh/kg, as calculated by Thackeray, Wolverton and Isaacs (2012). However, the specific energy value is also dependant on the cell and case design. In practice, the maximum achievable gravimetric energy per cell is around 210 Wh/kg, and for the battery, it is around 150 Wh/kg (THACKERAY; WOLVERTON; ISAACS, 2012), while the energy density can be as high as 650 Wh/l (GERSSEN-GONDELACH; FAAIJ, 2012).

Birke, Keller and Schiemann (2010) states that the hybrid-electric (HEV) and electric vehicles (EV) are boosting the industry to advance in the development of new technologies and materials related to these batteries. In the case of HEVs, the future trends are toward high power and low energy battery solutions, while for EVs medium power and high energy ones. This principle can be extended to aircraft as well. Future trends for Li-ion in Figure 4 shows that HEV cells will have to increase specific power, while EV cells will have to double their specific energy performance with little improvements in terms of power.

Figure 4 – Available and predicted specific power (left) and energy (right) trends for Li-ion based cells for HEVs and EVs.



Source: Birke, Keller and Schiemann (2010).

Fefermann *et al.* (2016) states that studies performed by Safran company show that for commuter applications the battery-level specific energy should be, at least, 500 Wh/kg, while studies on larger aircraft conducted by Boeing show the need of at least 600-750 Wh/kg, as reported by Ritzert *et al.* (2013). From Figs. 3 and 4, Li-ion and Li-poly batteries can provide good performance on current hybrid or electric vehicles and promising products in the next 15-20 years, but they are still not suitable for a wide range of aircraft applications.

Regarding safety, these batteries can be dangerous. In conditions of high drainage or recharge rate, the temperature can rise rapidly and reach high values, which can lead to the release of oxygen. If this oxygen reacts with some flammable substance, there is a high risk of explosion.

2.1.2 Li-air Batteries

The Li-air (or Li-O₂) batteries are quite promising (KUHNS; SIZMANN, 2012), possibly having specific energy values around 11500 Wh/kg, which is very close to the aviation fuel specific energy of 11900 Wh/kg. The Li-O₂ technology is characterized by the chemical reaction:



where the oxygen is dissolved in the electrolyte and reacts with the lithium on the surface of the porous cathode. The specific energy and density of the reaction are one of the highest of the considered electric energy technologies at 3458 Wh/kg and 3445 Wh/l (GALLAGHER *et al.*, 2014).

Notwithstanding, Li-air batteries only exist in laboratories. They have some issues with safety, and they are not capable of being charged and discharged at competitive rates. Moreover, there are also issues regarding poor energy efficiency and limited life cycles.

2.1.3 Li-S Batteries

Recently, the Lithium-Sulfur batteries have been considered one of the best options and promises for energy storage devices (THIELMANN *et al.*, 2012). The chemical reaction is characterized by:



and it has a high specific energy compared to standard Li-ion devices, reaching a theoretical value of 2567 Wh/kg and energy density of 2800 Wh/l (BRUCE *et al.*, 2012). They are already available on the market through British companies as OxisEnergy (Oxis Energy, 2019) and SionPower [44], as battery packs with specific energies around 250 Wh/kg, and planning to improve this value to the double within five years.

Moreover, a prototype with a specific energy of 600 Wh/kg and a power density of 150 Wh/l is already being tested in laboratory (NAZAR; CUISINIER; PANG, 2014). It is worth mentioning that sulphur is easy to access and cheap to buy, which makes this type of battery very attractive, since the costs of the materials involved are reduced. However, they currently have low life-cycle and low efficiency that does not permit the full extraction of the chemical energy.

2.1.4 Battery Forecasts

Gerssen-Gondelach and Faaij (2012) gathered the predictions and expectations for the characteristics and performances of the batteries for the year 2025, which are available in Table 1. Later, Zamboni (2018) updated those values from newer publications, extending the forecast to 2035.

Table 1 – Expected characteristics for batteries in 2035.

	Li-ion	Li-S	Li-air
Specific Energy [Wh/kg]	250-350	600-700	800-1500
Specific Power [W/kg]	500-600	350-500	300-400
Energy Density [Wh/l]	600-800	300-350	1000-1700
Charge/Discharge efficiency [%]	90-95	70-90	60-85
Cycle life [# cycles]	1000-3000	1000-2500	500-1000
Degree of Discharge [%]	70-90	90-100	70-90
Lifetime [years]	7-15	7-14	5-10
Cost (\$2010) [\$ / kWh]	250-350	250-500	400-800
Uncertainty	low	medium	high

Source: Zamboni (2018).

From Table 1, the forecasts show an expectation of improvement of the performance characteristics of Li-ion batteries. However, Bradley and Droney (2015) have been developing and studying requirements for hybrid aircraft projects and state that these aircraft will only be competitive if the batteries reach high specific energy levels. In the case of a single-aisle hybrid

aircraft for a regional transport, it is required a specific energy of at least 500 Wh/kg for parallel hybrid system, or 750 Wh/kg for series and mixed hybrid systems.

Therefore, Li-S and Li-air batteries should probably be the best options for future projects, since they can achieve high specific energy levels. However, there are still major challenges to board these batteries on a plane, such as project maturity, redundancy in operational safety, flammability testing, i.e., all that is necessary to ensure safety and reliability requirements.

2.2 Electric Motors and Systems

Another very important component in the architecture of hybrid and electric systems is the electric motor. In recent years, the automotive industry has been focusing on more powerful and more compact electric car designs, which pushed the development of new equipment and technologies. Lately, the aerospace industry has incorporated these new trends and has produced new applications of electric motors.

Petermaier (2015) has published a work describing an aeronautical propulsive application of electric motors, where key aspects regarding drive systems are underlined: electric machines must be efficient ($\eta > 95\%$), extremely lightweight ($W_{sp} > 6$ kW/kg), safe and redundant. Moreover, this technology must show to be scalable and thus it can be extended from existing small aircraft application to larger regional airplanes. Aircraft motors must be designed with a particular focus to achieve the lightest possible solution through some key steps (PETERMAIER, 2015):

- High performance magnetic materials: high electric frequencies to grant a high torque density;
- High performance cooling: increase motor efficiency reducing losses due to high temperatures in copper wires, using optimal coolers at high coolant temperature (90-100°C);
- Optimization of passive structural components through better computational and manufacturing techniques such as 3D printing;
- Optimization of motor design rotational speed: aircraft application benefits from direct motor-propeller connection, avoiding a gearbox.

All these aspects led Siemens to come up with the SP260D, an induction motor shown in Fig. 5. It has a maximum continuous power output of 260 kW at 2500 RPM and an impressive total mass of only 50 kg, resulting in a power density of 5 kW/kg (Siemens, 2016). This motor was used on the Extra 330LE (Fig. 5), an aerobatic plane that set a new speed world record in 2017. At the Dinslaken Schwarze Heide airfield in Germany, the electric aircraft reached a top

Figure 5 – Electric motor SP260D (left) and Extra 330LE (right).



Source: Siemens (2015), FLYER (2016).

speed of around 337.50 km/h over a distance of 3 km (Siemens, 2017). The speed achieved was 13.48 km/h faster than the previous record.

The power required by an aircraft is generally of a much higher magnitude than the engine power densities that are currently available. Scaling up these motors leads to unfeasible sizes. As the size of the motors increases, the external surface to internal volume ratio decreases, reducing the heat dissipation. In ground application, this problem is solved by using oversized conductor cross sections to minimize heat loss, which is very heavy. However, this is not suitable for aerospace applications.

This problem may be addressed in the future by using High Temperature Superconducting (HTS) motors. Superconducting materials have the unique property of being able to carry current with almost no resistive losses. This property only occurs when the superconducting material is below a certain critical temperature, magnetic field, and current density level. The superconducting motor concept could work at higher current values, which means a higher torque per unit mass and the possibility to downsize the motor and to avoid the need of a transmission. Moreover, it could also work at a low voltage, without the need of transformers and with fewer cells in series, increasing reliability (SHINZATO *et al.*, 2012).

2.3 Hybrid-Electric Aircraft Fundamentals

A synergy between the qualities of both conventional and full electric aircraft results in what is called hybridization, which means the integration of the propulsion system with energy stored source (batteries) and fuel source (conventional engine). The Degree-of-Hybridization (DoH) express the percentage of the total power required by the aircraft that comes from the electric system (PORNET; ISIKVEREN, 2015). Nonetheless, the most commonly used in the literature are the degree of hybridization for energy (H_E) and power (H_P) (ISIKVEREN *et al.*, 2014), defined as:

$$H_P = \frac{P_{electric}}{P_{total}} \quad (2.4)$$

and

$$H_E = \frac{E_{electric}}{E_{total}} \quad (2.5)$$

However, the degree of hybridization of power is not really a good parameter to measure how hybrid a design is. Bogaert (2015) asserts:

“For example, having a large electric motor that is only for a short while will result in a large degree of hybridization of power while only a very small part of the mission is ‘hybrid’. In that regard, the degree of hybridization of energy is a better parameter. However, it is also not ideal since the specific energy of fuel is much larger compared to the battery specific energy, and the efficiency of the electrical systems much higher than that of the gas turbine. This results in values of H_E being generally quite low (< 0.2) even though the total supplied electric motor energy (E_{em}) might be higher than the total supplied gas turbine energy ($E_{gasturb}$).”

Accordingly, another parameter is introduced by Isikveren *et al.* (2014): the supplied power ratio (Φ), which is defined as the total electric motor power over the entire mission in relation to the total shaft power over the entire mission.

$$\Phi = \frac{P_{em_{total}}}{P_{shaft_{total}}} \quad (2.6)$$

The advantage of this parameter is that it is more intuitive than the degree of hybridization of energy. The value of $\Phi = 0$ represents a conventional aircraft while the value of $\Phi = 1$ represents a fully electric aircraft. When using a constant power Split over the entire mission the supplied power ratio will be approximately the same as this constant power split (BOGAERT, 2015).

Figure 6 displays an example functional correlation between installed H_P and H_E for a dual-energy storage-propulsion-power system (DESPPS) based upon kerosene and batteries as energy carriers targeting YEIS 2035 and were derived from assumed step values of Φ .

There are many distinct architectures available to design a hybrid electric propulsion system. Some of them are classified in Table 2 and illustrated in Fig. 7. Conventional aircraft do not use electric power or electric energy for propulsion ($H_P = 0$, $H_E = 0$). Despite, all-electric (or full/universally-electric) aircraft use exclusively electrical energy and power for propulsion ($H_P = 1$, $H_E = 1$). Turboelectric aircraft use fossil fuel for energy storage but electrical power transmission instead of mechanical power to drive the propulsor(s) ($H_P > 0$, $H_E = 0$). Hybrid-electric aircraft combine the use of fuel and electrical energy storage and propulsive power ($H_P > 0$, $0 < H_E < 1$). Series hybrid designs generate electrical power using a combustion engine and deliver both battery and fuel energy to the propulsor via electrical buses ($H_P = 1$, $0 < H_E < 1$). Parallel hybrid architectures deliver combustion power to the propulsor mechanically ($H_P < 1$, $0 < H_E < 1$). The combustion engine may operate continuously and use electrical power to

Figure 6 – Example of a Degree-of-Hybridization trade-study conducted for a hypothetical Dual-Energy Storage-Propulsion-Power System (YEIS 2035).

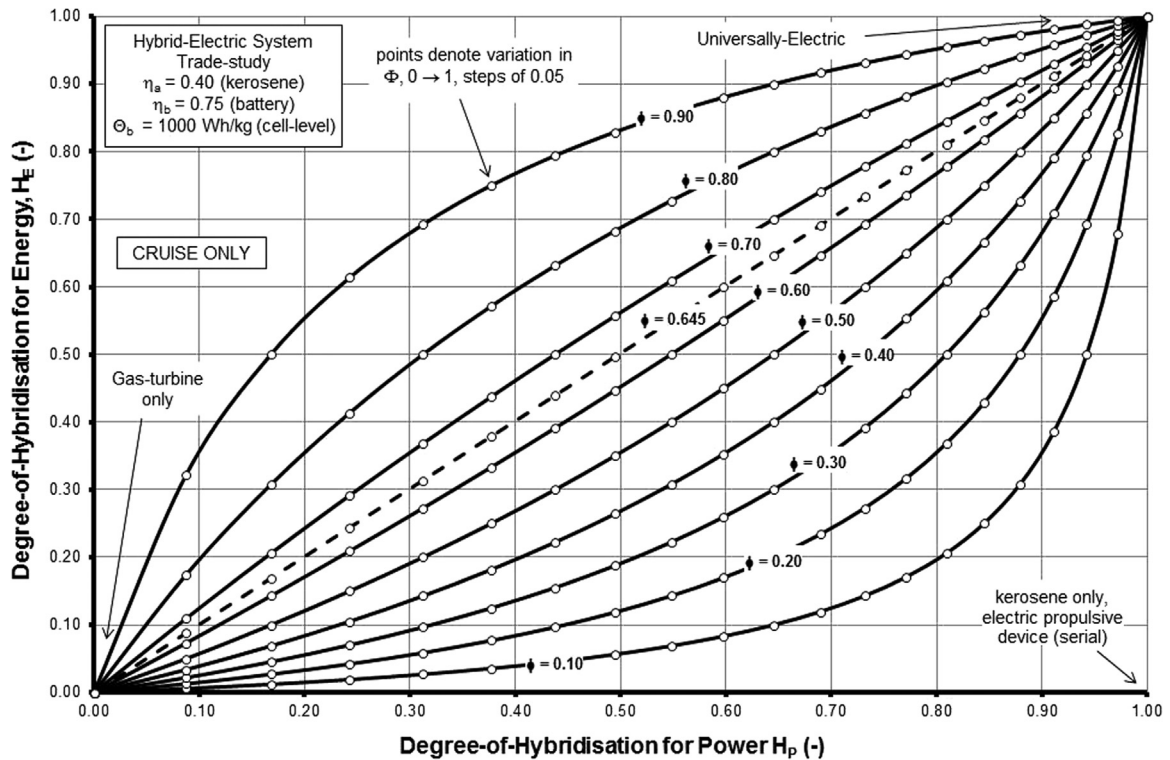
Source: Isikveren *et al.* (2014).

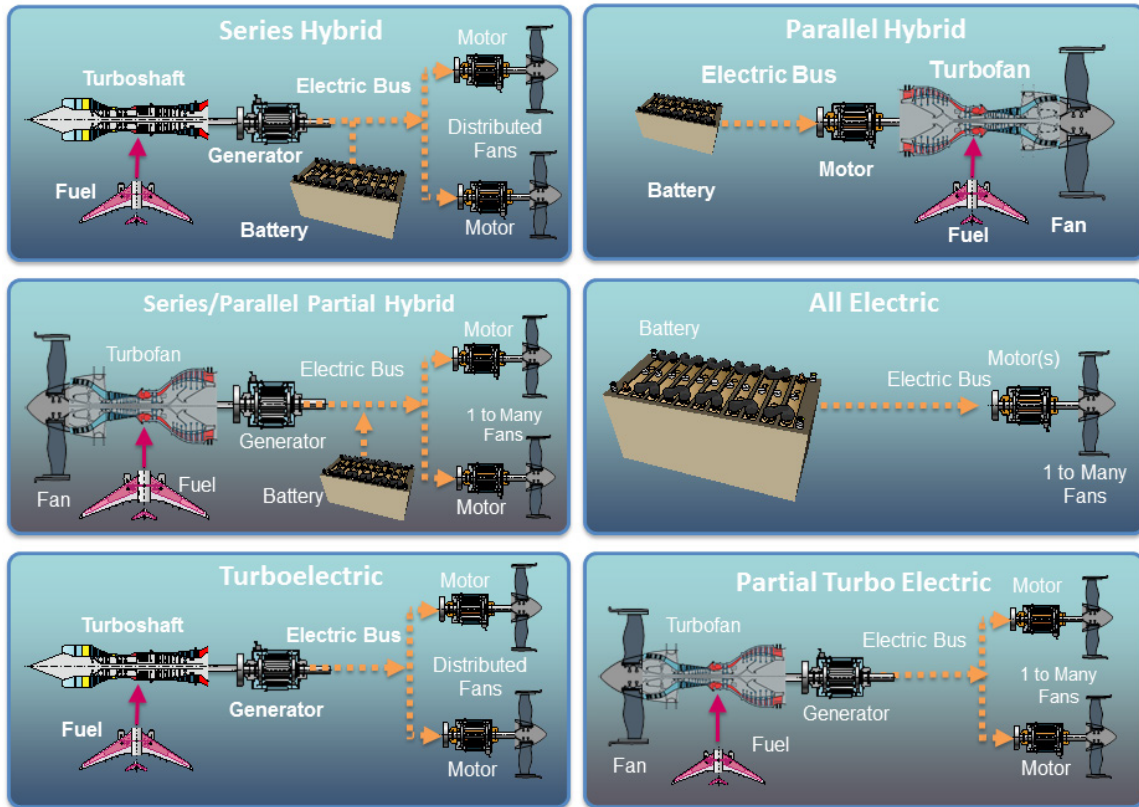
Table 2 – Classification of architectures for a hybrid-electric propulsion system.

Architecture	H_P	H_E
Conventional	0	0
All-Electric	1	1
Turboelectric	> 0	0
Series Hybrid	1	< 1
Parallel Hybrid	< 1	< 1

reduce fuel flow, or the engine may disconnect via a clutch to enable full-electric operation during some portion of the flight envelope.

In the design of a hybrid electric propulsion system, the choice of the best architecture for a certain project depends on its own applications and limitations. In road vehicles, for example, the series hybrid architecture has the lowest fuel consumption, as presented by Bayindir, Gözükcük and Teke (2011). However, Hung points out that it has a larger weight than a parallel architecture, which is crucial and determinant in aerospace applications (HUNG; GONZALEZ, 2012). In a design study of light aircraft, Friedrich and Robertson (2014) assert that the parallel configuration provides the highest efficiency for aerospace applications .

Figure 7 – Electric aircraft propulsion architectures.



Source: Sciences and Medicine (2016).

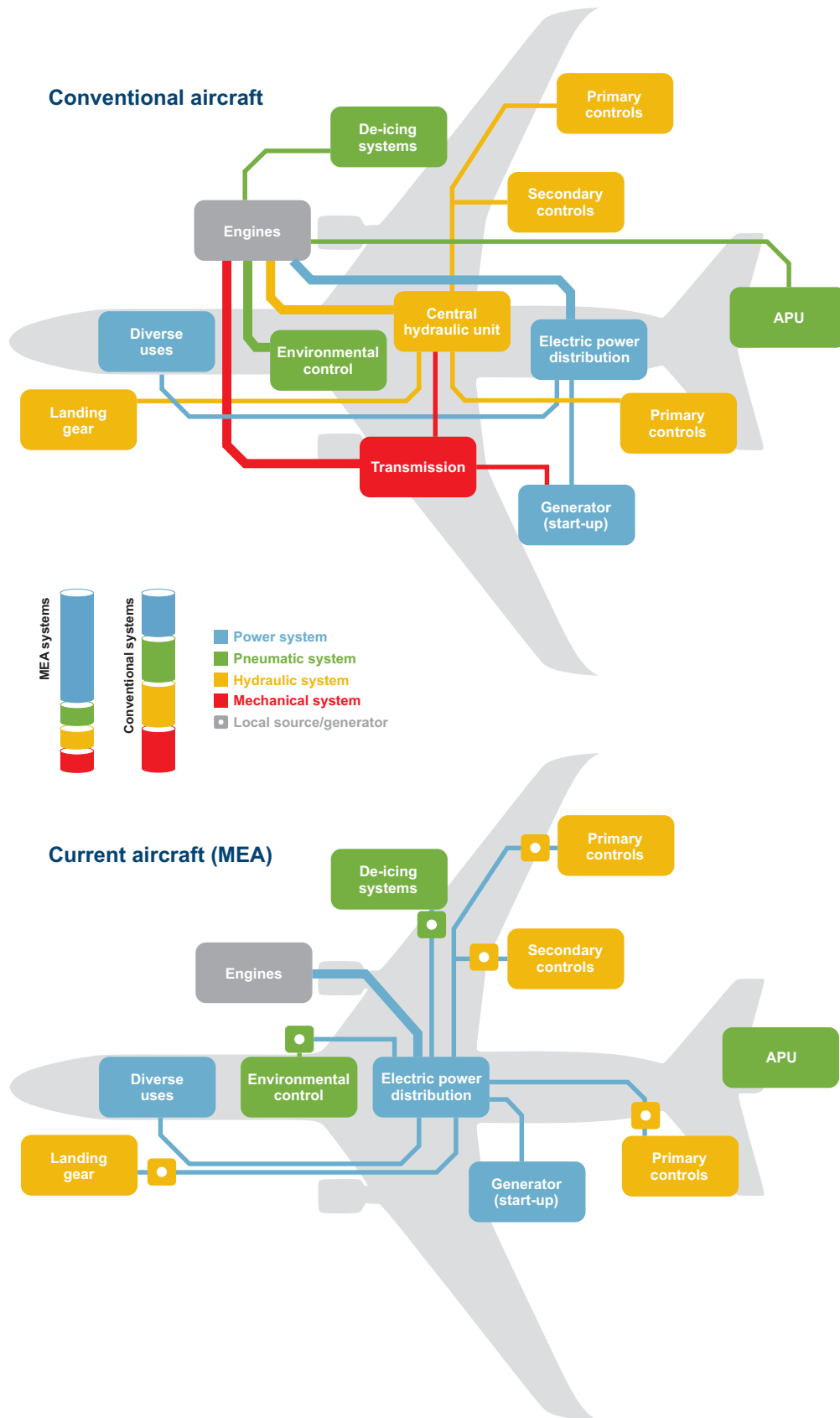
2.3.1 All-Electric Configuration

Before the idea of an all-electric aircraft, it was created the concept of More Electric Aircraft (MEA): jet-powered planes that maximize the use of electricity for all the other aircraft systems. Specifically, the MEA concept provides for the utilization of electric power for all non-propulsive systems, i.e., substitute partially or totally the pneumatic, hydraulic and mechanical subsystems by electrical ones (Fig. 8). Traditionally these non-propulsive systems are driven by a combination of different secondary power sources such as hydraulic, pneumatic, mechanical and electrical. Recent technological advances in the field of power electronics, fault-tolerant architecture, electro-hydrostatic actuators, flight control systems, high-density electric motors, power generation, and conversion systems have ushered the era of the MEA. The main examples of the use of MEA design concept could be noted in the Airbus A380 and in the Boeing 787.

Ultimately, the all-electric aircraft have all the subsystems and the propulsion exclusively electric, i.e., powered by electric motors. Electricity may be supplied by a variety of methods including batteries, ground power cables, solar cells, ultracapacitors, fuel cells, and power beaming. A schematic illustration of the all-electric architecture is depicted in Fig. 7.

A commercially interesting all-electric aircraft requires high specific energy of batteries (order of 1800-2000 Wh/kg) and values of specific power for the electric motors that can be

Figure 8 – Conventional and more electric aircraft, from .



Source: Aertec (2017).

achieved only with the use of fully-superconducting machines. But the forecasts say that these performances are not foreseen in the near future, thus the following architectures are much more explored.

2.3.2 Series and Turboelectric Configuration

In the series configurations, all the propulsive power is produced by electric motors. Depending on the degree-of-hybridization in terms of energy (H_E), there is a difference between the pure serial (turboelectric) and the series hybrid. They both share some common components such as fuel tanks, gas turbine engines, generators, electric power lines and electric components grouped in the PMAD (Power Management And Distribution), electric motors and finally the propulsive units (propeller or fan). Besides the turbo-electric configuration, the others have also an electric energy reservoir, usually in the form of batteries.

The turboelectric architecture (or pure series) is different when compared to other configurations because it does not depend on energy storage systems, such as batteries. However, high-power requirements demand progress in power electronics and powermachines technology. Since this configuration has no electrical storage system, the gas turbine engine must be able to provide all the power required, what oversizes this engine, decreasing the advantage of this architecture. Moreover, the turboelectric configuration is usually heavier than the conventional mechanical architecture, since it comprises more components, such as a generator. Thus, when compared to the traditional configurations, the turboelectric architectures may not be very competitive as expected, and even not meet the requirements of fuel saving. On the other hand, they present a great advantage: flexibility, i.e., due to the variability in positioning of the components, it is easy to set the layout in many ways, what is very appropriate for nonconventional concepts, such as distributed propulsion and boundary layer ingestion (BLI) designs (FELDER; KIM; BROWN, 2009).

Series hybrid architectures (Fig. 7) have an additional contribution of an electrical storage system (batteries), bringing some benefits to the propulsive system. Indeed, it could be possible to reduce the size of the gas turbine engine, since part of the aircraft required power will be supplied by the batteries. However, it has the weight penalty, since the current batteries have low specific energy, which results in heavy package of batteries.

An additional benefit of this configuration is that the gas turbine engine driving the generator can be designed to operate at a consistent and optimum engine speed, since this engine is not directly mechanically linked to the propellant of the aircraft. Moreover, this architecture allows simple coupling of components, avoiding those complex mechanical connections between the propeller, gas-turbine and electric motors (FRIEDRICH; ROBERTSON, 2015). Furthermore, likely the turboelectric configuration, the series hybrid is convenient for integrate many smaller fans/propellers distributed along the aircraft.

2.3.3 Parallel Configuration

Parallel architectures (Fig. 7) is a "mechanical coupling" system. The usual components of a parallel architecture include fuel tanks, engines, batteries, and electric motors. In the series architecture, there are generators, which are not found here.

The configuration has its engine and motor connected by a mechanical coupler. The mechanical coupling can be done in two ways: directly, where the axis of the electric motor is connected to the axis of the engine, or through a gearbox, where there is the sum of the mechanical powers of the two axes. This last option is interesting because it allows the easy coupling and uncoupling of the axes, which is feasible for smaller aircraft, but having clutches in high power and high-speed power drives is not efficient and easily done (CHAN; BOUSCAYROL; CHEN, 2010).

In this configuration, different control strategies can be used. If the power required by the transmission is higher than the output power of the engine, the electric motor is turned on so that both engines can supply power to the transmission. If the power required by the transmission is less than the output power of the engine, the remaining power is used to charge the battery pack (MENGISTU, 2011). Moreover, mechanical and electric power can be decoupled, what makes the system with high operating flexibility, enabling three modes of operation: purely combustion; purely electric and hybrid.

On the other hand, Miller (2004) comes up with other similar definitions, but in a different perspective. He splits the parallel hybrid-electric systems into three major types: mild, power-assist, and dual-mode. The types are nominally classified based on the sizing and participation of the electric motor. In the mild system, for example, the electric motor is relatively small and it is used to aid in acceleration and utilizes excess power to recharge the batteries. The power-assist parallel system uses a larger electric-motor and a more substantial battery pack, which warrants a modest downsizing of the engine. Likewise, the dual-mode parallel system utilizes a yet even larger electric motor and larger energy storage bank (battery). In other words, the higher the participation of the electric-motor and the battery pack, the lower the turboshaft engine sizing.

2.3.4 Series-Parallel Configuration

The series-parallel architecture (Fig. 7) is a combination of the advantages of the series and parallel configurations. However, there is a price to pay, which is the weight gain due to the complex layout system. When compared to the series hybrid configuration, the series-parallel architecture has an additional mechanical link, and when compared to the parallel configuration, the series-parallel architecture has an additional generator and control electronics (CHAU; WONG, 2002).

Usually, this configuration has one or more fans that can be driven directly by a gas turbine as well as other fans that are driven exclusively by electrical motors; these motors can be

powered by a battery or by a turbine-driven generator (SCIENCES; MEDICINE, 2016).

2.3.5 Partial Turboelectric Configuration

The partial turboelectric architecture is very similar to the parallel-series architecture, differentiating by not including batteries in its layout, as shown in Fig. 7. In other words, this configuration is a variant of the full turboelectric architecture that uses electric propulsion to provide part of the aircraft propulsive power, and the rest is provided by a turbofan driven by a gas turbine. Thus, the electrical components for this configuration do not need as much technological development as those required for the full turboelectric architecture (SCIENCES; MEDICINE, 2016).

Similar to what has been mentioned previously in the turboelectric configuration, this architecture also presents a flexibility of transmission of electrical power throughout the aircraft, which makes it an interesting option to be applied in the concepts of unconventional aircraft that use distributed and boundary propulsion layer ingestion (BLI).

2.3.6 Summary of Hybrid-Electric Architectures

Zamboni (2018) shows in Table 3 a summary of the main advantages and disadvantages of the hybrid-electric architectures aforementioned. Many authors say that the parallel configuration is better at this current technology, since it is lighter when compared to the others. Besides, series architectures have great potential for the future. As the technology of energy storage systems evolves, new and more energetic batteries will be available, allowing more system electrification, which reduces the participation of engines. An example would be the use of more electric motors, such as in the distributed propulsion, which has shown great advantages due to aero-propulsive interactions, such as drag reduction and increased aerodynamic efficiency (ISIKVEREN *et al.*, 2015).

2.4 Review of Hybrid-Electric Aircraft Projects

Several manned fixed-wing and electric aircraft have already flown, and there are already proposals to be sold. Figure 9 presents examples of electric aircraft that had their first flight since the beginning of the millennium. On the other hand, Figure 10 shows other major studies and projects developments in partnership with government agencies, large companies and also new ventures.

Table 3 – Summary of advantages and disadvantages of hybrid-electric architectures.

Architec.	Advantages	Disadvantages
Turbo-electric	<ul style="list-style-type: none"> • Does not depend on advances in energy storage technologies • High design freedom for propulsion-aircraft integration 	<ul style="list-style-type: none"> • High weight and low efficiency • Gas turbine engine is sized for peak power conditions • Depends on advances in HTS material technology
Series	<ul style="list-style-type: none"> • Decoupled engine can run at optimal RPM throughout the mission • High design freedom for propulsion aircraft integration • Power split between conventional and electrical power source is adjustable in flight • Batteries can be re-charged in-flight 	<ul style="list-style-type: none"> • High weight and low efficiency • Need a generator • Could depend on advances in HTS material technology
Parallel	<ul style="list-style-type: none"> • No need for a generator makes it lighter • Fewer energy conversions, more efficient • Power split between conventional and electrical power source is adjustable in flight • Engine could be down-sized to provide only average continuous power 	<ul style="list-style-type: none"> • Could need a complex gearbox • Power split changes are restricted due to risk of engine off-design operation • Engine is not decoupled from thrust and cannot run at optimal RPM • Mostly limited to conventional configurations for engine-aircraft integration
Series-Parallel	<ul style="list-style-type: none"> • Better design freedom when compared to parallel configuration • Batteries can be re-charged in-flight 	<ul style="list-style-type: none"> • Extra generator increases weight • Complex control strategy • Engine not fully decoupled from propeller
Partial turbo-electric	<ul style="list-style-type: none"> • Does not depend on advances in energy storage technologies • Good design freedom for electric motors-aircraft integration 	<ul style="list-style-type: none"> • Depending on degree of hybridization could be heavy and inefficient • Gas turbine engine is not decoupled from thrust generation

Source: Zamboni (2018).

Figure 9 – Summary of flyable, manned electric aircraft.

Name	Ist flight year	Arch.	Seats	MTOW [kg]	Max power [kW]	Specific energy battery [Wh/kg]	Range [nm] / Endurance	Remarks
Lange Antares 20E	2003	E	1	660	42	136	N.A.	1st electric aircraft with airworthiness certification; commercially available, motorglider
Fishman Electraflyer C	2008	E	1	283	13.5	N.A.	90 min	Converted motorglider; Li-Po battery
Boeing HK-36 FCD	2008	FC	1	860	75	N.A.	45 min	30 kW fuel cell; experimental
Yuneec E430	2009	E	2	470	40	154	N.A.	Clean-sheet composite airframe; commercialization abandoned
Siemens/Diamond E-Star	2011	SHE	2	800	70	N.A.	N.A.	30 kW Wankel engine; experimental
Pipistrel Taurus Electro G2	2011	E	2	450	40	N.A.	N.A.	Commercially available
Pipistrel Taurus Electro G4	2011	E	4	1500	150	180	244	Won NASA Green Flight Challenge (GFC); experimental
IFB Stuttgart eGenius	2011	E	2	950	60	204	244	Competed in NASA GFC; experimental
Embry-Riddle Eco-Eagle	2011	PHE	2	1075	105	125	170	Unofficial participant in GFC; 75 kW rotax, 30 kW electric; experimental
Fishman Electraslyer ULS	2012	E	1	238	15	N.A.	120 min	Commercially-available under US ultralight rules
Chip Yates Long ESA	2012	E	1	680	192	N.A.	N.A.	Experimental
Siemens/Diamond E-Star 2	2013	SHE	2	800	80	N.A.	N.A.	5 kW/kg motor; experimental
Airbus E-Fan	2014	E	2	600	60	207	60 min	2 x 30 kW fan; experimental
Cambridge SOUL	2014	PHE	1	235	20	144	N.A.	12 kW electric, 8 kW petrol; recharges in flight; experimental
Pipistrel Alpha Electro	2015	E	2	550	60	171	70	Commercially available
Airbus E-Fan 1.2	2016	SHE	2	600	60	N.A.	N.A.	2 x 30 kW fan, 50 kW range extender; experimental
Siemens Extra 300 (330LE)	2017	E	1	1000	260	N.A.	N.A.	95% eff. motor, > 5 kW/kg incl. inverter, 580 VDC; experimental

Source: Breijle and Martins (2018).

Figure 10 – Summary of electric fixed-wing aircraft concepts and studies.

Name	Target EIS year	Arch.	Seats	MTOW [kg]	Max power [kW]	Specific energy battery [Wh/kg]	Design Range [nmi]	Remarks
NASA X-57 "Maxwell"	2019	E	2	1360	0.144	130	N.A.	2 x 72 kW tip motors; manned demonstrator; leading-edge DP
NASA STARC-ABL	2035	TE	154	60000	2.6	N.A.	3500	-9.4% fuel burn; tube/wing configuration with tailcone BLI propopulsion
NASA N3-X	2045	TE	300	227000	50	N.A.	7500	-10% fuel burn due to electric propulsion; superconducting; HWB with BLI distributed propulsion
Boeing SUGAR Volt	2035	PHE	154	68040	1.0	750	3500	-10.9% fuel burn due to EP; struc-braced wing with battery pods
Bauhaus Luftfahrt Ce-Liner	2035	E	189	109300	33.5	2000	900	C-wing, supercond. motors, aggressive tech assumptions
Airbus VoltAir	2035	E	~33	~33000	N.A.	750+	~900	Superconducting electronics; BLI; laminar-flow wing
Airbus/R-R E-Thrust	2050	SHE	90	N.A.	9.0	1000	N.A.	Superconducting; BLI and high bypass ratio; embedded fans
ESAero/Wright ECO-150R	2035	TE	150	60-75k	12.7	N.A.	1650	FB ~737-700; 16 motors embedded in wing; no supercond.
Eviation Alice	2019	E	11	6350	0.780	260	560	3 pusher props; Kokam Li-ion batteries
XTI Tri-Fan 600	2024	SHE	6	2404	1.5	N.A.	1200	VTOL; tilt-fan configuration
Ampace Tailwind	2020s	E/SHE	N.A.	N.A.	N.A.	N.A.	350	Tail-mounted boundary layer ingestion thruster
Zunum	2020s	SHE	12	5216	1	N.A.	700	Conventional regional jet layout; straight NLF wing

Source: Brelje and Martins (2018).

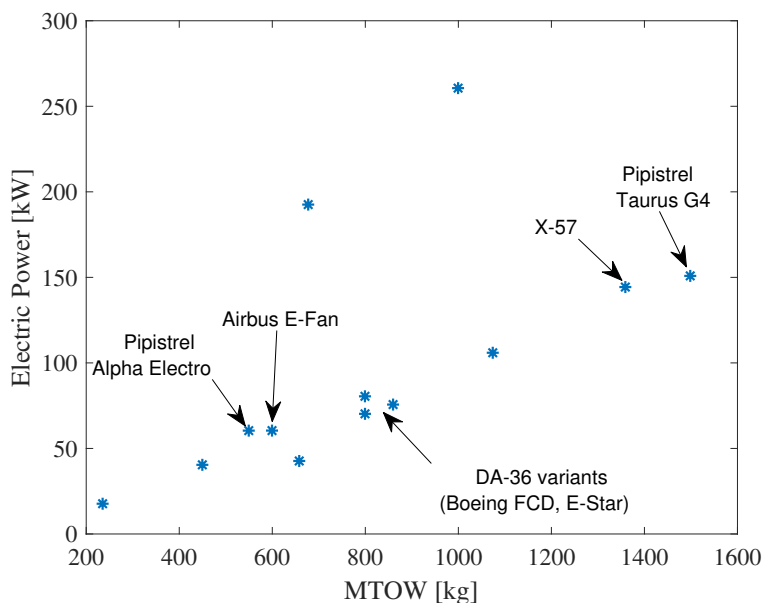
2.4.1 Commercial Products and Prototypes

The beginnings of electric aircraft concepts began many years ago, more than a century ago. It was the Brazilian Santos Dumont who first successfully powered an airship with an electric motor in 1883 (Encyclopaedia Britannica, 2019). Since then, several electric aircraft have been developed, as listed by Costello (2011). In the 1980s and 1990s, aircraft with high aspect ratio and solar panels were demonstrated by NASA and other researchers, resulting in the known high-altitude long-endurance (HALE) aircraft.

The first manned and fixed-wing electric aircraft was the Brditschka MB-E1, which flew for less than 10 minutes in 1973 (PORNET; ISIKVEREN, 2015). Recently, many electric motor gliders have entered the sales market. The first one that was certified was the Antares 20E (COSTELLO, 2011). Additionally, some companies in the aerospace industry created some demonstrators from glider airframes, such as the Boeing HK-36, Diamond DA-36 E-Star, and the Pipistrel Taurus Electro.

In 2011, the NASA/CAFE foundation Green Flight challenge inspired three new experimental electric aircraft with extended range: the Taurus Electro, the Embry-Riddle Aeronautical University's Eco-Eagle, and the IFB Stuttgart's eGenius. More recent demonstrators have focused on scaling up power to 100kW and above, such as the Extra 330LE. Figure 11 shows the evolution of the MTOWs of the aircraft and the electrical powers of each one of them. Most of them are manufactured based on motor glider airframes. There is a linear behavior of the evolution, which is due to the technological progress. NASA's X-57 Maxwell demonstrator is a project that applies the distributed propulsion concept with multiple electric motors.

Figure 11 – Progression of manned electric aircraft demonstrators. (Data from Table 9).



Source: Elaborated by the author.

In 2017, Airbus, Rolls-Royce, and Siemens formed a partnership whose aim was to develop a hybrid-electric aircraft, which has been called as “E-FAN X” (Fig. 12). The project is a derivative of the BAe-146 model and is intended to replace one of the four turbofan engines with a 2 MW electric motor. The intention is “to explore the challenges of high-power propulsion systems, such as thermal effects, electric thrust management, altitude and dynamic effects on electric systems, and electromagnetic compatibility issues” and is targeted for first flight by 2020 (Airbus, 2017).

Figure 12 – Airbus E-Fan X.



Source: ch-aviation (2018).

The E-Fan X will feature three turbofan engines and a two-megawatt electric motor, along with a power distribution center and “E-Supervisor” hybrid electric propulsion system. According to Siemens, the electric propulsion system obtains its power from a generator that is powered by a turbine in the fuselage. E-Fan X will also feature lithium-ion batteries with 700 kilowatts of power.

2.4.2 Recent Concepts and Studies

There are many companies and research centers from different universities developing and testing new concepts and prototypes of hybrid-electric aircraft that have not yet flown or are still going to wait a few years.

One of the pioneers was the Boeing company when launched the SUGAR (Subsonic Ultra-Green Aircraft) series. These studies evaluated several evolutionary and revolutionary designs to meet the NASA N+3 goals. The reports show comparisons between a hybrid concept and turbofan concepts with equal technology and mission rules.

All of the concepts were sized for 900 nm economic missions with 154 seats. The concepts were a tube-and-wing baseline with current technology (SUGAR Free); a tube-and-wing architecture with estimated 2030s technologies (Refined SUGAR); a high aspect ratio strut-braced tube-and-wing design with 2030s technology (SUGAR High); a hybrid-wing-body (HWB) configuration with turbofans and 2030s technology (SUGAR Ray); and a version of SUGAR High with parallel hybrid electric propulsion (Sugar Volt, Fig. 13).

Figure 13 – Boeing SUGAR Volt.



Source: Phys.org (2012).

In the first phase of the study, SUGAR Volt was the only concept capable of meeting NASA's N+3 fuel burn goal of -70% (compared to the SUGAR Free baseline). The Volt used 28% less fuel than the conventionally-powered SUGAR High. In the second phase, hybrid electric propulsion was extended to the conventional tube-and-wing and HWB configurations, and similar fuel burn improvements were found (25%-46% better than conventional propulsion for the HWB; 33%-55% better for the tube-and-wing) (BRADLEY; DRONEY, 2015). These studies included a detailed discussion of technology development risks, commercialization potential, and an agenda for future development of parallel hybrid technology.

In the last years, NASA has spent its time researching four concepts varying power scales. The best concept developed is the Scalable Convergent Electric Propulsion Technology and Operations Research (SCEPTOR) project, which was launched in 2014. This project has focused on evaluating the effects of higher power levels and distributed propulsion. SCEPTOR is closely related to a NASA propulsive concept known as LEAPtech (Leading Edge Asynchronous Propellers Technology), which introduces multiple small propellers distributed along the leading edge of the wing (MOORE, 2014). The main goal of LEAPtech is to reduce drag by increasing cruise wing loading of general aviation airplanes by 2.5 times. This is achieved by greatly increasing C_{Lmax} through blown lift, avoiding the need for complex and heavy multi-element flap systems.

From the SCEPTOR project, NASA came up with a manned aircraft: the X-57 Maxwell (Fig. 14). This is a derivation of the Italian Tecnam P2006T airframe, replacing the Tecnam's combustion engines by electric motors and propellers distributed along the wing, and powered by Li-ion batteries.

Figure 14 – NASA X-57 Maxwell.



Source: INSIDEEVs (2018).

From 2017 until the present day, several startups and aeronautical companies were created with the objective of launching new electric aircraft for carrying passengers, with certification Part 23, in the order of 1 MW of power. For example, Zunum Aero is a company funded by Boeing and JetBlue and is developing a 12-passenger hybrid electric regional aircraft. Wright Electric is trying to sell aircraft concepts for short-haul all-electric operation in partnership with EasyJet airline. Ampaire is a new venture promoting the "tailwind" concept, featuring an aft boundary layer ingesting propulsor and series hybrid configuration.

SIZING APPROACHES IN ELECTRIC AND HYBRID-ELECTRIC AIRCRAFT DESIGN

In this chapter, it is presented the main classification of aircraft design phases. Moreover, the conceptual design phase is addressed in more detail, where top-level requirements are defined and configurations are selected. Next, a generic sizing method is proposed, considering the concept of constraint diagrams (power loading vs. wing loading).

3.1 Aircraft Development Phases

The process of developing a new aircraft starts from the survey of the main requirements and market demands, where it is investigated the needs of customers and the new opportunities, such as increased number of passengers, newly available routes to reach and exploit, aging fleet members, and availability of new working concepts, ideas, and technologies.

After a definition of the type of aircraft, the project is carried out in several phases until, finally, the aircraft is manufactured and put into operation. According to Nicolai and Carichner (2010), the design process is usually divided into the following three phases:

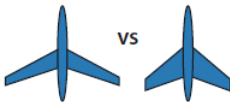
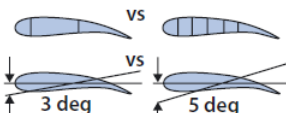
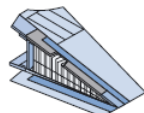
- *Conceptual Design*
 - Definition of the performance goals;
 - Evaluation of possible competing concepts;
 - Generation of many possible concepts;
 - Selection of a baseline design (3 views + data).

- *Preliminary Design*
 - Refined sizing of the baseline design concept;

- Parametric studies;
- Global design frozen with the possibility to change only few details.
- *Detail Design*
 - Detailed design of the whole vehicle down to each single detail;
 - Accurate evaluation of performances;
 - Fine tuning of the design;
 - Release of drawings for production.

Despite this classification, the activities between each of these phases are always interconnected and are summarized in Fig. 15.

Figure 15 – The three phases or levels of aircraft design.

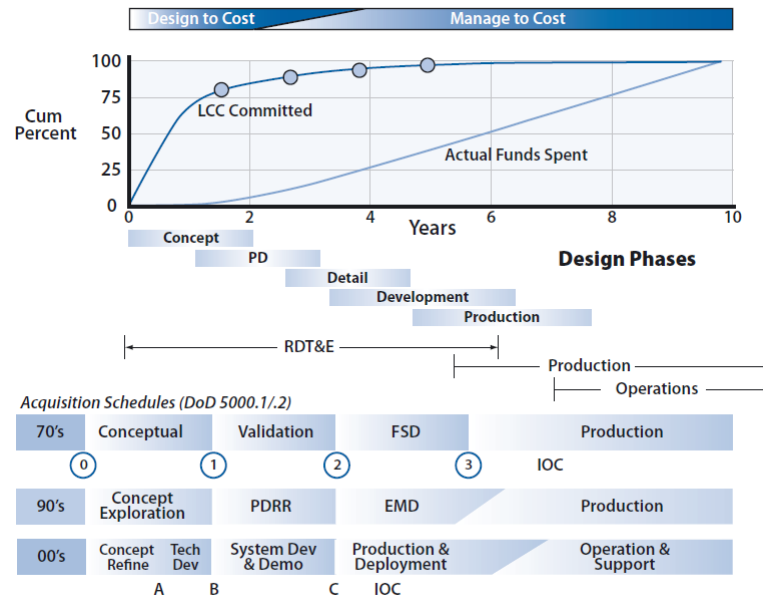
	Phase 1 Conceptual Design	Phase 2 Preliminary Design	Phase 3 Detail Design				
							
Known	Basic Mission Requirements Range, Altitude, & Speed Basic Material Properties σ/ρ E/ρ $\$/lb$	Aeroelastic Requirements Fatigue Requirements Flutter Requirements Overall Strength Requirements	Local Strength Requirements Producibility Functional Requirements				
Results	<table border="1" style="display: inline-table; vertical-align: top;"> <tr> <th>Geometry</th> <th>Design Objectives</th> </tr> <tr> <td>Airfoil Type R t/c λ Δ</td> <td>Drag Level Weight Goals Cost Goals</td> </tr> </table>	Geometry	Design Objectives	Airfoil Type R t/c λ Δ	Drag Level Weight Goals Cost Goals	Basic Internal Arrangement Complete External Configuration Camber & Twist Distribution Local Flow Problems Solved Major Loads, Stresses, Deflections	Detail Design <i>Mechanisms</i> Joint Fittings and Attachments Design Refinements as Result of Testing
Geometry	Design Objectives						
Airfoil Type R t/c λ Δ	Drag Level Weight Goals Cost Goals						
Output	Feasible Design	Mature Design	Shop Designs				
TRL	2 – 3	4 – 5	6 – 7				

Source: Nicolai and Carichner (2010).

Figure 16 shows the three phases of design in a typical government program acquisition according to DoD 5000.1 (DEFENSE, 2009). The years shown are extremely optimistic because there are always breaks in the schedule while the government issues a Request for Proposal, industry submits proposals, and the government evaluates the proposals, selects a winner, and gets its funding in place. Commercial programs move much faster because the aircraft builder controls the progress and funding of the program. Typical times from the decision to build the aircraft (Milestone 1 or B for the government; the start of preliminary design for commercial) to production is about 10 years for the government and 5 years for commercial.

Figure 16 also shows the importance of the conceptual design phase in that over 70% of the design features that drive life-cycle cost (LCC) are selected during that phase.

Figure 16 – Design phases integrated into the entire government program.

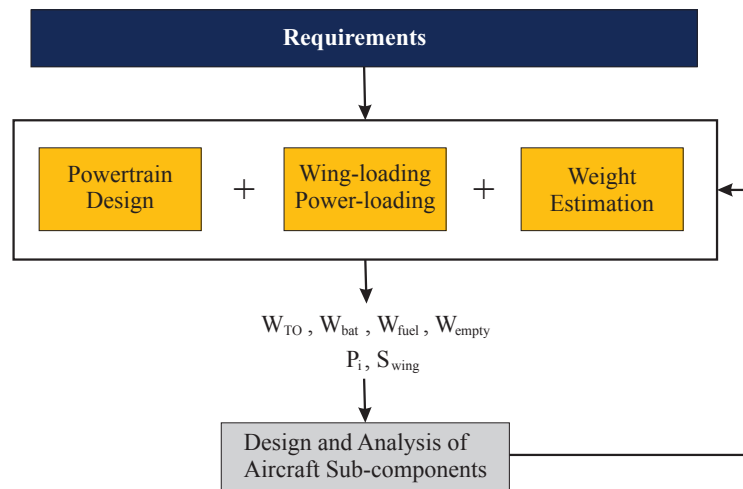


Source: Nicolai and Carichner (2010).

3.2 Aircraft Sizing Method - Conceptual Design Process

The conceptual design process of an aircraft is presented in the flowchart in Fig. 17 and discussed next.

Figure 17 – Conceptual design flowchart.



Source: Elaborated by the author.

3.2.1 Requirement Analysis

Apart from specifying the airworthiness rules (FLORIO, 2016) according to which the aircraft type has to be certified, TLRs (Top Level Requirements) define objectives and constraints in a degree of detail complying with the purpose of advanced design. The following is a typical

set of requirements and technical objectives for jet transports: payload, range, performance (speed, service ceiling, climb rate, climb gradient), comfort (payload / storage capability for military), sustainability aspects (noise and gas emission), airport accessibility (takeoff and landing distance, wheel loading, parking area, radius of turn), safety (survivability for military aircraft), operating cost (direct costs: crew, fuel, maintenance, etc.; and indirect costs: terminal space, loading equipment, etc.). Some of these aspects are discussed below.

3.2.1.1 Payload

This requirement drives the size of the aircraft. Only for personal and small general aviation aircraft, the pilot is considered as payload. In business, commuters and commercial aircraft, pilots and crew are considered as part of the operative weight budget (not of the payload).

3.2.1.2 Range

It is the maximum distance over which the payload can be transported, for example, US continental 5600 km (3000 nmi) or transpacific 14000 km (7600 nmi) without refueling. Policies concerning flight execution and fuel reserves are stated explicitly and a distinction can be made between economical and high-speed cruising conditions corresponding to different ranges. Regional airliners are mostly designed for multi-stage operations for which the number of flights are specified to be flown without intermediate refueling. Range drives the required amount of energy to propel the aircraft over its mission profile.

3.2.1.3 Cruise Speed/Altitude Capability

Often in combination with a minimum initial altitude, speed is the attribute that made of aviation what is today. Requirements may belong to standard and/or non-standard ambient conditions. The one-engine-inoperative (OEI) ceiling is important when flying over mountainous terrain or oceans. Moreover, speed drives the wing configuration and propulsion system choice. Typically, Mach numbers less than 0.6 imply in propeller-powered and no wing sweep (possible laminar flow) aircraft, and Mach numbers greater than 0.6 imply in turbofan-powered and wing sweep aircraft.

3.2.1.4 Takeoff Distance

It is the length of a runway needed to accelerate, lift off and climb to a prescribed obstacle height (military 50 ft; commercial 35 ft). It grows with: increased power loading (W/P), increased wing loading (the ratio between the aircraft weight and its lifting surface - W/S), higher airport altitude (thinner air), and greater ground field roughness.

3.2.1.5 Climb Requirements

Climb requirements can be given in terms of:

- Climb Rate (c , ROC, \dot{h}) [m/s]: the vertical component of the airspeed of the aircraft during climbing. It is the time derivative of the aircraft altitude.
- Climb Gradient (G) [%]: the ratio between the vertical and the horizontal traveled distances during the climb. For small flight path angles, the climb gradient is equal to c/V and to the flight path angle γ .

In other words, the climb rate (c) affects the maximum altitude that can be achieved in the shortest time, and the climb gradient (G) affects the maximum altitude that can be achieved with minimum traveled horizontal distance.

3.2.1.6 Airport Compatibility

It comprises the airfield classification, defining limitations to wing span and length, landing gear track and runway pavement loading.

3.2.1.7 Environmental Issues

It includes the maximum noise emission levels defined relative to certification requirements in FAR Chapter 36 and similar standards in ICAO Annex 16. For example, a cumulative limit of 30 dB below FAA Stage 4. Engine exhaust emission targets during take-off and landing are defined relative to internationally agreed criteria; in particular, CAEP/6 NO_x restrictions.

3.2.1.8 Reliability and Durability

Intense airliner utilization emphasizes the need to achieve a specified lifetime in terms of a number of flight hours and/or flight cycles.

Many airliners are conceived in the framework of family planning rather than a single mission. Several versions with increased or decreased range and/or payload are generated during the life cycle of the project. This requires evaluation during the conceptual design of several derivative designs having their cabin cross-section in common with the basic version.

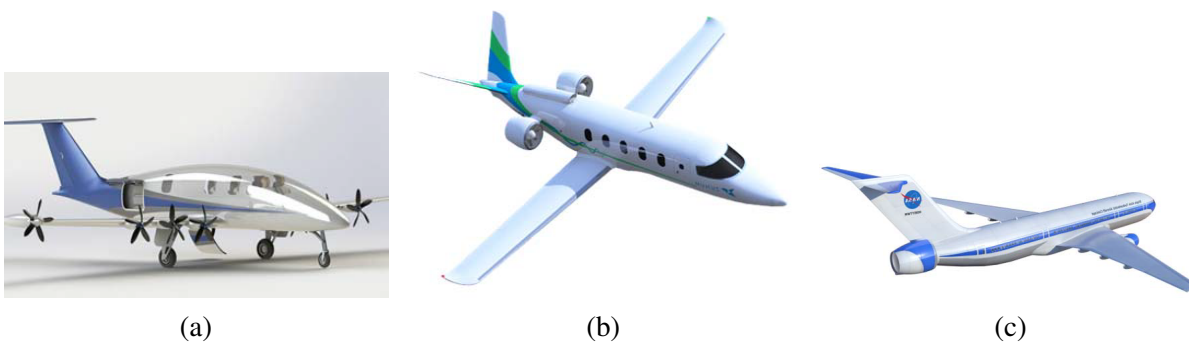
3.2.2 Configuration Selection

It is necessary to choose the best configuration among the several possibilities: wing position (high, mid or low), engine location (on the wing or on the fuselage), tail configuration (T-tail, crucifix or low tail), and undercarriage (tail-dragger or nose wheel configuration). For hybrid-electric aircraft, there are more options for propulsion integration (i.e. distributed propulsion), and more options for powertrain architecture.

The propulsion integration allows discussing various possibilities, what directly affects the aero-propulsive interaction. Currently, it has been proposed these three options:

- Distributed propellers + gas turbine in the tail cone: strong aero-propulsive interaction (Fig. 18a);
- Two ducted fans + gas turbine in the tail cone: little aero-propulsive interaction (Fig. 18b);
- Two turbofans + tail cone thruster: strong propulsive effects (Fig. 18c).

Figure 18 – Propulsion integration.



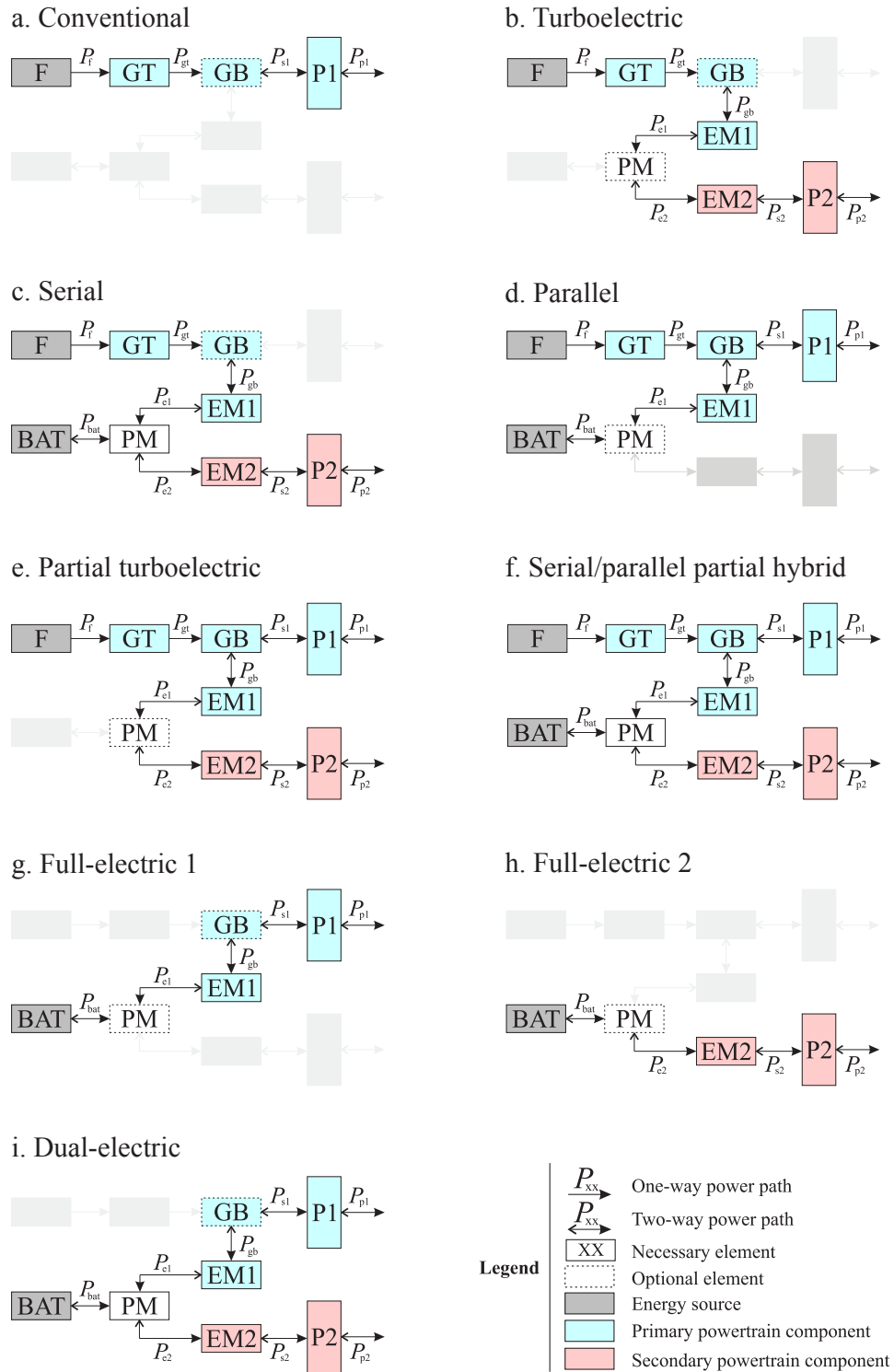
Source: Air&Space (2016).

The powertrain architecture may be chosen among the several possibilities presented in Section 2.3. As discussed previously, each one of them has its own advantages and disadvantages, leaving the choice of the best option that fits a given project to the responsible designer.

To simplify and follow the standard adopted by Sciences and Medicine (2016), this work will use the configurations and nomenclature proposed by Felder (2015), including a conventional powertrain for reference, as shown in Fig. 19. These representations energy sources, components which split power, components which transform one type of power into another, and the power paths that connect these elements. Inverters and transformers are modeled in a simplified way and associated to the electric machines or in the power management and distribution (PMAD, or “PM”) component. The components are divided into the elements which constitute the “primary” powertrain, and those that constitute the “secondary” powertrain. The primary components are, directly or indirectly, mechanically coupled to the gas turbine. The secondary components include the devices which power the electrically-driven propulsion system. The primary and secondary branches of the power train contain N_1 and N_2 identical instances of each component, respectively.

From Fig. 19, one can see that the first five architectures are limit cases of the sixth (the serial/parallel partial hybrid, SPPH). Thus, the SPPH architecture can be used as a generic model, while the remaining architectures can be obtained by setting specific power-control parameters to zero or one.

Figure 19 – Simplified models of the different powertrain architectures considered, including the power paths (indicated with lower-case subscripts), and powertrain components and energy sources (indicated with upper-case letters). Lines with two arrow heads indicate paths where the power can flow in both directions, with the positive direction shown by the filled arrowhead. Legend: “F” = fuel, “GT” = gas turbine, “GB” = gearbox, “P” = propulsor, “BAT” = batteries, “EM” = electrical machine (i.e. electric omotor or generator), “PM” = power management and distribution system.



Source: Felder (2015).

3.2.2.1 Definition of Power Control Parameters

The authors Voskuijl, Bogaert and Rao (2018), Isikveren *et al.* (2014), Perullo and Mavris (2014), Ang *et al.* (2018) have used different parameters to describe the powertrain, but there is no convention so far. Consequently, the parameters proposed here are based on previous definitions, but have been modified such that specific combinations of the power-control parameters can define the power train architecture.

The first parameter is the *supplied power ratio*, which can be expressed as

$$\Phi = \frac{P_{bat}}{P_{bat} + P_f} \quad (3.1)$$

where P_{bat} and P_f are the power from the battery and the fuel, respectively. Thus, the supplied power ratio represents the amount of power drawn from the electrical energy source (batteries) with respect to the total amount of power drawn from all energy sources (battery plus fuel).

The second power-control parameter is the *shaft power ratio*, which represents the amount of shaft power produced by the secondary electrical machines with respect to the total amount of shaft power produced, defined as

$$\varphi = \frac{P_{s2}}{P_{s1} + P_{s2}} \quad (3.2)$$

Another parameter is the *gas turbine throttle*, defined as

$$\xi_{GT} = \frac{P_{GT}}{P_{GT,max}} \quad (3.3)$$

which represents the power produced by the gas turbine with respect to the maximum power it can produce in the given flight condition. This power can be related to the installed sea-level static power of the gas turbine $P_{GT,max,SL}$.

The altitude lapse applied here is the simplest one, presented below, and assumes that the engine power is directly dependent on the density ratio:

$$P = P_{SL} \left(\frac{\rho}{\rho_{SL}} \right) = P_{SL} \sigma \quad (3.4)$$

where P , ρ and σ are power, air density, and air density ratio at altitude, respectively; and P_{SL} and ρ_{SL} correspond to sea-level values.

3.2.2.2 Solving the Powertrain Equations

Considering the architecture *f* in Fig. 19, the powertrain model has ten unknowns variables, which correspond to the ten power paths. Thus, ten equations are necessary to solve the system. Evaluating the component efficiencies, it is possible to write the first seven equations by applying a power balance for each generic component i :

$$\sum P_{out} = \eta_i \sum P_{in} \quad (3.5)$$

where the left-hand side indicates the powers that leave each component, and on the right-hand side the powers that enter the components multiplied by the efficiencies of the components.

There are missing three other equations to complete the system. So using the Φ (which relates P_{bat} to P_f), φ (which relates P_{s1} to P_{s2}), and the total required propulsive power $P_p = P_{p1} + P_{p2}$, it is possible to set the linear system as

$$\begin{bmatrix} -\eta_{GT} & 1 & 0 & 0 & 0 & 0 & 0 & 0 & 0 & 0 \\ 0 & -\eta_{GB} & 1 & 1 & 0 & 0 & 0 & 0 & 0 & 0 \\ 0 & 0 & 0 & -\eta_{P1} & 0 & 0 & 0 & 0 & 1 & 0 \\ 0 & 0 & -\eta_{EM1} & 0 & 1 & 0 & 0 & 0 & 0 & 0 \\ 0 & 0 & 0 & 0 & -\eta_{PM} & -\eta_{PM} & 1 & 0 & 0 & 0 \\ 0 & 0 & 0 & 0 & 0 & 0 & -\eta_{EM2} & 1 & 0 & 0 \\ 0 & 0 & 0 & 0 & 0 & 0 & 0 & -\eta_{P2} & 0 & 1 \\ \Phi & 0 & 0 & 0 & 0 & (\Phi - 1) & 0 & 0 & 0 & 0 \\ 0 & 0 & 0 & \varphi & 0 & 0 & 0 & (\varphi - 1) & 0 & 0 \\ 0 & 0 & 0 & 0 & 0 & 0 & 0 & 0 & 1 & 1 \end{bmatrix} \begin{pmatrix} P_f \\ P_{gt} \\ P_{gb} \\ P_{s1} \\ P_{e1} \\ P_{bat} \\ P_{e2} \\ P_{s2} \\ P_{p1} \\ P_{p2} \end{pmatrix} = \begin{pmatrix} 0 \\ 0 \\ 0 \\ 0 \\ 0 \\ 0 \\ 0 \\ 0 \\ 0 \\ P_p \end{pmatrix} \quad (3.6)$$

Therefore, knowing the total aircraft required power and the component efficiencies, it is easy to find the power splits across the powertrain, allowing a component sizing as well.

3.2.3 Power Constraints: Wing and Powertrain Sizing

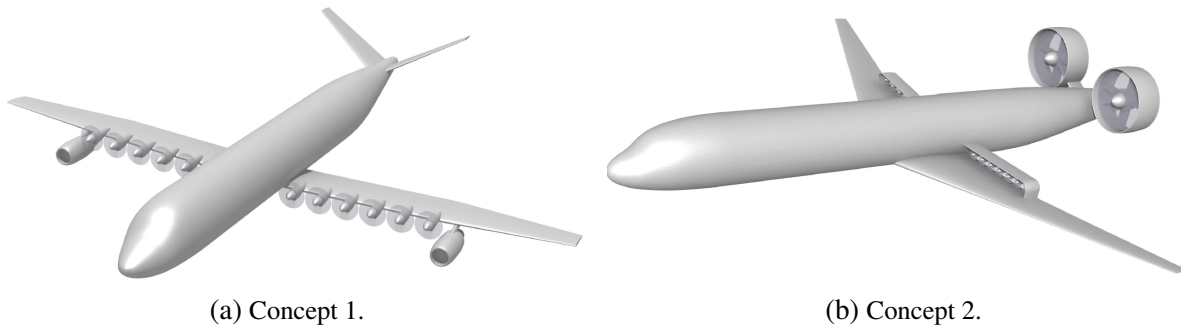
The definition of the wing area and the installed power are, initially, the main step when designing an aircraft. Currently, the studies performed around the world have been considering different configurations for the powertrain, such as *distributed propulsion* (DP), which is the spreading of propulsive elements (i.e., fans, propellers, or jets) over the airframe in a beneficial manner (GOHARDANI; DOULGERIS; SINGH, 2011). This approach has estimated improvements propulsive efficiency through, for example, reduced wing area (BORER *et al.*, 2016) or increased effective bypass ratio (FELDER; KIM; BROWN, 2009). Thus, it is discussed here hybrid systems that present synergistic benefits when combined with distributed propulsion, being referred to as *hybrid-electric distributed propulsion* (HEDP).

For the following modeling, it is considered examples of HEDP aircraft layout illustrated in Fig. 20. The concept shown in Fig. 20a contains two gas turbines which constitute the primary powertrain branch ($N_1 = 2$), and twelve propulsors driven by electric motors which form part of the secondary powertrain branch ($N_2 = 12$).

3.2.3.1 Thrust, Lift and Drag Decomposition

In conventional aircraft designs, propulsive effects are not taken into account in aerodynamic calculations (lift and drag). In other words, the sizing methods are simplified. However, when having configurations with distributed propulsion, it is important to take into account these effects, since they directly modify the aerodynamic flow throughout the aircraft, which results in different lift and drag components. Nonetheless, the DP contributes directly to the thrust.

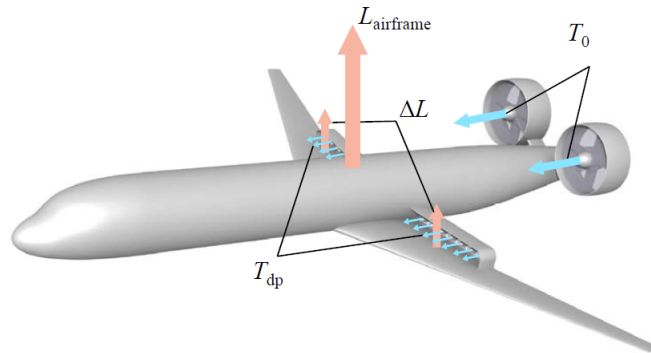
Figure 20 – Representation of two HEDP aircraft: one featuring leading-edge distributed propellers powered by two thermal engines in a serial configuration (a), and one featuring over-the-wing DP combined with a propulsive empennage (b).



Source: Vries, Brown and Vos (2018).

Taking Concept 2 (from Fig. 20b) as example, the DP and the airframe produce components of lift and thrust as depicted in Fig. 21.

Figure 21 – Lift and thrust produced by the propulsive system.



Source: Elaborated by the author.

The total thrust of the aircraft (T) is the sum of the component produced by the two ducted fans at the rear of the fuselage (T_0), and the component produced by the array of distributed propulsors installed over the wing (T_{dp}), which presents strong interaction effects with the airframe. Thus,

$$T = T_0 + T_{dp} \quad (3.7)$$

The T_{dp} component is affected by the presence of the wing. To evaluate the effect of the airframe on propulsor performance, it is necessary to account for the effects of elements such as wing, nacelle, fuselage, and so on (ESDU International PLC, 1985). Additionally, since the powertrain is expressed by component efficiencies (see Eq. 3.5), it is convenient to express the interaction effects in terms of changes in propulsive efficiency of the distributed propulsion system (η_{dp}):

$$\eta_{dp} = \eta_{dp,isolated} + \Delta\eta_{dp}(T_{dp}, L_{airframe}, S, \dots) \quad (3.8)$$

where T_{dp} is defined as the total thrust produced by the distributed propulsors, $\eta_{dp,isolated}$ is the propulsive efficiency that these propulsors would have without any other element (ducts, nacelles, wing, fuselage, etc.), and $\Delta\eta_{dp}$ is the change in propulsive efficiency when installed on the aircraft.

The total lift produced by the aircraft can be expressed as

$$L = L_{airframe} + \Delta L(T_{dp}, L_{airframe}, S, \dots) \quad (3.9)$$

where ΔL is the increase in aircraft lift due to the thrust generated by the distributed propulsors, which depends on thrust, airframe lift and a fraction of wing area. Nonetheless, the aero-propulsive interaction generates effects on the overall drag of the aircraft, as expressed:

$$D = \underbrace{D_0 + \Delta D_0(T_{dp}, S, \dots)}_{\text{zero-lift drag}} + \underbrace{D_i(L_{airframe}) + \Delta D_i(T_{dp}, L_{airframe}, S, \dots)}_{\text{lift-induced drag}} \quad (3.10)$$

where D_0 is the zero-lift drag without distributed propulsors, ΔD_0 is the increase in zero-lift due to the DP system. This increase can be caused by interaction with jets or slipstreams at zero lift, by variations in angle of attack in order to maintain zero lift, or by changes in wetted area due to pylons, nacelles, and other external elements of the propulsion-system installation. Moreover, D_i is the lift-induced drag of the aircraft without DP, and ΔD_i is the change in lift-induced drag due to the DP system.

As usual, it is convenient to represent the lift and drag contributions as non-dimensional coefficients, i.e., lift and drag coefficients. It can be done dividing those contributions by the dynamic pressure of the freestream (q_∞) and the reference area of the wing (S), obtaining the following:

- For lift:

$$C_L = \frac{L}{q_\infty S} \quad (3.11)$$

$$C_L = C_{L_{airframe}} + \Delta C_L(T_{dp}, C_{L_{airframe}}, S, \dots) \quad (3.12)$$

- For drag:

$$C_D = \frac{D}{q_\infty S} \quad (3.13)$$

and assuming a parabolic shape for the airframe drag polar $\left(C_{D_i} = \frac{C_{L_{airframe}}^2}{\pi e \mathcal{R}} \right)$, where e is the Oswald factor and \mathcal{R} is the aspect ratio of the wing. Thus,

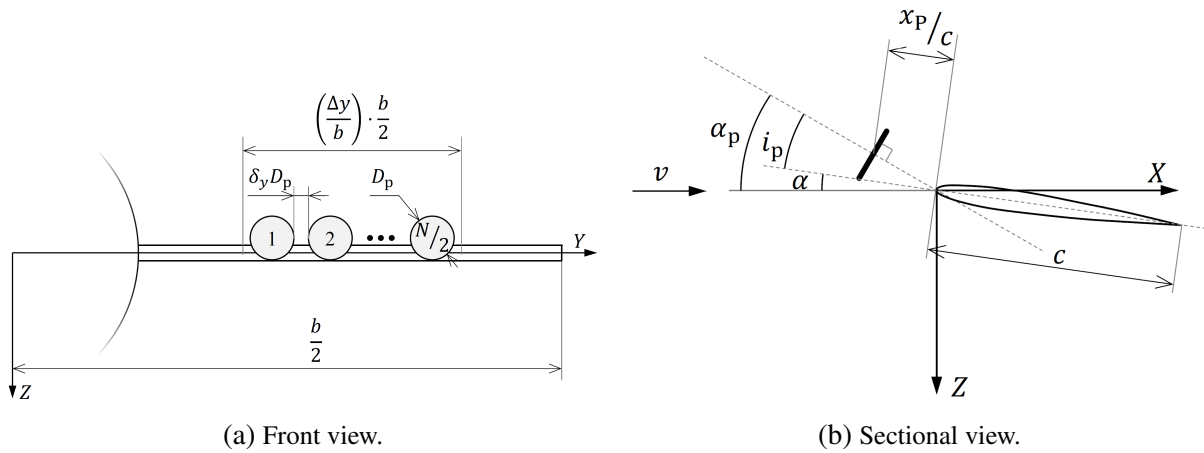
$$C_D = C_{D_0} + \Delta C_{D_0}(T_{dp}, S, \dots) + \frac{C_{L_{airframe}}^2}{\pi e \mathcal{R}} + \Delta C_{D_i}(T_{dp}, S, C_{L_{airframe}}, \dots) \quad (3.14)$$

Therefore, the aero-propulsive interaction effects of the distributed propulsors are expressed by means of these "Deltas", which are estimated using detailed aerodynamic analyses. For the conceptual sizing phase, surrogate models or simplified aerodynamic models have been used, as presented in the following section.

3.2.3.2 Aero-Propulsive Interaction Model

Consider a tube-and-wing aircraft featuring leading-edge distributed propulsors, illustrated as Concept 1 in Fig. 19a. Taking a semi-wing, a simplified geometrical description is shown in Fig. 22.

Figure 22 – Simplified DP-system representation, indicating the main geometrical parameters.



Source: Vries, Brown and Vos (2018).

It is assumed a rectangular planform wing of span b and chord c . There are N propulsors ($N/2$ per semi-wing) spread over the wing, but not near the wing root or tip. These propulsors have a diameter of D_p and are aligned in spanwise direction with a gap of $\delta_y D_p$. A lateral clearance of $\delta_y/2$ is supposed at each end of the array, and the propulsors are positioned at an angle α_p relative to the freestream velocity vector. For a certain quantity of propulsors and fraction of wingspan occupied by the DP array ($\Delta y/b$), the diameter of the propulsors can be calculated as

$$D_p = \frac{b \cdot (\Delta y/b)}{N(1 + \delta_y)} \quad (3.15)$$

where N and $(\Delta y/b)$ are selected as design variables, while the diameter of the propulsors is selected as dependent variable.

Relating the wing span b to wing aspect ratio \mathcal{R} , i.e., $b = \sqrt{\mathcal{R} \cdot S}$, Eq. 3.15 can be rewritten and normalized as follows:

$$\frac{D_p^2}{W} = \frac{(\Delta y/b)^2}{N^2(1 + \delta_y)^2} \frac{\mathcal{R}}{(W/S)} \quad (3.16)$$

where it is possible to determine the propulsor-disk area needed per unit of aircraft weight W as a function of geometrical parameters and the wing loading (W/S). When designing a DP system,

it is important to check whether the diameter of the propulsors are feasible or not. If a large number of propulsors is selected for a small span interval and the aircraft required thrust is too high, the thrust to be produced by the propulsors may not be feasible.

To move forward and to estimate the values of ΔC_L and ΔC_{D_i} , it is proposed the method addressed by Patterson, Daskilewicz and German (2015). This method represents the propellers as actuator disks and the wing as a flat plate, incorporating a semi-empirical correction for finite slipstream height. The model includes several assumptions:

- The velocity increases as the actuator disk is computed assuming uniform axial inflow;
- Variations in lift due to swirl are neglected (actuator disk assumption);
- The flow over the wing is attached;
- The airfoil is symmetric, and thus zero lift is produced at $\alpha = 0$;
- The effect of each propeller on the adjacent ones is neglected;
- The effect of the propellers on the wing is limited to the spanwise interval occupied by the disks ($\Delta y/b$);
- Within this spanwise interval, the effect on the wing is considered uniform in spanwise direction (which is more accurate if $\delta_y \ll 1$);
- The wing is supposed to be fully immersed in the slipstream, i.e., half of the slipstream flows under the wing and half over the wing.

Since there are too many simplifications, the method may not be very accurate, what requires further analysis, especially because the stall behavior of the wing is not taken into account in cases of high-lift conditions or at high propeller incidence angles. However, due to the simplicity of the method, it becomes very useful for the conceptual design phase.

After calculating the propeller disk area per unit weight (D_p^2/W - disk loading), the next step is to calculate the axial induction factor at the propeller disk (a_p) as a function of the thrust-to-weight ratio of a single propeller ($T_p/W = \chi(T/W)/N$) and the disk loading, where $\chi = T_{dp}/T$ is uniquely related shaft power ratio (φ) according to:

$$\chi = \begin{cases} \frac{1}{1 + \frac{\eta_{p2}}{\eta_{p1}} \left(\frac{\varphi}{1 - \varphi} \right)}, & \text{if the DP system belongs to the primary branch} \\ \frac{1}{1 + \frac{\eta_{p1}}{\eta_{p2}} \left(\frac{1 - \varphi}{\varphi} \right)}, & \text{if the DP system belongs to the secondary branch} \end{cases} \quad (3.17)$$

Thus, using actuator disk theory (VELDHUIS, 2005):

$$a_p = \frac{\Delta V_p}{V} = \frac{1}{2} \left(\sqrt{1 + \frac{8}{\pi \rho V^2} \frac{(T_p/W)}{D_p^2/W}} - 1 \right) \quad (3.18)$$

where ΔV_p is the velocity increase by the propeller disk.

Next, it is necessary to evaluate the velocity induced by the propulsors at the quarter-chord location. Then, it is expressed the axial position of the propeller as a fraction of its radius:

$$\frac{x'_p}{R_p} = \frac{(x_p/c) + 1/4}{(R_p/c)} \quad (3.19)$$

where the ratio between the propeller radius and the wing chord R_p/c can be calculated using:

$$\frac{R_p}{c} = \frac{1}{2} \sqrt{\left(\frac{D_p^2}{W}\right) \left(\frac{W}{S}\right) \mathcal{R}} \quad (3.20)$$

Hence, it is possible to calculate the contraction ratio of the slipstream at the wing ($R_{c/4}/R_p$) using:

$$\frac{R_{c/4}}{R_p} = \sqrt{\frac{1 + a_p}{1 + a_p \left(1 + \frac{x'_p/R_p}{\sqrt{(x'_p/R_p)^2 + 1}}\right)}} \quad (3.21)$$

Finally, from conservation of mass in incompressible flow, it follows that:

$$a_{c/4} = \frac{1 + a_p}{(R_{c/4}/R_p)^2} - 1 \quad (3.22)$$

Therefore, it is possible to determine the velocity increase due to the thrust generated by the propellers at wing quarter chord. Using the derivation of Patterson, Daskilewicz and German (2015), the sectional lift coefficient increase can be calculated as:

$$\Delta c_l = 2\pi \left[(\sin \alpha - a_{c/4} \beta \sin i_p) \sqrt{(a_{c/4} \beta)^2 + 2a_{c/4} \beta \cos(\alpha + i_p) + 1} - \sin \alpha \right] \quad (3.23)$$

where α is the geometric angle of attack of the wing, i_p is the angle between the propeller axis and the wing chord (i.e., $i_p = \alpha_p - \alpha$), and β is a finite-slipstream correction factor.

The angle of attack of the wing is unknown, so it has to be estimated using the three-dimensional lift coefficient, as approximated by Roskam (1985):

$$\alpha \approx \frac{C_{L_{\text{airframe}}}}{2\pi \mathcal{R}} \left[2 + \sqrt{\mathcal{R}^2 (1 - M^2) \left(1 + \frac{\tan^2 \Lambda_{c/2}}{1 - M^2}\right) + 4} \right] \quad (3.24)$$

where M is the freestream Mach number, $\Lambda_{c/2}$ is the wing half-chord sweep angle.

The value of β is no trivial. So it is used an approach proposed by Patterson (2016), who describes a surrogate model based on CFD simulations of an actuator disk in front of a two-dimensional wing with a modified NACA 0012 airfoil.

Therefore, having the lift coefficient increase from Eq. 3.23, it is possible to calculate the change in drag coefficient, which is split into two components:

$$\Delta c_d = \Delta c_{d_0} + \Delta c_{d_i} \quad (3.25)$$

where Δc_{d_0} is the increase in friction drag on the wing surface due to increased dynamic pressure in the slipstream, which is calculated as:

$$\Delta c_{d_0} = a_{c/4}^2 c_f \quad (3.26)$$

where c_f is the sectional skin friction coefficient, for which a value of 0.009 is assumed (BIBER, 2011). On the other hand, the Δc_{d_i} term is the change in lift-induced drag of the wing due to the propeller-induced lift. The authors Patterson and Borer (2017) usually include this term in the drag polar by modifying the Oswald factor; however, it is not easy to get an accurate estimation of the Oswald factor for a generic aspect ratio, so this term is approximated as (BIBER, 2011):

$$\Delta c_{d_i} = \frac{2C_{L_{\text{airframe}}}\Delta c_l}{\pi R} \quad (3.27)$$

The lift and drag coefficients calculated so far are two-dimensional coefficients and represent an average value for the DP system. So, assuming the effect of the propellers on the wing is limited to the spanwise interval they occupy, the three-dimensional coefficients can be related to the corresponding average sectional coefficients as:

$$\Delta C_L = \Delta c_l \left(\frac{\Delta y}{b} \right) \quad (3.28)$$

$$\Delta C_{D_0} = \Delta c_{d_0} \left(\frac{\Delta y}{b} \right) \quad (3.29)$$

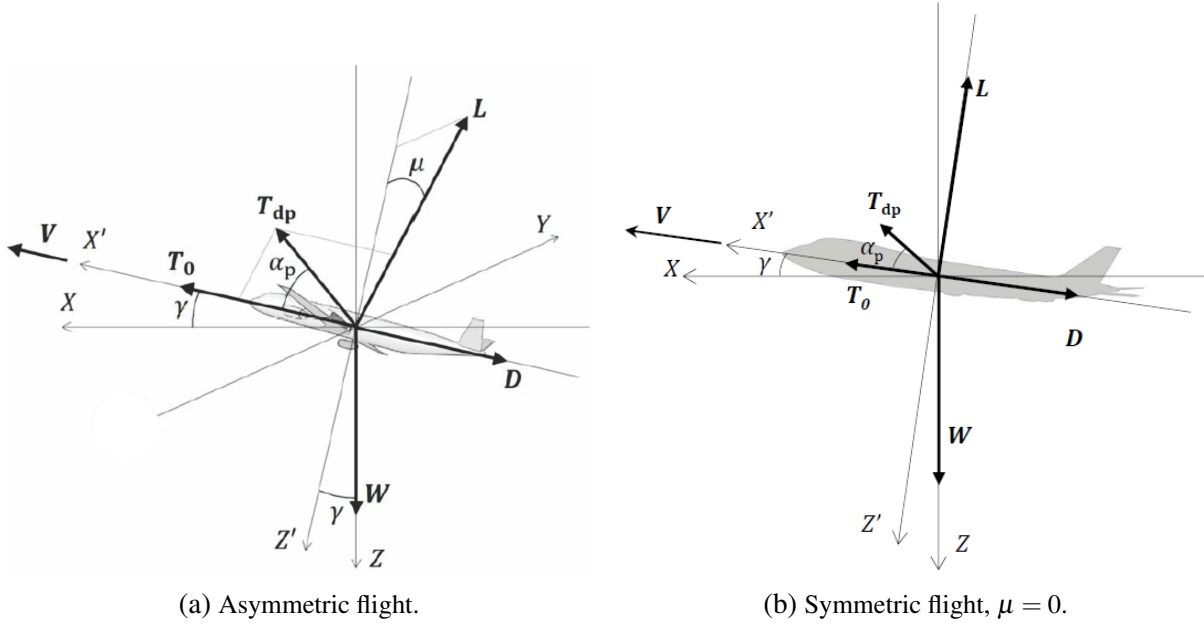
$$\Delta C_{D_i} = \Delta c_{d_i} \left(\frac{\Delta y}{b} \right) \quad (3.30)$$

Finally, since the effect of the wing on propeller performance is relatively small, especially when compared to other wing-mounted distributed-propulsion layouts, such as over-the-wing propellers (MARCUS *et al.*, 2018), the effect of the wing on the propellers is neglected, and thus $\Delta \eta_{dp} = 0$, even though it is actually non-zero (VELDHUIS, 2005).

3.2.3.3 Derivation of Performance Constraint Equations

The main forces acting on an aircraft in flight are shown in the free-body diagram in Fig. 23, where W is the weight of the aircraft, V the velocity vector, γ the flight path angle, and μ the

Figure 23 – Simplified DP-system representation, indicating the main geometrical parameters.



Source: Vries, Brown and Vos (2018).

bank angle. For conventional aircraft, there is only the thrust component aligned to the velocity vector (T_0); however, here there is an additional component (T_{dp}), which is produced by the DP system.

Applying Newton's second law along the X' , Y' and Z' axes, it is possible to write the following equilibrium equations, respectively:

$$T_0 + T_{dp} \cos \alpha_p - W \sin \gamma - D = \frac{W}{g} \frac{dV_{X'}}{dt} \quad (3.31)$$

$$L \sin \mu + T_{dp} \sin \alpha_p \sin \mu = \frac{W}{g} \frac{dV_{Y'}}{dt} \quad (3.32)$$

$$L \cos \mu + T_{dp} \sin \alpha_p \cos \mu - W \cos \gamma = \frac{W}{g} \frac{dV_{Z'}}{dt} \quad (3.33)$$

where g is the gravitational acceleration and $dV_{X'}/dt$, $dV_{Y'}/dt$, $dV_{Z'}/dt$ are the acceleration of the aircraft along the X' , Y' and Z' axes, respectively. In this work, the acceleration in Z' axis is assumed to be zero ($dV_{Z'}/dt = 0$) for all maneuvers. $dV_{Y'}/dt$ represents the centrifugal acceleration, which can be calculated as:

$$\frac{dV_{Y'}}{dt} = \frac{V^2}{R_{\text{turn}}} \quad (3.34)$$

where R_{turn} is the local turn radius of the aircraft trajectory. The flight path angle of the aircraft (γ) can be related to the rate of climb ($\dot{h} = dh/dt$, where h is altitude of the aircraft) as:

$$\sin \gamma = \frac{\dot{h}}{V} \quad (3.35)$$

Recovering that $\chi = T_{dp}/T$, it is possible to rewrite Eq. 3.31 as:

$$\frac{T}{W} = \frac{1}{1 - \chi(1 - \cos \alpha_p)} \left(\frac{D}{W} + \frac{\dot{h}}{V} + \frac{1}{g} \frac{dV}{dt} \right) \quad (3.36)$$

where T/W is called as the total thrust-to-weight ratio of the aircraft. Using Eqs. 3.10 and 3.14, it is possible to expand the drag component (D) in Eq. 3.36 in order to express the contributions as non-dimensional coefficients, that is:

$$\frac{T}{W} = \frac{\frac{q_\infty}{(W/S)} \left(C_{D_0} + \Delta C_{D_0} + \frac{C_{L_{airframe}}^2}{\pi e AR} + \Delta C_{D_i} \right) + \frac{\dot{h}}{V} + \frac{1}{g} \frac{dV}{dt}}{1 - \chi(1 - \cos \alpha_p)} \quad (3.37)$$

Since ΔC_{D_0} and ΔC_{D_i} are functions of T/W , Eq. 3.37 becomes a transcendental equation in function of T/W , W/S and $C_{L_{airframe}}$. Thus, it is necessary to couple Eq. 3.37 to another equation of W/S , which comes from the equilibrium equation along the Z' (Eq. 3.33). Thus, inserting Eq. 3.12 in Eq. 3.33 and reorganizing terms, it gets:

$$\frac{W}{S} = \frac{q_\infty \cos \mu (C_{L_{airframe}} + \Delta C_L)}{\sqrt{1 - \left(\frac{\dot{h}}{V} \right)^2} - \chi \sin \alpha_p \cos \mu \left(\frac{T}{W} \right)} \quad (3.38)$$

which is a transcendental equation as well.

Therefore, solving Eqs. 3.37 and 3.38 together, it is possible to establish a combination of T/W and W/S which guarantees equilibrium flight for a given velocity and airframe lift coefficient. One can propose to solve both equations analytically; however, the expressions of the ‘‘Deltas’’, as presented in previous sections, are complicated, what means that these equations have to be solved iteratively.

As described by Vries, Brown and Vos (2018), performance requirements for turn maneuvers can be expressed in terms of bank angle, turn radius, turn rate, or load factor. If the required bank angle is specified, then Eqs. 3.37 and 3.38 can be solved as explained previously. However, if the turn radius R_{turn} is given as a requirement, the bank angle has to be calculated using the equilibrium equation along the Y axis. Reorganizing and substituting the terms in Eq. 3.33, it gets:

$$\sin \mu = \frac{\frac{1}{g} \frac{V^2}{R_{turn}}}{\frac{q_\infty}{W/S} (C_{L_{airframe}} + \Delta C_L) + \chi \sin \alpha_p \left(\frac{T}{W} \right)} \quad (3.39)$$

On the other hand, if the turn rate ω is specified, then it can be related to the turn radius through $V = \omega R_{turn}$. Finally, if the load factor n is specified as a requirement, then it can be related to the turn radius using $n = \sqrt{1 + (V^2/gR_{turn})^2}$.

3.2.3.4 Constructing the Performance Constraint Diagram

The performance constraint diagram is a well-known method used for many book authors, such as Torenbeek (2013) and Roskam (1985), to represent different performance constraints of the aircraft and the resulting feasible design space in terms of wing loading and thrust-to-weight ratio (or power-loading). The main advantage of this diagram is that it can be used to calculate the required wing area and powerplant that is able to meet all performance requirements of the design.

Usually, the two axes represent parameters such as (y-axis) thrust-to-weight ratio (T/W) and (x-axis) wing loading (W/S). However, for HEDP aircraft, the use of power-loading (W/P) on the y-axis is better for some reasons. First, there are propellers installed, so power loading is more suitable for the case. Secondly, the power produced by the propulsive elements is required to size the components of the powertrain, and not thrust. Finally, when selecting the optimum design, it is convenient to select the powertrain that has to produce the least amount of power (which is directly related to energy consumption), not thrust.

Traditionally, among all the T/W and W/S combinations that allow meeting the mission performance, the designer should choose the design point that yield the aircraft with the lowest cost and weight. Therefore, the optimal design point is chosen for:

1. the *highest possible wing loading*, i.e., smallest wing, and
2. the *lowest possible thrust-to-weight ratio* or *highest possible power loading*, i.e., smallest engine.

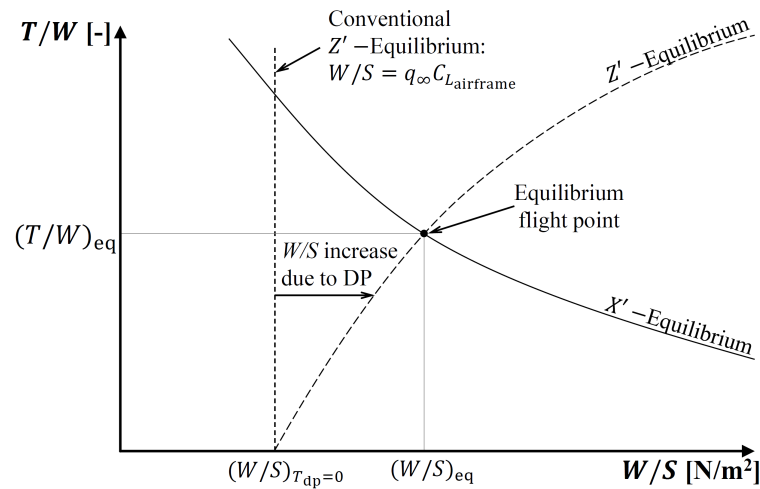
To switch a thrust-to-weight ratio (T/W) curve into a power loading (W/P) curve, the following relation can be used:

$$\frac{W}{P} = \frac{1}{V(T/W)} \quad (3.40)$$

For a given flight condition, i.e., for a certain velocity and lift coefficient, Eqs. 3.37 and 3.38 generate the curves shown in Fig. 24. The intersection of these curves gives the equilibrium flight point, that is, the combination of T/W and W/S where the required flight condition is satisfied with no additional accelerations. This point of intersection can be obtained iteratively solving both Eqs. 3.37 and 3.38 together. If the aero-propulsive interactions effects were neglected, the curve generated by Eq. 3.38 becomes a straight line: $W/S = q_{\infty} C_{L_{\text{airframe}}}$. Thus, the potential benefit of distributed propulsion can clearly be identified in Fig. 24; in other words, for a given airframe lift coefficient, the wing loading of the aircraft can be increased, and an aircraft with a higher wing loading has a smaller wing area relative to its mass, as compared to an aircraft with a lower wing loading.

As mentioned above, for a given flight condition (i.e., velocity and lift coefficient), the solution of Eqs. 3.37 and 3.38 provides a single *point* in the constraint diagram. In order to

Figure 24 – Wing-loading versus thrust-to-weight-ratio diagram indicating the curves obtained from the equilibrium of forces along the X' axis (Eq. 3.37) and Z' axis (Eq. 3.38) for a given velocity and airframe lift coefficient.

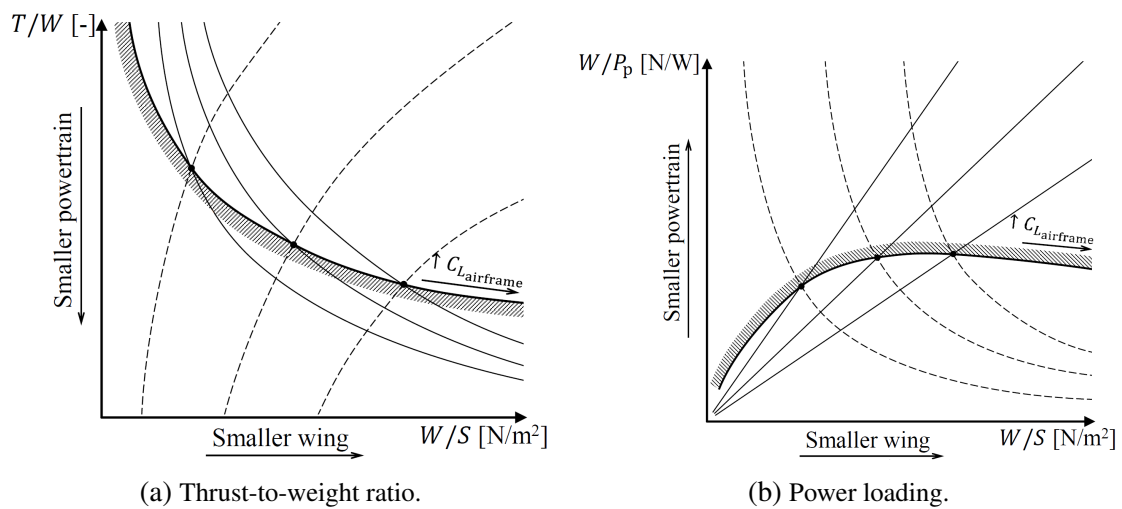


Source: Vries, Brown and Vos (2018).

obtain performance constraint *curves*, it is necessary to vary the velocity and/or the airframe lift coefficient parametrically. Thus, four types of performance constraint can be discussed:

- *Constraints at constant flight speed*: this represents the cruise phase, where for a given and constant flight speed, as the assumed lift coefficient increases, a smaller wing (i.e., higher wing loading) is required to generate the same total lift, which is illustrated in Fig 25.

Figure 25 – Wing-loading versus thrust-to-weight-ratio diagram (a) and wing-loading power-loading diagram (b), indicating the constraint curve obtained by evaluating the equilibrium flight points for different airframe lift-coefficient values at constant flight speed.



Source: Vries, Brown and Vos (2018).

- *Constraints at constant airframe lift coefficient*: it occurs during climb phase, where a stall margin has to be maintained. For example, if a climb gradient requirement must be met at

1.4 times the reference stall speed V_{SR}^1 , then the aircraft must be able to fly at $C_{L_{max}}/1.4^2$, where $C_{L_{max}}$ is the total maximum lift coefficient (including aero-propulsive effects²).

- *Constraints at fixed flight speed and airframe lift coefficient:* it is applied for approach phase, where due to stall constraint, the aircraft must be able to achieve a determined speed at $C_{L_{max}}$. Since both parameters are fixed (velocity and C_L), a single point in the diagram is obtained. In order to make clear the visualization, a straight and vertical line is plotted in the diagram at the wing loading corresponding to the point obtained. This line indicates a wing loading that cannot be exceeded under any circumstances.
- *Semi-empirical constraints:* it occurs during takeoff and landing, where Eqs. 3.31, 3.32 and 3.33 are not representative, since there are external forces (from runway surface) that act on the aircraft, which is varying its acceleration. Thus, some semi-empirical methods (TORENBEEK, 2013; RAYMER, 1999) are used to determine the takeoff distance and landing distance constraints. The methods combine four parameters (W/S , W/P or T/W , $C_{L_{max}}$ and σ), which are actually the most influencing for the takeoff distance (S_{TO}). Hence, they are put together in the so-called Takeoff Parameter (TOP):

$$TOP_{jet} = \left(\frac{W}{S}\right)_{TO} \left(\frac{W}{T}\right)_{TO} \frac{1}{C_{L_{TO}}} \frac{1}{\sigma} \quad (3.41)$$

$$TOP_{prop} = \left(\frac{W}{S}\right)_{TO} \left(\frac{W}{P}\right)_{TO} \frac{1}{C_{L_{TO}}} \frac{1}{\sigma} \quad (3.42)$$

From Fig. 26 it is possible to enter with a takeoff distance (S_{TO}) and obtain the parameter TOP.

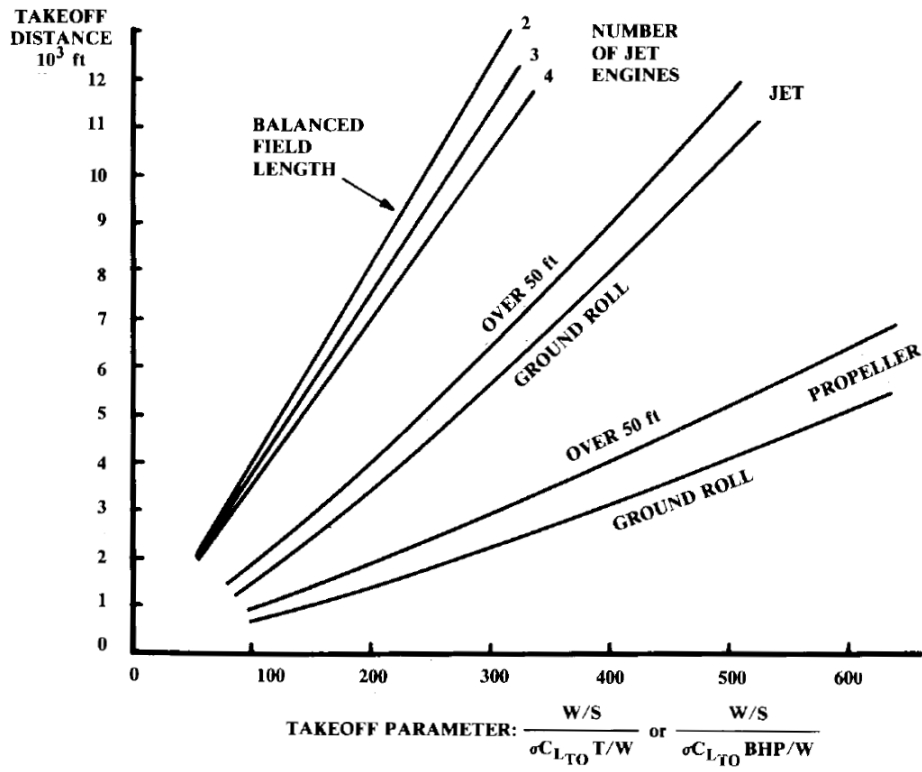
Lastly, the curves can be plotted on a constraint diagram and, finally, obtaining the *feasible design space*, a region under the curves where all performance constraints are satisfied for any of the W/P and W/S combinations.

As already discussed, for fuel-based aircraft, the goal is to identify the combination of maximum wing loading and minimum thrust loading (maximum power loading for propeller aircraft) that allow meeting all the given performance requirements, for certain assumptions on \mathcal{R} and $C_{L_{max}}$. Here, for HEDP aircraft, picking a design point depends on the figure of merit that the designer wants to minimize, as discussed in Chapter 4.

¹ The reference stall speed V_{SR} is defined in 14 CFR §1.2 and 14 CFR §25.103.

² The future airworthiness regulations might change such that the performance requirements can be met in powered conditions, instead of in engine-idle conditions. Some benefits of DP systems cannot be achieved with the current regulations, so they are being debated (PATTERSON; BORER, 2017)

Figure 26 – Takeoff distance estimation.



Source: Raymer (1999).

ASSESSMENT OF ELECTRIFICATION ON CONCEPTUAL AIRCRAFT DESIGN

In the following chapter, the method presented in Chapter 3 is validated with the paper of reference. A thin-haul aircraft proposal is selected to be the example of method application. Constraint diagrams are plotted and discussed, highlighting the aero-propulsive interactions due to the distributed propulsive system installed. Furthermore, it is evaluated how the optimum design point affects the final aircraft design.

4.1 Top-Level Requirements and Assumptions

In Chapter 3 it was presented a method to calculate the thrust, lift and drag changes due to aero-propulsive interactions of distributed propulsion systems, what has led to a set of modified constraint equations. These equations are collected in a power loading vs. wing loading diagram in order to provide a visual representation of the design space. Thus, to validate the method, the following example will be compared to the one evaluated by Vries, Brown and Vos (2018).

Therefore, first of all, it is necessary to come up with the top-level requirements of the project. So, consider a regional transport aircraft comparable to the ATR 72-600, with a range of 825 nmi and a payload of 73.6 kN. The aircraft flies at a cruise altitude of 18000 ft and Mach number of 0.41, and the approach speed must be no greater than 115 knots. In addition, the aircraft must be able to keep a climb gradient of 2.1% at 1.4 times the reference stall speed V_{SR} with one engine inoperative (OEI) (CS25, 2012). Moreover, the aircraft must be able to takeoff with a field length of less than 1333 m. All of these requirements are summarized in Table 5.

To get started, it is necessary to list some important design parameters selected to meet those requirements, which includes aspect ratio, half-chord sweep, taper ratio, and so on. Even more important is to choose the type of powertrain architecture to be used. For the validation,

Table 5 – Top-level aircraft requirements.

Parameter	Value
Payload, W_{PL} [kN]	73.6
Cruise altitude, h_{cr} [ft]	18000
Cruise Mach number, M_{cr} [-]	0.41
Range, R [nmi]	825
Approach speed, V_{app} [knots]	115
OEI climb gradient, h/V [%]	2.1
OEI climb speed, V_{climb} [knots]	$1.4V_{SR}$

only the conventional configuration (Fig. 19a) will be evaluated. Thus, for this configuration, a series of parameters has to be assumed with respect to the aircraft technology. So, the design and technology parameters used are gathered in Table 6.

Table 6 – Design and technology parameters assumed.

Parameter	Value
Aspect ratio, A [-]	12
Half-chord sweep, $\Lambda_{c/2}$ [deg]	0
Taper ratio, [-]	0.62
Root thickness-to-chord ratio, [-]	0.18
N^o of primary propulsors, N_1 [-]	2
Gearbox efficiency, η_{GB} [-]	0.96
Gas turbine efficiency, η_{GT} [-]	0.3

For each phase of a generic mission, the aerodynamic parameters depend on the aircraft configuration (i.e., clean, takeoff, or landing). Thus, some aerodynamic properties are assumed and shown in Table 7, for each constraint.

Table 7 – Aerodynamic properties assumed.

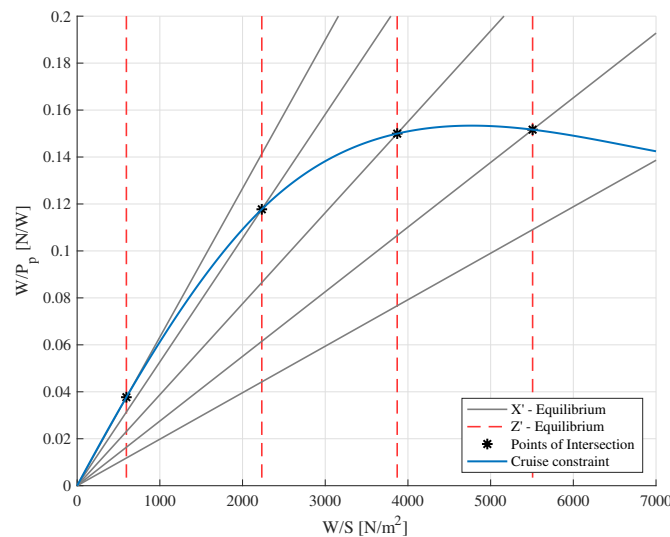
Parameter	Cruise	Approach	Takeoff	OEI climb
Flap configuration	clean	landing	takeoff	landing
Landing gear position	retracted	extended	extended	retracted
Zero-lift drag coefficient, C_{D_0}	0.02	0.085	0.035	0.65
Oswald factor, e	0.85	1.00	0.95	1.00
Maximum lift coefficient, $C_{L_{max,airframe}}$	-	2.8	2.2	2.8
Propulsive efficiency (primary), η_{p1}	0.9	0.8	0.75	0.8

4.2 Validation of the Constraint Diagram

Solving Eqs. 3.37 and 3.38, and evaluating the constraint at constant flight speed, i.e., the cruise performance constrain discussed in section 3.2.3.4, it is possible to find the first curve of the constraint diagram of the aircraft, as shown in Fig. 27. Unlike in Fig. 25b, the

Z' -Equilibrium curves are straight lines here because the conventional powertrain architecture does not have DP system, which means that there is no aero-propulsive interactions that “bend” the curves. Furthermore, the lift coefficient was varied while keeping constant the cruise speed, what generated a series of curves. Finally, finding the points of intersection of X' -Equilibrium and Z' -Equilibrium equations, it is possible to plot the constraint curve (in blue), which in this case is the cruise constraint. This curve represents the total power loading (W/P_p) for the aircraft related to this cruise constraint, where the feasible design space is below the green curve. If one wants to break it down and find the power loading for a specific component, just take the system of equations 3.6 and solve for the component of interest.

Figure 27 – Cruise constraint construction.

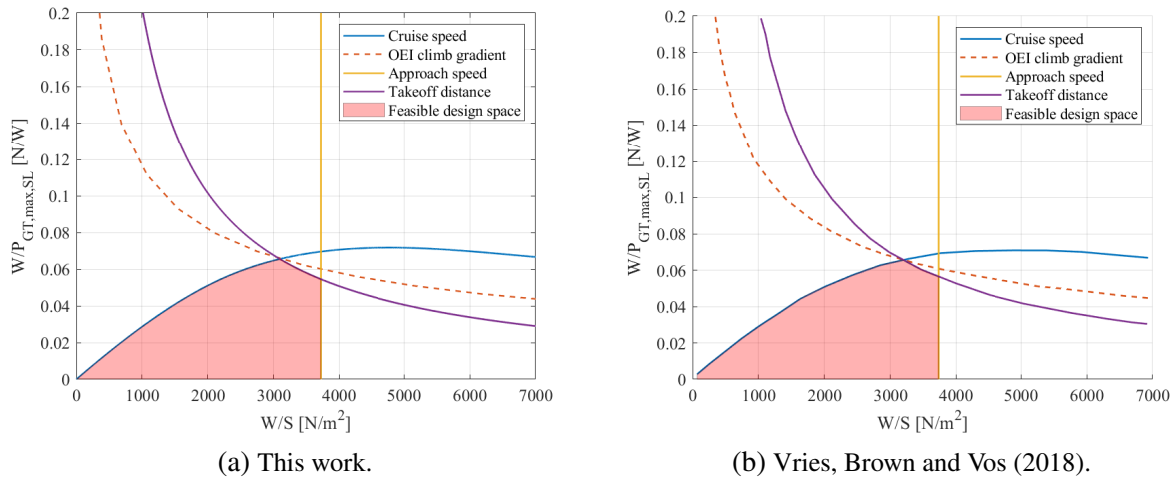


Source: Elaborated by the author.

Then, moving forward, and evaluating the other three types of performance constraints discussed in section 3.2.3.4, it is possible to find the final constraint diagram of the conventional aircraft. Since the paper of Vries, Brown and Vos (2018) has only the power loading diagram for the gas turbine, here it is done the same. So, making the breaking down of the total power loading using the efficiencies, it is possible to find the constraint diagram for the gas turbine component, as shown in Fig. 28.

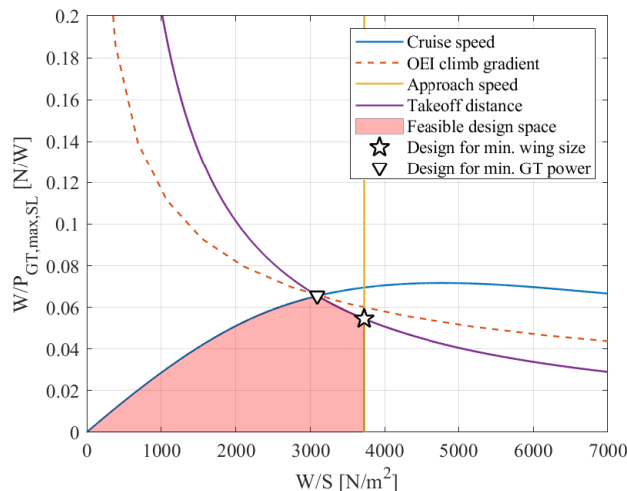
Therefore, Fig. 28 shows that the current work is able to compute the constraint diagram accordingly, when compared to the paper of reference (VRIES; BROWN; VOS, 2018). Furthermore, the next step is to choose the optimum design point. As discussed in previous sections, traditionally, the optimal design point is chosen for the highest possible wing loading and the highest possible power loading. In other words, if the designer is looking for the smallest wing, he or she has to pick the rightmost point within the feasible design space; however, if the designer is looking for the smallest engine, he or she has to pick the the the highest point of the curve within the feasible design space. These two options (or points) are highlighted in Fig. 29.

Figure 28 – Gas turbine power loading diagrams for aircraft with conventional powertrain architecture.



Source: Elaborated by the author.

Figure 29 – Optimum design points and feasible design space in constraint diagram.



Source: Elaborated by the author.

Having the validation confirmed, the following section presents how this methodology can be applied in an example of a type of aircraft that has been largely discussed currently: thin haul aircraft.

4.3 Application Example

Thin haul transportation refers to the air transportation of passengers on very small capacity aircraft over ultra-short distances (JUSTIN *et al.*, 2017). This type of operation has received attention in the last debates on aircraft electrification, as these hybrid and electric aircraft can make this type of transport feasible again.

Air transportation from small and medium airports is severely restricted by harsh eco-

conomic realities. In the deregulated market, carriers choose to provide service only if and when operations are sufficiently profitable (BHATTACHARYYA; PRITCHETT; GERMAN, 2017). But even with the Essential Air Service (EAS) program¹, it is not economically feasible for established airlines operating large aircraft to serve the majority of the thousands of airports (and potential routes) in the United States. Many of the routes that can support service by airlines can only do so at very low frequency, diminishing the value to passengers. Many carriers have found a solution in using smaller airports either with higher-frequency scheduled flights with smaller aircraft or by offering an on-demand air taxi service. Despite the higher per-seat-mile cost of operating smaller aircraft, demand has been shown to increase on routes once a reasonable frequency and availability can be achieved.

From this context, the AIAA launched as a proposal of the Design Competition² of 2018-2019 the design of a domestic transport aircraft for these thin haul scheduled or on-demand operations servicing small airports and short routes. So, this aircraft will be used as reference for the first example of application of the method presented previously. The requirements and constraints of the aircraft are summarized in Table 8.

Table 8 – Requirements and constraints of the thin haul aircraft.

Parameter	Value
Number of passengers	4-6
Payload, W_{PL} [lbs]	800
Range, R [nmi]	250

Since the proposed aircraft is in the market of the Piper PA-46 and Cirrus SR22, other requirements were assumed, as shown in Table 9.

Table 9 – Requirements and constraints of the thin haul aircraft.

Parameter	Value
Cruise altitude, h_{cr} [ft]	17500
Cruise Mach number, M_{cr} [-]	0.3
Approach speed, V_{app} [KCAS]	110
OEI climb gradient, \dot{h}/V [%]	2.1
OEI climb speed, V_{climb} [knots]	$1.4V_{SR}$
Takeoff field length, S_{TO}	2375

For this aircraft, two powertrain architectures will be evaluated: a conventional and a serial with a distributed propulsion system, similar to Fig. 20a. The respective selected design parameters are shown in Table 10, and the aerodynamic assumptions in Table 11.

¹ Essential Air Service (EAS) is a program of the U.S. government whose purpose is to guarantee that small communities that were served by certificated air carriers before airline deregulation in 1978 maintain a minimal level of scheduled air service. Thus, maintaining a minimal level of scheduled air service to these communities that otherwise would not be profitable

² Available at: <www.aiaa.org/designcompetitions>

Table 10 – Selected design parameters for the thin haul aircraft.

Parameter	Value
Aspect Ratio, \mathcal{AR} [-]	10
Half-chord sweep, $\Lambda_{c/2}$ [deg]	0
N ^o of primary propulsors, N_1 [-]	2
N ^o of secondary propulsors*, N_2 [-]	8
DP span fraction*, $\Delta y_{dp}/b$ [-]	0.6
Spacing between DP propulsors*, δ_y [-]	0.01
Axial position of DP propulsors*, x_p/c [-]	-0.2
EM efficiency*, η_{EM1} or η_{EM2} [-]	0.96
PMAD efficiency*, η_{PM} [-]	0.99
Gearbox efficiency, η_{GB} [-]	0.96
Gas turbine efficiency, η_{GT} [-]	0.3

* Asterisks indicate parameters which are only applicable to the hybrid-electric concept.

Table 11 – Aerodynamic assumptions for the thin haul aircraft.

Parameter	Cruise	Approach	Takeoff	OEI climb
Flap configuration	clean	landing	takeoff	landing
Landing gear position	retracted	extended	extended	retracted
Zero-lift drag coefficient, C_{D_0}	0.021	0.106	0.055	0.65
Oswald factor, e	0.78	0.88	0.81	0.88
Maximum lift coefficient, $C_{L_{\max,airframe}}$	-	2.5	2.0	2.5
Propulsive efficiency (primary)*, η_{p1}	0.9	0.8	0.75	0.8
Propulsive efficiency (secondary)*, η_{p2}	0.85	0.75	0.7	0.75
Supplied power ratio*, Φ	0.05	0.2	0.1	0.2

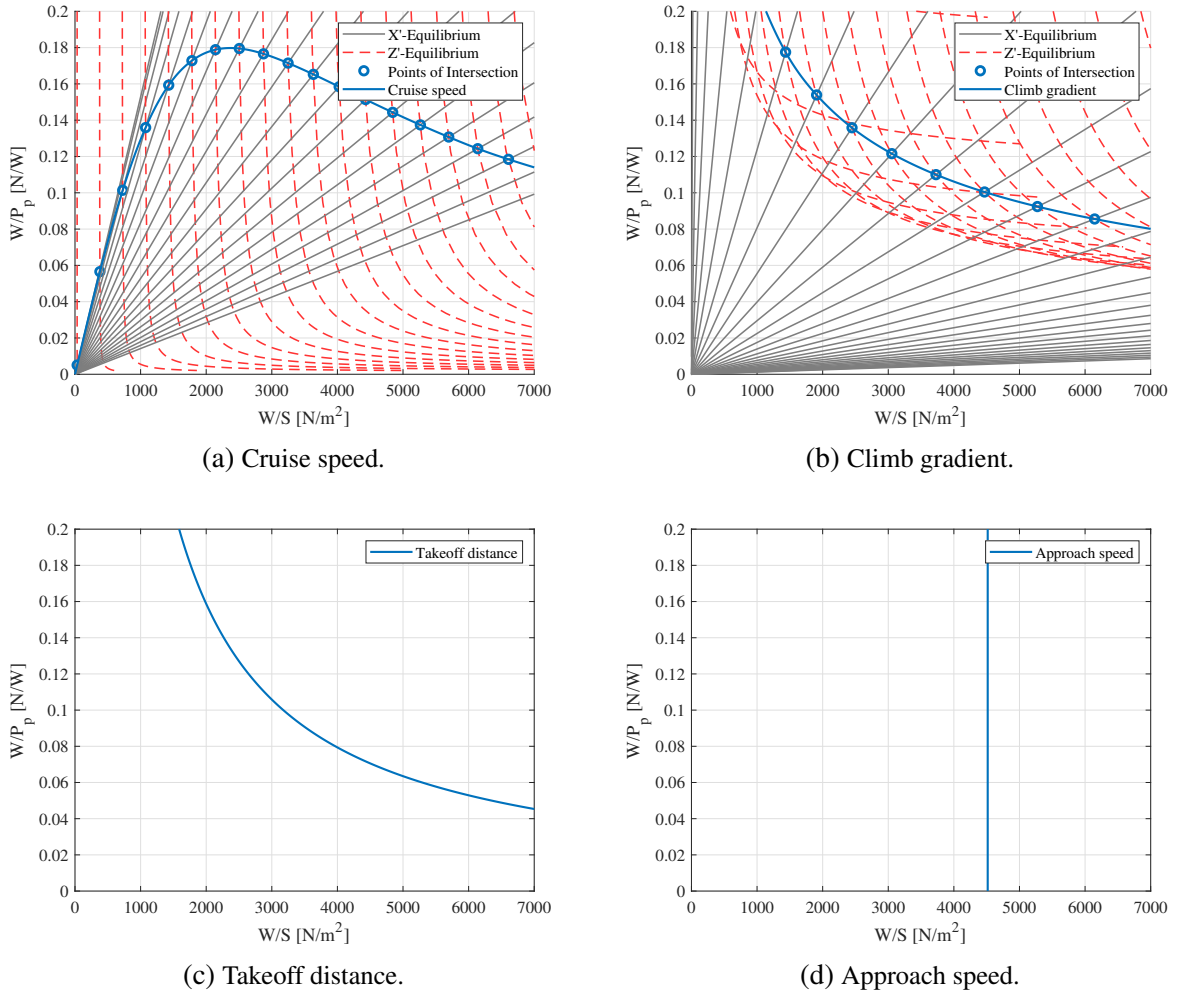
* Asterisks indicate parameters which are only applicable to the hybrid-electric concept.

Then, solving Eqs. 3.37 and 3.38, it is evaluated the four types of performance constraints, as discussed previously. The four constraint curves for the serial configuration are shown in Fig. 30.

Combining the four constraint curve from Fig. 30, and doing the same process for the conventional configuration, it is possible to plot the total power-loading diagrams for both powertrain architectures, which are shown in Fig. 31. Comparing both diagrams, one can notice that the feasible design space is bigger for the serial architecture. This happens because for the serial configuration there is a distributed propulsion system installed, which produces aero-propulsive interactions, causing an increase of lift. Thus, the feasible design space provides better choices for the optimum design points, as will be discussed next.

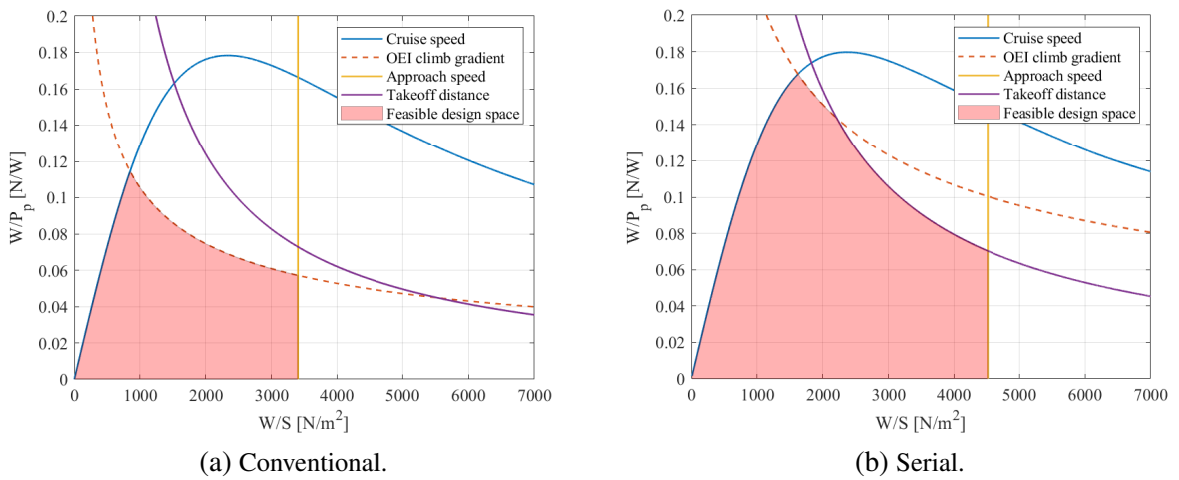
Making the breaking down of the power-loading in terms of the components, i.e., in terms of gas turbine, electric motors, and batteries, it is possible to plot the four power-loading diagrams depicted in Fig. 32. Comparing the $W/P_{GT,\max,SL}$ for the conventional architecture (Fig. 32a) with the $W/P_{GT,\max,SL}$ for the serial architecture, one can see that the feasible design

Figure 30 – Construction of the four constraint curves for the serial configuration.



Source: Elaborated by the author.

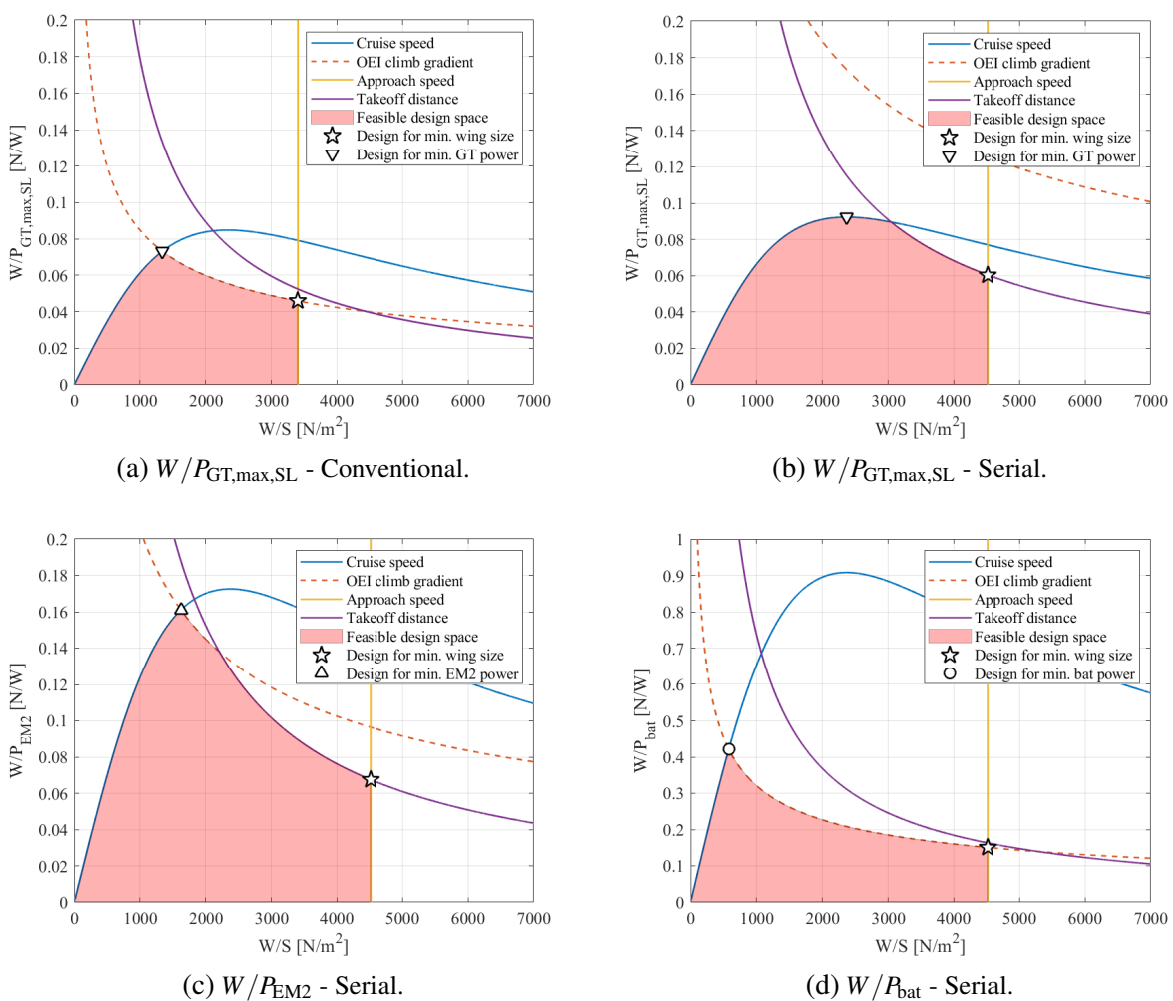
Figure 31 – Total power loading diagrams for aircraft with conventional and serial powertrain architecture.



Source: Elaborated by the author.

space increased for the serial configuration. Nonetheless, when comparing, for example, the cruise speed curve (in blue) for both configurations, the curve shows higher values for the serial architecture. This happens because in the hybrid-electric configuration, there is a battery participating of the cruise phase, which means that less power is required from the gas turbine. Since any change in power is inversely proportional in the ratio W/P , the curve increases. The same behavior can be observed for the other curves, but with different proportions due to the equation involved.

Figure 32 – Component power-loading diagrams for the thin-haul aircraft with conventional and serial powertrain architecture.



Source: Elaborated by the author.

Regarding the approach speed curve, it is worth noting that the line moves forward, increasing considerably the design space, which directly affects the choice of the optimum design point. This happens because the distributed propulsive system installed generates aeropropulsive interactions which produces a “Delta” C_L . Since the approach speed constraint is straightforwardly related to lift coefficient, the increment in C_L results in an improvement of that requirement. Following the same reasoning, the climb and takeoff constraint curves increase due

to this aerodynamic gain.

Still in Figs. 32a and 32b, the choice of the optimum design point, as discussed previously, depends on what the designer is looking for. In other words, in this case, if he or she wants a smaller wing, the point marked with a “star” has to be chosen. On the other hand, if he or she wants to design for minimum gas turbine power, the point marked with an upside-down triangle has to be chosen. In addition, it is interesting to see that in Fig. 32a the climb is the one responsible to limit the design of the gas turbine point, while in Fig. 32b the climb curve is far from the feasible design space. Moreover, the “star” point will always be the most up and right point.

Moving forward, and repeating the same analysis for the other components, i.e., for the electric motor and battery, two other optimum design points are shown in Figs. 32c and 32d, where the regular triangle represents the choice of design for minimum electric motor power, and the regular circle represents for minimum battery power. Finally, it is important to say that most people would select the design point for maximum wing loading, which usually corresponds to the smallest wing size. However, this is not always the best option. Due to the large impact of the powertrain on MTOW, it may be more beneficial to select one of the other design points, or even a different combination of wing loading and power loading that minimizes MTOW or another figure of merit. This can lead to increased component power-loading, and therefore reduced powertrain weight – assuming that the reduction in powertrain mass is not outweighed by the increase in wing mass.

Therefore, the diagrams are great forms of initial analysis for the conceptual design of an aircraft. However, although a parametric analysis has not been performed here, the constraint curves are very sensitive to the parameters assumed (aerodynamic and technological), which makes this stage of the study extremely important. In addition, as the choice of design point influences the aircraft as a whole, if the goal is to enable an airline operation, such as thin-haul, the reduction of fuel consumption is very important, so an optimization study of energy consumed on a generic mission should be performed. This is what will be presented in the next chapter.

ENERGY SIZING APPROACH AND OPERATIONAL ANALYSES

In the following chapter, it is presented the concept of typical mission and its phases. A methodology is proposed for aircraft dimensioning based on the required powers and energies spent in each phase of the mission. Also, it is sized the weight of powertrain (engines and electric motors), batteries and fuel, and a mission optimization is performed to evaluate the optimum degrees-of-hybridization in each flight phase, where the objective functions are to minimize fuel consumption and minimize the maximum takeoff weight.

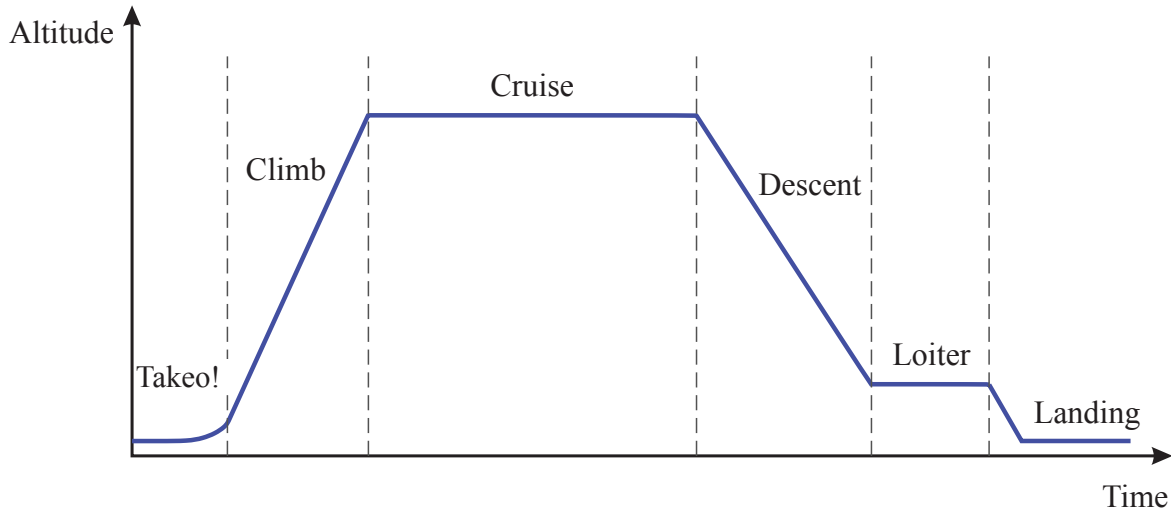
5.1 Typical Mission of an Aircraft

In the design of any aircraft, it is extremely important to know the requirements and specifications of the project, since they are responsible for determining the direction and details of the project. Therefore, it is important to define:

- (i) *Purpose of the aircraft*: typical use of the aircraft;
- (ii) *Typical missions*: description of the typical mission of the aircraft, i.e., time and altitude of operation during a typical flight;
- (iii) *Target of performance*: maximum speed, maximum range, stall speed, and so on;
- (iv) *Desired features*: materials used, ease of construction, affordable maintenance;
- (v) *Requirements*: basis of certification adopted, aeronautical legislation requirements that must be fulfilled.

Thus, for this work, it is necessary to define a typical mission to study the design and performance analysis of the aircraft. To do so, consider the typical mission profile shown in Fig. 33, where each phase means:

Figure 33 – Typical mission profile.



Source: Elaborated by the author.

- *Takeoff*: this phase comprises the moment which the aircraft leaves the gate and accelerates until it reaches sufficient speed to leave the ground;
- *Climb*: the aircraft climbs from the altitude of the airport to the pre-established cruising altitude;
- *Cruise*: at this stage, the aircraft flies at a constant altitude and speed until it reaches the expected range;
- *Descent*: phase in which the aircraft ends the cruise regime and begins to descend to a certain altitude to prepare for landing;
- *Loiter*: the aircraft keep flying over for a certain amount of time at a certain altitude until it gets permission to land;
- *Landing*: moment when aircraft touches the ground and decelerates until reaching minimum speed, and finally, park at the airport.

After those definitions, it is presented a design procedure that is able to size and all-electric or hybrid-electric aircraft by evaluating the concept of energy per phase of flight.

5.2 Energy Sizing

One of the main advantages of the electrification of an aircraft is the reduction of fuel consumption. After all, this has a direct impact on airline profits, which are mainly responsible for orders and purchases of new aircraft, especially large ones. But at the same time, reducing fuel consumption enables other smaller aircraft operations, connected routes and smaller cities, which are not so profitable, such as the thin haul, as discussed earlier. In this context, the electrification of aircraft can make such ideas viable.

When it comes to fuel consumption, it is the same thing as energy expenditure. So, if it is possible to reduce energy consumption during a typical mission of an aircraft, it is also possible to reduce fuel consumption. Moreover, if other sources of energy are used, such as batteries, this fuel consumption can be further reduced. Therefore, the following method proposes an energy study per mission phase, i.e., the calculation of the energy consumption spent in each flight phase. This then allows the sizing of the fuel and/or battery weight that would be required for that mission. Part of the following formulation was extracted from Rossi (2018).

First of all, the takeoff weight of an aircraft can be divided as follows:

$$W_{TO} = W_{\text{empty}} + W_{\text{bat}} + W_{\text{fuel}} + W_{PT} + W_{PL} \quad (5.1)$$

where W_{empty} is the empty weight of the aircraft, W_{bat} the battery weight, W_{fuel} the fuel weight, W_{PT} the powertrain components weight, and W_{PL} the payload weight. To deal with the empty weight in an uniform way with conventional aircraft design techniques, batteries are considered as fuel at this level, thus empty weight corresponds to structure and systems together.

The empty weight W_{empty} can be estimated from takeoff weight (W_{TO}) using statistical regression proposed by Roskam (1985), as follows:

$$\log_{10} W_{TO} = A + B \log_{10} W_{\text{empty}} \quad (5.2)$$

where coefficients A and B are taken from Table 12.

Table 12 – Statistical regression values relating empty weight to takeoff weight.

Aircraft Type	A	B
Homebuilt	0.3411	0.9519
Single-engine propeller driven	-0.1440	1.1162
Twin-engine propeller driven	0.1063	1.0351
Agricultural	-0.4398	1.1946
Business Jet	0.2678	0.9979
Regional turboprop	0.3874	0.9647
Transport jet	0.0833	1.0383
Military bomber, transport, patrol	-0.2009	1.1037

Source: Roskam (1985).

The payload weight (W_{PL}) can be estimated by adding the weight of the crew (including pilot) without luggage (N_{crew}) and the weight of passengers with luggage (N_{pax}), as follows:

$$W_{PL} = (N_{crew} \cdot 78 + N_{pax} \cdot 102)g \quad (5.3)$$

As a first guess, the maximum takeoff weight can be initially considered as four times the payload weight ($MTOW = 4W_{PL}$), and the powertrain weight (W_{PT}) depends on the architecture chosen and, consequently, the number of components and electric motors (in case of DP system). Thus, having those weight estimated, it is important to estimate the aerodynamic data.

5.2.1 Aerodynamic Data Estimation

To get started, it is necessary to assume some parameters, such as the aspect ratio (\mathcal{R}), which can be chosen comparing other aircraft models, and the wing loading (W/S). The wing loading value depends on how the choice is made. It may come from the optimum design point from the constraint diagram presented in Chapter 4, or using the following expression:

$$\left(\frac{W}{S}\right) = \frac{\rho_0 V_{ST}^2}{2C_{L_{max}}} \quad (5.4)$$

where ρ_0 is air density, V_{ST} the minimum stall speed and $C_{L_{max}}$ the maximum lift coefficient with flaps-down. Then, having the takeoff weight and the wing loading, it is possible to compute the wing reference surface:

$$S = \frac{W_{TO}}{\left(\frac{W}{S}\right)} \quad (5.5)$$

and the wing span is obtained from aspect ratio \mathcal{R} (selected previously), as $b = \sqrt{\mathcal{R} \cdot S}$. Having the wing span, a reference chord can be calculated as $c_{ref} = S/b$, since at this stage step there is no geometric information.

To estimate the parasite drag coefficient, the method proposed by Roskam (1985) is used. The zero-lift drag coefficient C_{D_0} is related to parasite area f , and its value can be obtained by a statistical regression relating f and the wetted area S_{wet} , which is related to takeoff weight. The set of equations is:

$$C_{D_0} = \frac{f}{S} \quad (5.6)$$

$$\log_{10} f = a + b \log_{10} S_{wet} \quad (5.7)$$

$$\log_{10} S_{wet} = c + d \log_{10} W_{TO} \quad (5.8)$$

where a , b , c and d are regression values which depend on the type of aircraft. Combining the previous equations, and converting to S.I. units, the parasite drag coefficient becomes:

$$C_{D_0} = \frac{0.3048^2}{S} 10^{a+b[c+d \log_{10}(2.2W_{TO})]} \quad (5.9)$$

The parameters a and b are available in Table 13. To get their values, it is necessary to estimate the aircraft friction coefficient c_f from the Reynolds number (Re_c) evaluated at cruise speed and altitude, using the previous reference chord c_{ref} , as follows:

$$c_f = \frac{0.1488}{Re_c^{0.2}} \quad (5.10)$$

and the c and d values are available in Table 14. Furthermore, having the zero-lift drag coefficient estimated, the polar drag relations can be defined for clean and takeoff configurations, respectively:

$$C_D = C_{D_0} + \frac{C_L^2}{\pi e AR} \quad (5.11)$$

$$C_{D_{TO}} = C_{D_0} + \Delta C_{D_{gear}} + C_{D_{flap}} + \frac{C_L^2}{\pi e_{TO} AR} \quad (5.12)$$

Table 13 – Correlation coefficients for parasite area.

c_f	0.0090	0.0080	0.0070	0.0060	0.0050	0.0040	0.0030	0.0020
a	-2.0458	-2.0969	-2.1549	-2.2218	-2.3010	-2.3979	-2.5229	-2.6990
b	1.0000	1.0000	1.0000	1.0000	1.0000	1.0000	1.0000	1.0000

Source: Roskam (1985).

Table 14 – Statistical regression values relating wetted surface to takeoff weight.

Aircraft Type	c	d
Homebuilt	1.2362	0.4319
Single-engine propeller driven	1.0892	0.5147
Twin-engine propeller driven	0.8635	0.5632
Agricultural	1.0447	0.5326
Business Jet	0.2263	0.6977
Regional turboprop	-0.0866	0.7699
Transport jet	0.0199	0.7531
Military bomber, transport, patrol	0.1628	0.7316

Source: Roskam (1985).

Finally, having the aerodynamic data estimation, it is possible to characterize the mission phases in terms of performance.

5.2.2 Performance Estimation

In order to estimate the energy expended in each flight phase of the mission, it is necessary to estimate the power required and the elapsed time in each phase. Then, by relating both values, it is possible to calculate the energy ($\Delta E = P \cdot \Delta t$).

5.2.2.1 Takeoff

The takeoff phase is split into two parts: ground run and airborne. In both cases, the power required values are unknown due to the acceleration over time, but they can be obtained by solving implicit equations related to the distance traveled. The total takeoff run is divided by (ROSKAM, 1985) as:

$$L_{TO} = L_{GR} + L_{AB} \quad (5.13)$$

where it is considered $L_{TO} = 1.66L_{GR}$. Thus, to calculate the required power during ground run (P_{GR}), it is necessary to find a value of P that satisfies:

$$L_{GR} = \int_0^{V_{TO}} \frac{M_{TO}V}{\frac{P}{V_{TO}} - \frac{1}{2}\rho_{TO}V^2SC_{D_{TO}} - \mu(W_{TO} - \frac{1}{2}\rho_{TO}V^2SC_{L_{TO}})} dV \quad (5.14)$$

where the take-off speed must be greater than the stall speed.

The airborne is considered to be performed as an arc characterized by a radius R and a climb angle γ , as follows:

$$L_{AB} = R \sin \gamma \quad (5.15)$$

$$h_{AB} = R(1 - \cos \gamma) \quad (5.16)$$

where h_{AB} is the obstacle height, which has a value of 35 ft for Part-25 certified aircraft and 50 ft for Part-23. The climb angle γ is used to obtain the required power, as follows:

$$P_{AB} = \frac{1}{2}\rho_{TO}V_{TO}^3SC_{D_{TO}} + W_{TO}V_{TO} \sin \gamma \quad (5.17)$$

Then, the takeoff power P_{TO} is maximum value between P_{GR} and P_{AB} :

$$P_{TO} = \max [P_{GR}, P_{AB}] \quad (5.18)$$

and the takeoff time can be simply estimated considering the whole distance at takeoff speed:

$$\Delta t_{TO} = \frac{L_{TO}}{V_{TO}} \quad (5.19)$$

and, finally, the required energy for takeoff phase is obtained by multiplying the takeoff power with takeoff time:

$$E_{TO} = P_{TO} \cdot \Delta t_{TO} \quad (5.20)$$

5.2.2.2 Climb

The power required for the climb phase is obtained considering and average air density at midway altitude between takeoff and cruise, as follows:

$$P_{CL} = \frac{1}{2}\rho_{CL}V_{CL}^3SC_{D_{CL}} + V_{VCL}W_{CL} \quad (5.21)$$

where V_{VCL} is the vertical velocity (rate of climb). Moreover, the elapsed climb time is defined as the time that the aircraft takes to climb from the airport altitude (h_{airport}) to cruise altitude (h_{cruise}) at a certain rate of climb:

$$\Delta t_{CL} = \frac{h_{\text{cruise}} - h_{\text{airport}}}{V_{VCL}} \quad (5.22)$$

Finally, the required power energy during climb phase is computed as:

$$E_{CL} = P_{CL} \cdot \Delta t_{CL} \quad (5.23)$$

and the horizontal distance traveled during climb is then calculated using average climb speed:

$$R_{CL} = V_{CL} \Delta t_{CL} \quad (5.24)$$

5.2.2.3 Descent

Likewise the procedure performed for the climb phase, the required power for descent phase is calculated, as follows:

$$P_{DS} = \frac{1}{2} \rho_{DS} V_{DS}^3 S C_{D_{DS}} + V_{V_{DS}} W_{DS} \quad (5.25)$$

where $V_{V_{DS}}$ is the vertical speed, and it is negative since the aircraft is descending. The elapsed descent time is defined as the time that the aircraft takes to descent from the cruise altitude (h_{cruise}) to loiter altitude (h_{loiter}) at a certain rate of decent:

$$\Delta t_{DS} = \frac{h_{\text{loiter}} - h_{\text{cruise}}}{V_{V_{DS}}} \quad (5.26)$$

Finally, the required power energy during descent phase is computed as:

$$E_{DS} = P_{DS} \cdot \Delta t_{DS} \quad (5.27)$$

and the horizontal distance traveled during descent is then calculated using average descent speed:

$$R_{DS} = V_{DS} \Delta t_{CL} \quad (5.28)$$

5.2.2.4 Cruise

At the cruise phase, the required power is simply obtained as:

$$P_{CR} = \frac{1}{2} \rho_{CR} V_{CR}^3 S C_{D_{CR}} \quad (5.29)$$

The time needed to complete a cruise range depends on the cruise speed and the range expected:

$$\Delta t_{CR} = \frac{R_{CR}}{V_{CR}} \quad (5.30)$$

where the R_{CR} is the range remaining after deducting the horizontal distances traveled during climb and descent phase. Thus,

$$R_{CR} = R_{\text{total}} - R_{CL} - R_{DS} \quad (5.31)$$

Finally, the cruise energy spent during cruise phase is calculated, as follows:

$$E_{CR} = P_{CR} \cdot \Delta t_{CR} \quad (5.32)$$

5.2.2.5 Loiter

At the loiter phase, what is required is a certain amount of time that the aircraft has to fly while waiting. Eshelby (2000) shows that, for a propeller-driven aircraft, the best airspeed to reach the longest endurance is the airspeed of minimum required power (V_{mp}), which it is the same as saying that the best attitude is the one that maximizes the ratio $C_L^{1.5}/C_D$. This concept is also used for hybrid-electric aircraft, since the objective is minimize the energy spent during this phase. Thus, the speed of minimum required power is defined as:

$$V_{mp} = \frac{1}{\sqrt[4]{3}} V_{md} \quad (5.33)$$

where V_{md} is speed of minimum drag:

$$V_{md} = \sqrt{\frac{2W_{LT}}{\rho_{LT}S}} \sqrt{\frac{1}{\pi e AR C_{D0}}} \quad (5.34)$$

Additionally, the loiter speed cannot be lower than 1.2 times the stall speed ($1.2V_{stall}$). Then, the loiter speed is selected as:

$$V_{LT} = \max[V_{mp}, 1.2V_{stall}] \quad (5.35)$$

Then, the required power is

$$P_{LT} = \frac{1}{2} \rho_{LT} V_{LT}^3 S C_{D_{LT}} \quad (5.36)$$

and the energy spent during loiter phase is calculated, as follows:

$$E_{LT} = P_{LT} \cdot \Delta t_{LT} \quad (5.37)$$

where Δt_{LT} is the loiter time required.

5.2.3 Mission Evaluation

Having all of those required power and energy spent per mission phase, it is possible to size the gas turbine, the electric motors, and the batteries. The gas turbine and the electric motors are sized for the maximum required power that occurs in some phase of the flight. In other words, the motors need to be able to provide the required power of any stage, so if they are able to provide at the time of greatest need, the other phases offer no problem. Then, the maximum required power, and its phase, is thus calculated:

$$P_{\max} = \max[P_{TO}, P_{CL}, P_{CR}, P_{DS}, P_{LT}] \quad (5.38)$$

Additionally, the energy required to accomplish the mission is the sum of all the energies of each phase:

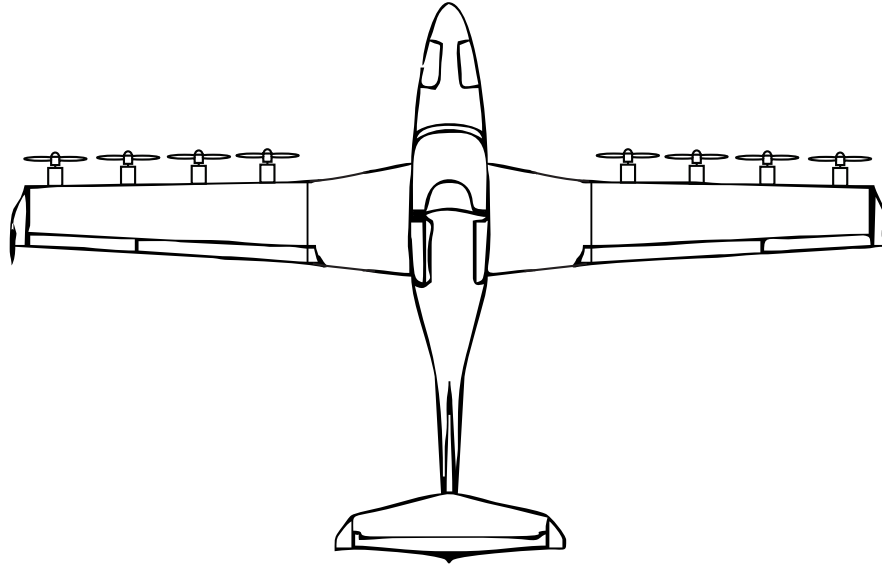
$$E_{\text{total}} = E_{TO} + E_{CL} + E_{CR} + E_{DS} + E_{LT} \quad (5.39)$$

But these energies can be rewritten in terms of the equivalent required power during a elapsed time for each phase:

$$E_{\text{total}} = P_{TO}\Delta t_{TO} + P_{CL}\Delta t_{CL} + P_{CR}\Delta t_{CR} + P_{DS}\Delta t_{DS} + P_{LT}\Delta t_{LT} \quad (5.40)$$

Now, for the following analysis, assume that the aircraft has N propulsors distributed along each semi-wing, as shown in Fig. 34. In addition, assume a powertrain architecture as the serial defined in Fig. 19. The degree-of-hybridization in terms of power used here is defined as:

Figure 34 – Sketch of aircraft with N propulsors distributed along each semi-wing.



Source: Elaborated by the author.

$$\psi = \frac{P_{bat}}{P_{bat} + P_{gt}} \quad (5.41)$$

and each phase has its own value for ψ . Then, using the serial powertrain, and solving for the gas turbine power with the respective efficiencies, it is possible to obtain the power that is supplied by the gas turbine in each flight phase, as follows:

$$P_{gt, \text{phase } i} = \left(\frac{1}{\eta_{pm}\eta_{em2}\eta_{p2}} \right) \left[\frac{1 - \psi_{\text{phase } i}}{\psi_{\text{phase } i} + \eta_{gb}\eta_{em1}(1 - \psi_{\text{phase } i})} \right] P_{\text{phase } i} \quad (5.42)$$

where $\psi_{\text{phase } i}$ and $P_{\text{phase } i}$ are the correspondent degree-of-hybridization and aircraft required power in each flight phase, respectively. Therefore, the gas turbine can be sized from the flight phase that it needs to provide the maximum power, because if it is able to provide such power at the moment it is most requested, it will be scaled for the other flight phases. Thus,

$$P_{gt, \text{max}} = \max[P_{gt, TO}, P_{gt, CL}, P_{gt, CR}, P_{gt, DS}, P_{gt, LT}] \quad (5.43)$$

However, this required power corresponds to the power at that phase altitude. Since the engine is affected by altitude, it is necessary to estimate the required power at sea-level ($P_{gt, SL} =$

$P_{gt,max}/\sigma_{\text{phase},P_{gt,max}}$). Thus, Having the required power at sea-level for the gas turbine, it is possible to estimate its weight using the regression relation defined by Roskam (ROSKAM, 1985):

$$W_{gt} = 0.1860 \cdot P_{gt,SL} \cdot g \quad (5.44)$$

where $P_{gt,SL}$ is expressed in kW.

To size the battery, it is necessary to know the degree-of-hybridization (ψ) used in each phase. Then, it is calculated the power split that comes from the battery in each phase as well. Finally, assuming a specific energy of the battery (e_{bat} [Wh/kg]), the battery weight is thus calculated:

$$W_{bat} = \frac{\sum_{i=1}^{\text{n of phases}} (P_{\text{bat,phase } i} \cdot \Delta t_{\text{phase } i})}{e_{bat}} \cdot g \quad (5.45)$$

where $P_{\text{bat,phase } i}$ is defined as:

$$P_{\text{bat,phase } i} = \left(\frac{1}{\eta_{pm}\eta_{em2}\eta_{p2}} \right) \left[\frac{\psi_{\text{phase } i}}{\psi_{\text{phase } i} + \eta_{gb}\eta_{em1}(1 - \psi_{\text{phase } i})} \right] P_{\text{phase } i} \quad (5.46)$$

Additionally, for safety and to maintain a good battery life, batteries are only discharged until reaching the state-of-charge minimum (SOC_{\min}) of 25%. Then, assuming the battery will only discharge 75% of its energy, the final weight battery is thus estimated:

$$W_{\text{bat,new}} = \frac{W_{\text{bat,old}}}{1 - SOC_{\min}} \quad (5.47)$$

Moreover, similarly to what was done to calculate the battery weight, and knowing the fuel specific energy (e_f) and the engine efficiency (η_{gt}), which usually is assumed to be 0.3, it is possible to estimate the power supplied in the form of fuel and, consequently, the fuel weight consumed. The set of equations is:

$$P_{\text{fuel,phase } i} = \left(\frac{1}{\eta_{gt}\eta_{pm}\eta_{em2}\eta_{p2}} \right) \left[\frac{1 - \psi_{\text{phase } i}}{\psi_{\text{phase } i} + \eta_{gb}\eta_{em1}(1 - \psi_{\text{phase } i})} \right] P_{\text{phase } i} \quad (5.48)$$

$$W_{\text{fuel}} = \frac{\sum_{i=1}^{\text{n of phases}} (P_{\text{fuel,phase } i} \cdot \Delta t_{\text{phase } i})}{e_f} \cdot g \quad (5.49)$$

Likewise the battery, a reserve (SOF) of 10% of fuel is usually kept for safety. Then, the fuel weight is updated:

$$W_{\text{fuel,new}} = \frac{W_{\text{fuel,old}}}{1 - SOF} \quad (5.50)$$

Furthermore, it is possible to estimate the weight of the electric motors. A suitable population of electric motors is reported in Table 15. Thus, considering a linear relationship resulting from the regression, it is obtained:

$$W_{em} = \left(1.9309 + 0.1933 \cdot \frac{P_{\text{max}}}{2N\eta_{p2}} \right) \cdot g \quad (5.51)$$

Table 15 – Electric motors examples.

Electric Motor	Aircraft	Power [kW]	Mass [kg]
Siemens SP260D	Extra 330LE	260	50
Emrax 348	N.Av.	170	40
N.Av.	Pipistrel Alpha Electro	85	14
N.Av.	Pipistrel Taurus Electro	40	11

where P_{max} is expressed in kW and N is the number of electric motors.

Finally, the powertrain weight here is only estimated with the weight of the engine and electric motors:

$$W_{PT} = W_{gt} + 2N \cdot W_{em} \quad (5.52)$$

The battery and fuel weights are not considered in the powertrain weight because they have explicit components in weight breakdown equation (Eq. 5.1). Since the previously considered empty weight estimation was based on a population of conventional aircraft, a correction must be provided, as follows:

$$W_{empty,new} = W_{empty,old} - W_{PT} \quad (5.53)$$

An example of how this methodology is applied is discussed next.

5.3 Example of Energy Sizing Optimization

The energy sizing method showed an approach where the aircraft is sized regarding the required power and energy. When the figure of merit is reduction of fuel consumption, the choice of some design parameter, such as number of propulsors and the degree-of-hybridization in each phase, is very important, changing the final design and, consequently, the fuel consumption. Thus, the following example will address a design optimization of a general aviation aircraft, where the objective functions are minimize the fuel consumption and minimize the maximum takeoff weight.

First of all, it is necessary to define the requirements of the project. The selected general aviation aircraft here is expected to carry four passengers, one pilot, and fulfill the other requirements listed in Table 16. Moreover, the aerodynamic and technological assumptions made are detailed in Table 17, and efficiencies assumed (i.e., electric motors, gearbox, and so on) are the same from Chapter 4.

Many parameters have been defined so far, but are still missing the definition of the number of propulsors installed in each semi-wing and the respective degrees-of-hybridization per flight phase. In this case, the total weight of propulsors does not change with the number of propulsors, because for a certain amount of required power, the weight of each propulsor will be calculated, but later the weights of all of them will be summed up, resulting in similar

Table 16 – Requirements for the general aviation aircraft of example.

Parameter	Value	Unit
Number of passengers	3	-
Number of pilots	1	-
Stall speed	60	KTAS
Cruise speed	160	KTAS
Climb/descent speed	105	KTAS
Climb rate	500	fpm
Descent rate	-350	fpm
Takeoff field length	325	m
Cruise altitude	8000	ft
Loiter altitude	1000	ft
Loiter time	45	min
Range	300	km

Table 17 – Assumptions for the general aviation aircraft of example.

Parameter	Value	Unit
Takeoff lift coefficient	1.6	-
Landing lift coefficient	2.0	-
Wing aspect ratio	10.5	-
Oswald efficiency (clean)	0.90	-
Oswald efficiency (takeoff)	0.85	-
Landing gear ΔC_{D_0}	0.02	-
Takeoff flaps ΔC_{D_0}	0.02	-
Propeller efficiency	0.85	-
Battery specific energy	500	Wh/kg
Fuel specific energy	12000	Wh/kg

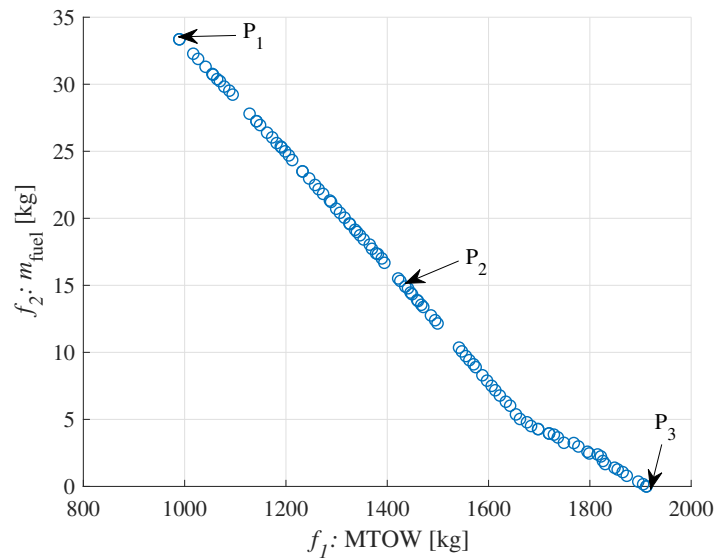
total weights, i.e., their weight only depends on the total required power. However, the degrees-of-hybridization can generate different combinations, which would result in different performances. Thus, they are chosen to be the design variables (x) of the optimization problem proposed here, which is characterized, as follows:

$$Multi\text{-objective optimization problem} : \begin{cases} \min(W_{fuel}) \quad \text{and} \quad \min(W_{TO}) \\ x : [\psi_{TO}, \psi_{CL}, \psi_{CR}, \psi_{DS}, \psi_{LT}] \\ 0 \leq \psi_{\text{phase}, i} \leq 1 \end{cases} \quad (5.54)$$

In the optimization, the maximum takeoff weight (W_{TO}) receives an initial value corresponding to four times the payload weight ($W_{TO_{\text{initial}}} = 4 \cdot W_{PL}$). The algorithm thus estimates the weight of batteries, fuel, powertrain, and empty-weight that would be necessary to accomplish the mission; however, the required powers calculated during this process were based on that initial maximum takeoff weight. So, the algorithm runs iteratively until the maximum takeoff weight converges to a final value.

Then, using the NSGA II ¹, it was possible to run the optimization. The algorithm was executed several times with a number of populations of 100, generations equal to 500, crossover index of 20 and mutation index of 20. These parameters were also changed, but all the results converged to the same. The solution, i.e., the Pareto-optimal front is available shown in Fig. 35.

Figure 35 – Pareto-front that represents the solution for the optimization problem.



Source: Elaborated by the author.

The result shows that to minimize the fuel consumption for this type of mission it is necessary to increase the amount of batteries onboard. However, as the weight of the batteries increases, the weight of the aircraft increases as a whole, and because the empty weight is dependent on the maximum takeoff weight, it also increases. Therefore, to reduce the fuel weight, the total weight of the aircraft is considerably increased.

Moreover, in Fig. 35 three points of the solution were selected: P_1 , P_2 , and P_3 . These points represent three different options for the aircraft design. P_1 is the condition where the aircraft has the highest fuel consumption, and it happens when all degrees-of-hybridization are equal to zero ($\psi_{\text{phase}, i} = 0$), i.e., in this case, the configuration represents a conventional aircraft. At the other end, P_3 is the condition where the aircraft consumes no fuel, i.e., it implies a full-electric configuration; therefore, the aircraft energy is only supplied by batteries, increasing the takeoff weight to the maximum. The other points between P_1 and P_3 have different combinations of degrees-of-hybridization. Therefore, the choice of the point within the Pareto-front depends on what the designer wants to benefit most. The details of the design for the three points selected are displayed in Table 18.

¹ The NSGA II (Non-dominated Sorting Genetic Algorithm II) is a multi-objective algorithm based on genetic algorithms and was proposed by Deb et al. (DEB *et al.*, 2000) as an evolution of the NSGA algorithm. It combines the current population with the previous population to preserve the best individuals. In addition, it is based on the concept of dominance, i.e., it classifies the total population in fronts (Pareto-optimal front) according to the degree of dominance.

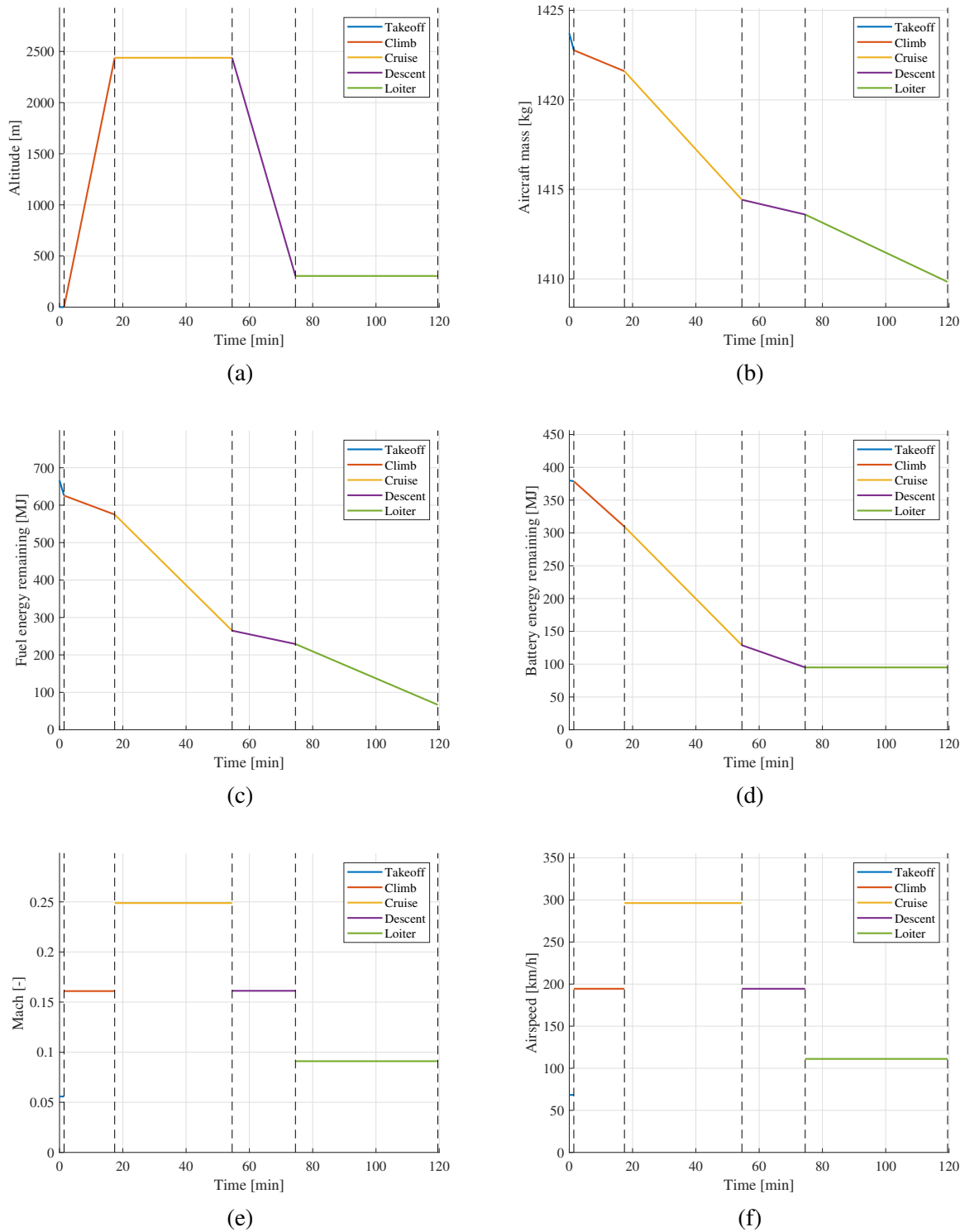
Table 18 – Results of the optimization.

Parameter	P_1	P_2	P_3
ψ_{TO}	0	0.10	1
ψ_{CL}	0	0.82	1
ψ_{CR}	0	0.66	1
ψ_{DS}	0	0.76	1
ψ_{LT}	0	0	1
m_{empty} [kg]	507.8	749.2	1037.3
m_{bat} [kg]	0	211.1	446.6
m_{fuel} [kg]	33.4	15.4	0
m_{PT} [kg]	64.3	63.9	43.6
m_{PL} [kg]	384	384	384
m_{TO} [kg]	989.5	1423.6	1911.5

Selecting the point P_2 as an example, it is possible to visualize how some parameters varied over time during the mission, as shown in Fig 36, where takeoff is in blue, climb in red, cruise in yellow, descent in purple, and loiter in green. The black dashed lines represent the start and end time of each phase. Figure 36a shows the altitude variation at each flight phase, and Fig. 36b depicts the aircraft mass reduction due to the fuel burn. Figs. 36c and 36d show how the energy storage (battery and fuel) is spent, which is totally related to the degree-of-hybridization selected. It is worth remembering that both the battery and the fuel finish the mission with the minimum of required reserve: 25% for the battery and 10% for the fuel. Also, Fig. 36e shows the respective Mach number, which is calculated using the mean velocity and speed of sound at each phase.

Still using point P_2 , it is possible to illustrate the power in each component of the powertrain, since the components' efficiencies and the degrees-of-hybridization are already known. So, the visual representation of the powertrain architecture for each mission phase is shown in Fig 37, and the total weight breakdown of the aircraft is illustrated in Fig. 38.

Furthermore, it is worth remembering that the specific energy of the battery is a very important parameter that affects directly the solution of the optimization problem. After all, having a "more energetic" battery, it is possible to fulfill the mission without increasing the maximum takeoff weight. Thus, to better visualize this effect, Fig. 39a presents how the solution changes as the specific energy of the battery is increased. For the case of $e_b = 1500$ Wh/kg, the $MTOW$ for full-electric aircraft is much smaller if compared to the other solutions. Also, the point for conventional configuration does not change, since there is no battery installation in conventional architecture. Moreover, if the specific energy of the battery is fixed in 500 Wh/kg, and the required total range of the mission were increased, the maximum takeoff weight would also increase considerably, as shown in Fig. 39b. Since the battery considered is not "very energetic", to carry 3 passengers and 1 pilot for a distance of 700 km, the aircraft would have an $MTOW$ of more than 4 tons, which is unfeasible. In addition, as the range increases, the point

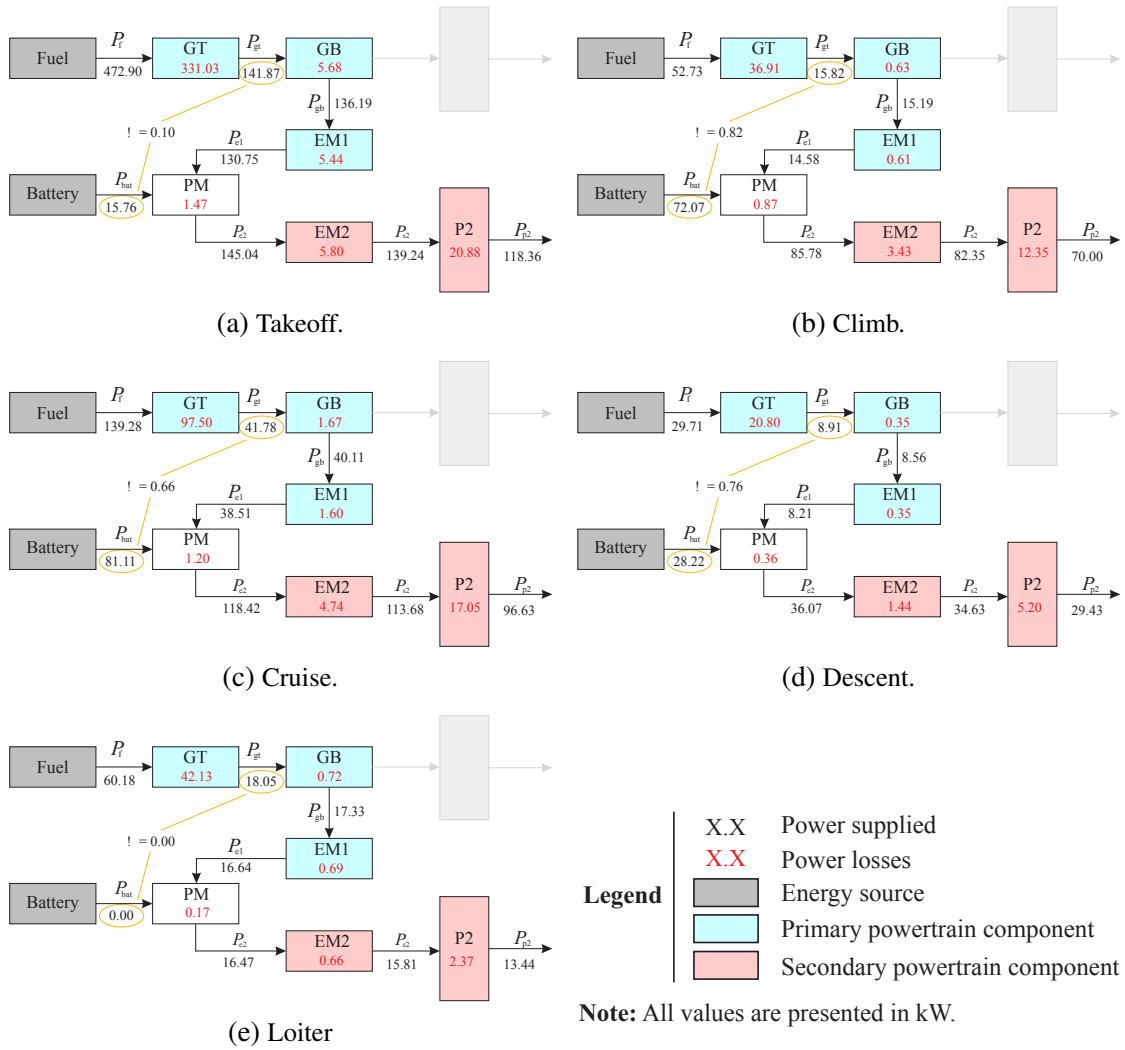
Figure 36 – Variation of some parameters during the mission for the selected point P_2 .

Source: Elaborated by the author.

for conventional configuration also increases, since more fuel is needed to fly such distances.

To better exemplify, it is performed the combination between those battery specific energies and required ranges. Fig. 40 shows how the conventional aircraft changes when the

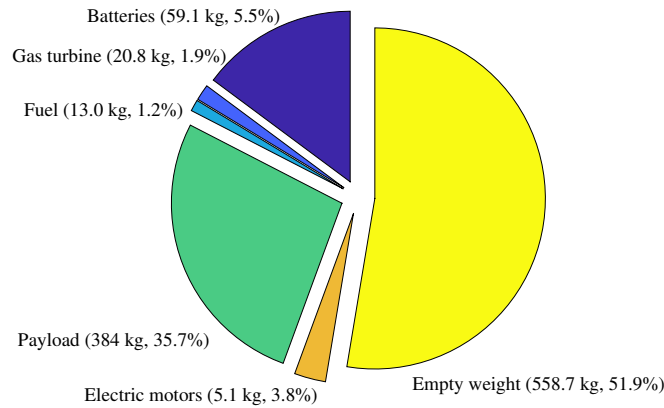
Figure 37 – Visual representation of the powertrain architecture for each mission phase.



Source: Elaborated by the author.

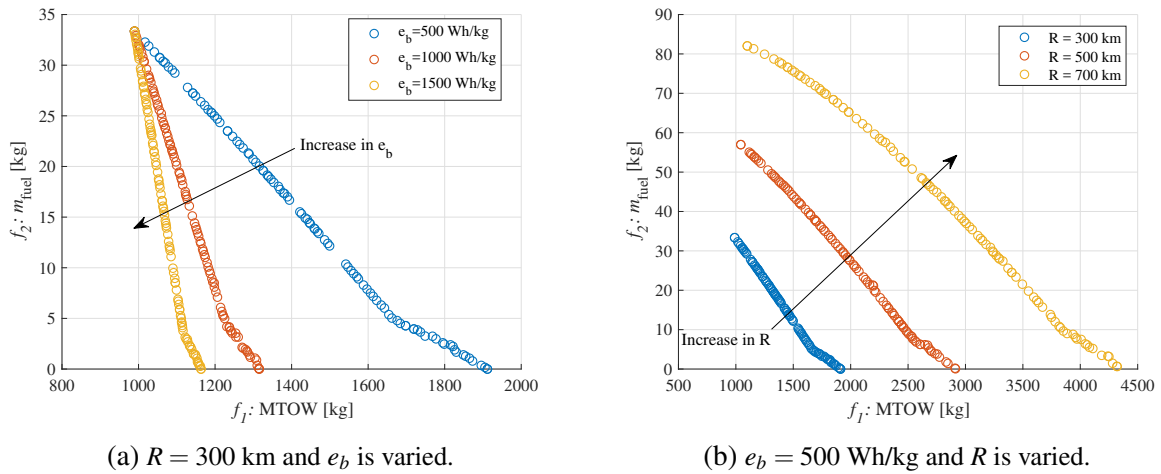
Figure 38 – Weight breakdown of the aircraft.

$$\psi_{to} = 0.10, \psi_{cl} = 0.82, \psi_{cr} = 0.66, \psi_{ds} = 0.76, \psi_{lt} = 0.00$$



Source: Elaborated by the author.

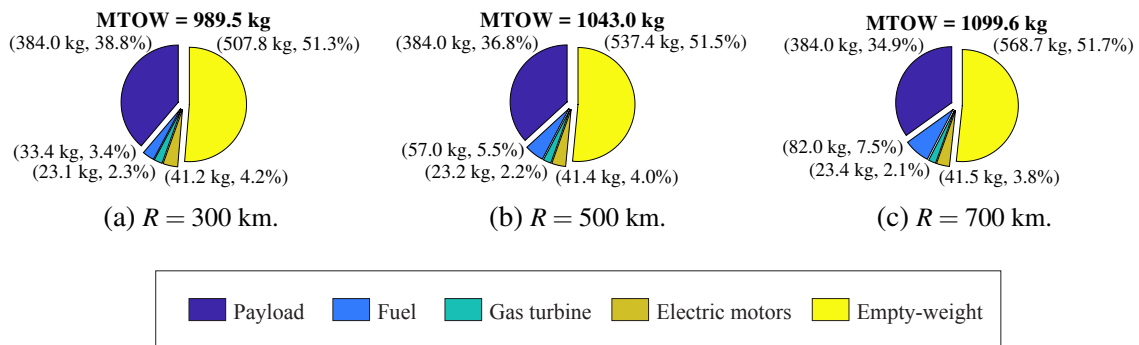
Figure 39 – Parametric analysis for the mission regarding e_b and R .



Source: Elaborated by the author.

range increases. In this case, more fuel is necessary, then the aircraft becomes heavier. Thus, the same analysis is done but for the full-electric architecture and the results are shown in Fig. 41.

Figure 40 – Weight breakdown for conventional configuration and different ranges.

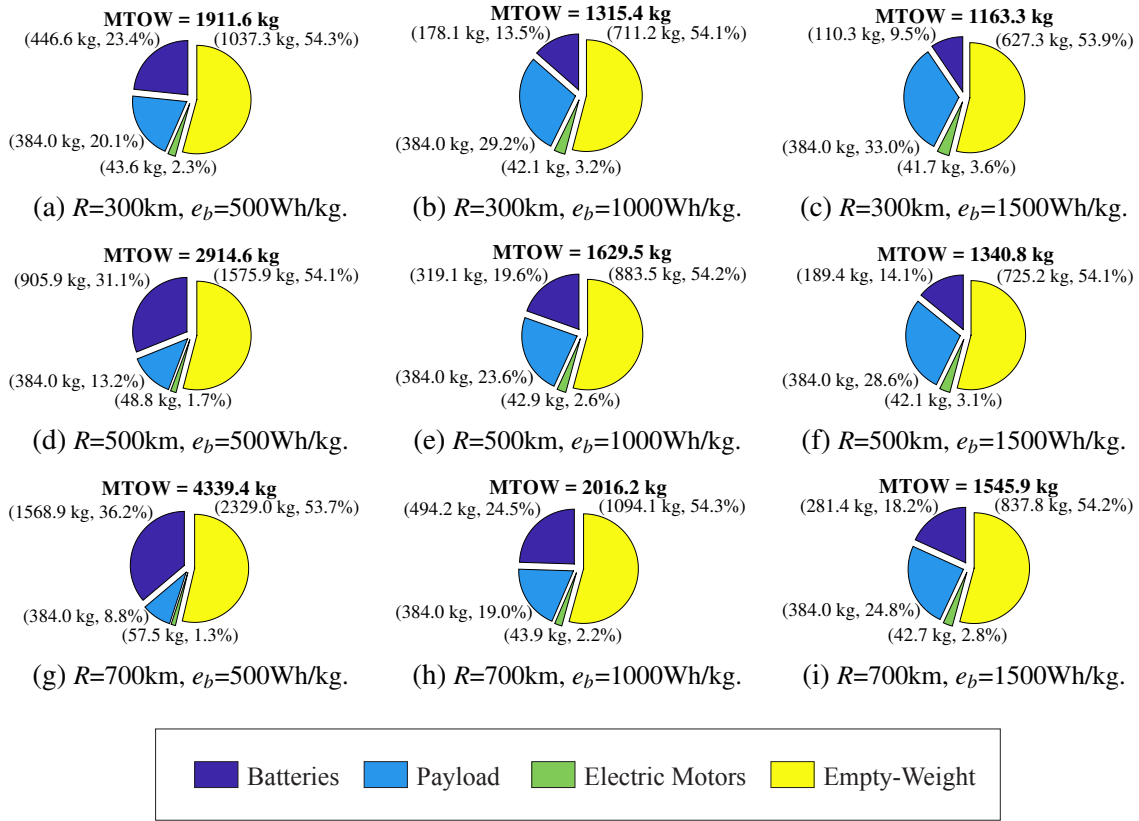


Source: Elaborated by the author.

It is interesting to note that for any range, as the specific energy of the battery increases, the battery weight decreases. Also, for any specific energy of the battery, when the range increases, more energy of the mission is required, which results in more battery installed; however, it is worth noting that for higher specific energies of the batteries, the maximum takeoff weight of the aircraft becomes feasible, no matter the range, i.e., the more energetic the batteries are, the closer it gets to the larger full-electric aircraft.

In summary, the mission profile is extremely important in this optimization problem. After all, the number of passengers, type of aircraft, total range, and loiter time are parameters that affect the overall required power and, consequently, the energy spent during the mission. In other words, in cases of intercontinental flights, where there is a great number of passengers and a long range to be traveled, the energy required for the entire mission would be huge, which would imply in tons of batteries. Therefore, the current battery technology is not suitable for

Figure 41 – Weight breakdown for full-electric configuration and different ranges and specific energy of the batteries.



Source: Elaborated by the author.

these type of mission, establishing the need for disruptive advances in technologies for the next years.

EFFECTS OF ELECTRIFICATION AND NEW CHALLENGES

This chapter presents some benefits enabled by electrification and contrasts them with the known risks. Furthermore, some effects produced by the electrification in aircraft design are discussed.

6.1 Direct Electrification Effects

Even with the technological advance and, consequently, the increase of the specific energy of batteries, the electrification brings with it the increase of weight due to the installation of several components associated to the hybrid-electric architecture chosen. However, a great and direct effect of electrification is the partial or total replacement of fuels.

As seen in Chapter 5, for short flights and smaller aircraft, the specific energies of the current batteries are already able to partially meet the requirements, generating good results. In this way, as this specific energy increases, it is possible to incorporate even more the electrification in the design of large aircraft, which require a large amount of energy per mission. Moreover, if electric energy gets cheaper than aviation fuel per unit of energy, then there will be a great reduction in operating costs, which is a big advantage of this type of technology. Depending on how this electricity is produced, i.e., if renewable electricity generation is assumed, there is a direct reduction of carbon emissions.

Full-electric aircraft still have the advantage of not dealing with issues related to engine thermal cycling. In this case, for having only batteries installed, if the aircraft use superconducting wires and new power electronics, the electrical efficiency can reach values close to 1. Additionally, in the case of turboelectric aircraft, there is the presence of gas turbines, which experience thermodynamic losses. However, if the aircraft has only batteries installed, and a ground engine is used to recharge them, that engine will be more efficient, since it is not dealing with altitude

effects.

In addition, it is possible to reduce maintenance cost by exchanging combustion engines and fossil fuels for electric motors and batteries, since this set of equipment would have fewer moving parts than its combustion counterpart. This would make aircraft operation more consistent and predictable.

6.2 Propulsion Effects

In conventional aircraft, the rotation of propellers and fans is mechanically coupled to turbine engines. In hybrid-electric architectures, it is possible to disconnect these components, since the electric motors are responsible for turning the propellers/fans. Thus, the turbine engines can operate in their optimal rotation of greater efficiency and lower consumption. Moreover, electric propulsion may enable higher bypass ratio (BPR) and decoupling the number of fans from the number of engines.

Boundary layer ingestion (BLI) is able to increase propulsive efficiency by ingesting slower air from the fuselage or wing boundary layer. The suction from the fan inlet changes the pressure distribution upstream, and fan outflow energizes the wake. Some authors still discuss whether the effect of BLI is considered to be a drag loss or an increase in η_p efficiency (GRAY *et al.*, 2017). The benefits caused by BLI are proportional to the percentage of boundary layer flow captured at the fan inlet (WELSTEAD; FELDER, 2016). Fig. 42 shows the Nova aircraft, a concept with BLI developed by Onera designers, and Fig. 43 shows a cutaway of the propulsive fuselage hybrid-electric concept made by Bauhaus Luftfahrt

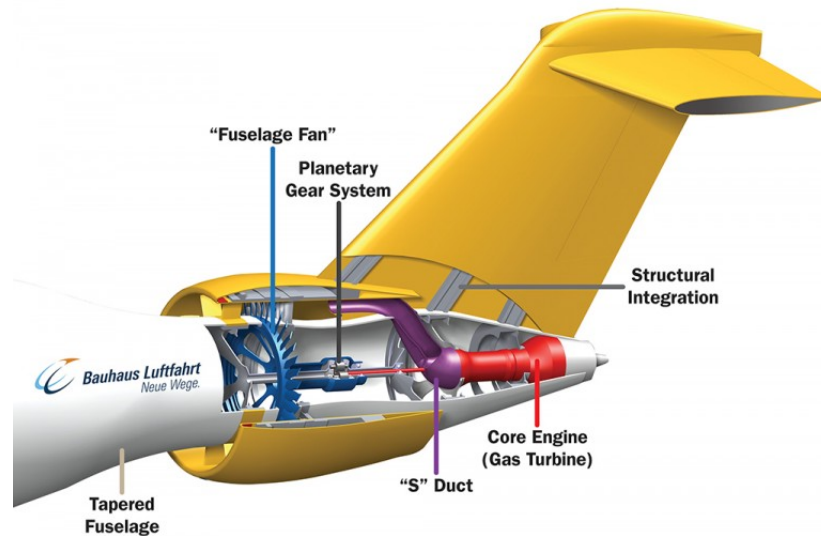
Figure 42 – Nova aircraft developed by Onera designers.



Source: AINonline (2015).

The BLI system is already possible using conventional engines, as presented in the MIT/Aurora D-8 concept by Yutko *et al.* (2017). Nonetheless, electric motors have great potentials to make boundary layer ingestion more feasible, since these electric motors can be scaled. Usually, combustion engines when scaled down in size, they lose in performance and

Figure 43 – Bauhaus Luftfahrt’s propulsive fuselage hybrid-electric concept.



Source: Michele (2016).

efficiency, while electric motors scale mostly linearly (MOORE, 2014). Moreover, when it comes to distributed propulsion, electric motors have smaller sizes, which enables their application at wing tip (see Fig. 14) and tailcone.

6.3 Aerodynamic Effects

Due to their versatility, the electric motors allow a range of possibilities in the definition and installation of the propulsive system, which generates new potential aerodynamic benefits. The distributed propulsive system may generate three of these aerodynamic benefits: installation drag reduction, large increase in lift, and swirl cancellation. Most benefits are still unproven and depend on the mission and configuration, but they are expected to reach a value of between 0 and 8% (JANSEN; DUFFY; BROWN, 2017).

Engine nacelles and pylons produce propulsion installation drag, i.e., friction, interference, and wave drag. Along with nacelle and fan weight, these propulsive aerodynamic drags become a constraint on turbofan bypass ratio. Wick, Hooker and Zeune (2015) showed a reduction of 8% in installation drag by using distributed propulsors along the wing on a transonic military transport concept.

The large increase in lift produced by distributed propulsion enables higher wing loading, which decreases wetted wing area, viscous drag, and cruise drag. Moreover, having a higher C_L , the constraints of approach speed and takeoff field length can be overcome with smaller wings. The NASA LEAPtech wing and X-57 demonstrator (see Fig. 14) have estimated that it is possible to reach an aerodynamic efficiency (L/D) of 20 and to achieve an increase in C_L from 1.7 to 2.4 (DEERE *et al.*, 2017); however, a loss of power can result in a sudden stall. The current aviation legislation says that transport-category aircraft cannot use these types of benefits to

meet certification requirements for stall (14 CFR 25.103) and approach speeds (14 CFR 25.125). However, there is nothing stated in commuter and general aviation aircraft regulations (Part 23).

Finally, wingtip propulsors have been proposed as an approach to cancel some swirl and wingtip vortices. Some studies have been performed in order to prove these aerodynamic effects. Examples include the study published by Miranda and Brennan (1986) that comprises experimentally-validated low-fidelity results and the thesis presented by Sinnige (2018) that presents aerodynamic and aeroacoustic interaction effects for tip-mounted propellers.

6.4 Sizing Effects

As discussed previously, the distributed propulsion can increase the wing loading, which means a smaller wing. In addition, DP can produce effects that generate benefits in the sizing of control surfaces and engines, such as during a one-engine-inoperative (OEI) condition. The regulation 14 CFR 25.121 states that an aircraft with more than one engine must be able to continue its takeoff at a minimum climb gradient even after losing one of its engines. This requirement makes manufacturers size their engines to ensure this performance, i.e., an oversized engine. In addition, to maintain the lateral direction of the aircraft, the rudder must be dimensioned for this asymmetry thrust situation. In other words, the OEI condition makes the aircraft heavier, more expensive and draggier.

In contrast, the application of DP has been studied to ensure directional control of the aircraft in diverse situations, which generates a great redundancy of operation. For example, in case of loss of one or more fans, compensating motors on the same side may be throttled up to higher burst power to cancel out the yawing moment, which relieves rudder action, leading to smaller vertical tails, lower weight, and lower drag. The same idea applies to the bird strike requirement. However, other constraints may limit these benefits, such as stability and crosswind landing.

Furthermore, as presented in previous Chapters, the hybrid-electric architecture enables the downsizing of engines, since battery are used to supply part of the power required by the aircraft, especially in phases that most require power and also in cases of engine failure. As a consequence, when it comes to downsizing engine, there is also a reduction in weight and costs. Moreover, turbine engines change their performance with altitude, while electric fans do not when powered by batteries.

6.5 Weight Effects

The biggest and most discussed disadvantage of electric propulsive systems is weight. The increase in weight is due to the energy storage system (batteries) and their respective transmission systems and equipment.

The weight of batteries, as shown in the previous chapter, is directly related to the battery specific energy (e_b) and the expected range. It is important to note that conventional aircraft lose a lot of weight during a cruise flight because fuel is burned, while electric aircraft remain with a "dead weight" of batteries. That is why intercontinental flights using batteries are still impractical. The electric aircraft that has greater range is the Pipistrel Taurus G4 (see Table 9) with 244 nmi.

Increments of weight due to electronics and equipment can be positive or negative, depending on the architecture, mission, and technology level. For example, the XTI Tri-Fan aircraft switched from a triple turboshaft design to a series hybrid electric architecture and got a weight reduction of 37% (MCKENNA, 2017). On the other hand, the ECO-150R propulsion system got three times heavier (SCHILTGEN; FREEMAN, 2016). In addition, the DP system requires more aircraft structure to be reinforced against fan-blade loss (14 CFR 33.94), which adds more weight.

In summary, it is a vicious cycle, i.e., low specific energies (e_b) generate heavier batteries and higher takeoff weights. This increases structural loads and empty weight, which directly reduces range. Therefore, today's technology limits long-range, manned and full-electric aircraft.

6.6 System Safety Effects

Electrification brings new challenges related to safety and redundancy, many of which are still unknown. However, at the same time, electrification can solve traditional problems that present a lot of risks. In a full-electric aircraft, there is no fuel, so there is no risk of explosion of jet fuel. However, in this type of aircraft this risk is replaced by the risk of fire in batteries, such as what happened in the Li-ion batteries used in the Boeing 787, where the batteries caught fire and the FAA¹ ordered to ground the entire 787 fleet (Scientific American, 2014). In addition, manufacturers, engineers, and regulatory agencies already have enough knowledge on how to ensure the safety of traditional fuels, while the batteries still lack maturity in this case.

After the Boeing 787 episode, the FAA released the circular advisory AC 20-184 which serves as a guide for testing and installations of Li-ion batteries and other correlated systems. The primary hazard is thermal runaway, i.e., when the battery rises sharply at its temperature and pressure, a fire may occur on the outside, which can release toxic gases. Thermal runaway can happen when the battery is overcharged, over-discharged, and in case of short-circuits.

Furthermore, electrification may present some benefits related to crashworthiness, but they are still uncertain. Jet fuels are hazards in the event of a crash; however, it is unknown how the batteries behave in this situation, since there are no records of full-electric aircraft that has

¹ The Federal Aviation Administration (FAA) is a governmental agency of the Department of Transportation of the United States that is responsible to inspect and rate civilian aircraft and pilots, enforce the rules of air safety, and install and maintain air-navigation and traffic-control facilities.

fallen to the ground.

Another hazard is the high-voltage electrical systems, i.e., depending on the current generated by a short circuit in the distribution system, it is possible to generate an electric arc, which can cause a fire inside the aircraft. In addition, high-voltage systems can be dangerous during maintenance or during handling by operators on the ground. So, it would require special procedures, as is the case of hydraulic systems.

The high-power systems have also been studied in more detail, which includes fault tree analysis of loss of thrust and superconducting fault protection considerations. Moreover, the electrical components and wires have their own efficiencies, they release a lot of heat by Joule effect. Assuming that all electrical inefficiency results in resistive heating, a large amount of heat will be generated inside the aircraft, increasing the temperature, which sets new challenges in control and heat dissipation.

In summary, electrification can bring great operational and safety benefits, especially in failure conditions and eliminating fuel hazards. However, it brings a new challenge, which is dealing with the unpredictability of the batteries, in addition to their danger of catching fire.

6.7 Noise and Heat Signature Effects

Noise reduction is another advantage that is much discussed and expected by all. However, there are not many papers that quantify such benefits. One of the most relevant is the study of the noise reduction in the SUGAR High and SUGAR Volt. The results showed that SUGAR Volt had noise levels of only 1 EPNdB when compared to SUGAR High.

Most authors state that the use of electric fans eliminates the jet noise, but there is still noise from propeller blades (BPF noise). Bryson *et al.* (2016) predict that a 1 MW electric motor will produce lower sound pressure levels when compared to the noise of a low-pressure ratio fan.

In military applications, it is very important to reduce, or even eliminate, noise and heat signatures, since it can be decisive in combat, for example. That is what Donateo and Ficarella (2017) studied when they designed a UAS with an electric mode to eliminate thermal signature.

6.8 Current Challenges and Future Research and Technology Needs

The development of full-electric and hybrid-electric aircraft opens up a range of challenges and future research fields, so much so that a systematic approach is being made around the world. Moreover, the challenges are scattered across all areas of engineering and humanity, including political and governmental actions. In summary, some of them can be listed as:

- Energy storage:
 - Specific energy, cycle life, safety, cost, packaging factor, safe transportation of batteries, battery swapping, battery standards, battery disposal;
- Electrical components:
 - Power level, specific power, efficiency, high voltage, thermal management & higher temperature components;
 - Research: permanent magnet generator, AC distribution/control;
- Thermal management:
 - Low impact solutions, higher temperature components;
- Certification process & standards:
 - FAR Part 23 and 25, ASTM and SAE (New committee E40 and new/modified standards for existing committees);
- Noise methods and analysis early in the design process;
- Structural considerations of battery and system integration (including thermal);
- Distributed propulsion:
 - Need better tools for both aero effects and control authority, effect on flight control surfaces;
- Modeling and simulation;
- Ground infrastructure:
 - Who pays for the cost of infrastructure needed for electric propulsion;
- Policy implications;
- Business case development:
 - Currently it is just start-ups convincing venture capitalists to spend money;
 - Need for cost modeling.

CONCLUSIONS AND PERSPECTIVES

In this work, studies were carried out on the conceptual design of full-electric and hybrid-electric aircraft, besides presenting methodologies for the initial development, based on performance requirements, finishing with the sizing and estimation of overall weights, highlighting benefits and limitations.

Initially, as factors that motivated new research in this field, the carbon emission reduction goals and other environmental issues raised by organizations such as the United Nations and NASA were presented. A review of literature and theory was carried out, where the main types of technologies and equipment were presented. After introducing the concepts and fundamentals related to electrification in propulsive systems, the main propulsive architectures and configurations currently discussed were listed, highlighting their advantages and limitations in each case. To illustrate, many prototypes that have already flown were presented along with new designs that are under development.

Furthermore, the work introduced the development phases of an aircraft, giving focus to the conceptual phase. A methodology was proposed to begin the initial estimation of the aircraft, based on operational requirements, such as payload, range, cruise speed, takeoff distance, and climb. Then, it was discussed the formulation for constructing the power constraints. The constraints come from equilibrium equations applied in each flight phase, and they are evaluated together in order to generate a single design space in the plot. Moreover, the advantages brought by the installation of a distributed propulsive (DP) system were discussed, and the effects produced by the aero-propulsive interactions were modeled, regarding number of propulsors and fraction of the wing that is occupied by them.

Later on, the method was validated with the paper of reference and an application example was presented for thin haul aircraft. Due to its operating characteristics – air transportation of passengers on very small capacity aircraft over ultra-short distances – this type of operation used to be so far not very profitable; however, the electrification of propulsive systems come to make

it feasible. Therefore, the requirements of the design were presented and the results showed how the DP system affected positively the final design, i.e., the DP system generates a “Delta” C_L , improving the overall lift, which makes the design feasible space in the constraint diagram increase. This upgrade improves the location of the optimum design points, which results in better design features, such as smaller wings, engines, and batteries.

Having a optimum design point of interest, i.e., a wing loading defined, it was possible to size the aircraft using energy mission approach. It was presented a typical mission of an aircraft and the main flight phases were classified in takeoff, climb, cruise, descent, and loiter. For each one of these phases, a formulation was addressed to quantify the required power to operate in a certain condition and, consequently, the amount of energy spent. Assuming a hybrid-electric propulsive system, it was possible to size and estimate the weights of each component of the aircraft. Since the degrees-of-hybridization per flight phase affect directly the final weight breakdown of the aircraft, an optimization problem was proposed to find the operational strategy in order to minimize the fuel consumption and the maximum takeoff weight. The results showed that for the aircraft in analysis the mission specifications totally determines the final weight breakdown, i.e., if the range expected increases, the maximum takeoff weight increases as well, even more significantly for cases of full-electric aircraft. Thus, the specific energy of the batteries is crucial to make the electrification of the design feasible. In other words, if the battery is “more energetic”, aircraft is capable of carrying out longer missions.

Finally, the advance of technologies is the main factor that will determine the progression of full-electric and hybrid-electric aircraft projects. Moreover, the electrification brings a bunch of benefits, but a lot of issues as well. Thus, it was presented the effects of electrification in the propulsion, aerodynamics, sizing, weights, system safety, noise, and heat signature. Moreover, it is highlighted the current challenges and future research and technology needs, where most of them have been discussed in debated and panels of international congress and committees.

At the end of the development of this work, from the analysis carried out and the results obtained, the following suggestions are proposed as future work:

- Better integration of the choice of the optimum design point with the energy sizing approach;
- Implementation of other aero-propulsive models for different and non-conventional concepts of aircraft;
- Replacement of the regression curves used to size the electric motors and engines by estimates of specific power of each component;
- During the energy sizing approach, to remove the wing weight from the empty weight, and size the wing based on the optimum design point chosen;
- Performance study of VTOL (vertical take-off and landing) aircraft;

- Implementation of a MDO (multidisciplinary design optimization) to advance in the conceptual design, including boxes of flight mechanics, aerodynamics, structural analysis, and cost estimation, where the tools used were developed *in situ*.

BIBLIOGRAPHY

Aertec. **Infographic More Electric Aircraft**. 2017. <<https://aertecsolutions.com/2017/06/22/infographic-mea/?lang=en>>, Last accessed on 2019-02-23. Citation on page 47.

AINonline. **Onera Pitches Greener, Wider Structure for A320 Replacement**. 2015. <<https://www.ainonline.com/aviation-news/air-transport/2015-06-30/onera-pitches-greener-wider-structure-a320-replacement>>, Last accessed on 2019-02-23. Citation on page 110.

Airbus. **Airbus, Rolls-Royce, and Siemens team up for electric future Partnership launches E-Fan X hybrid-electric flight demonstrator**. 2017. <<https://www.airbus.com/newsroom/press-releases/en/2017/11/airbus--rolls-royce--and-siemens-team-up-for-electric-future-par.html>>, Last accessed on 2019-2-12. Citation on page 55.

Air&Space. **NASA Wants Ideas for the Next Electric Airplane**. 2016. <<https://www.airspacemag.com/daily-planet/air-electric-180960646/>>, Last accessed on 2019-02-23. Citation on page 64.

ANG, A.; RAO, A. G.; KANAKIS, T.; LAMMEN, W. Performance analysis of an electrically assisted propulsion system for a short-range civil aircraft. **Proceedings of the Institution of Mechanical Engineers, Part G: Journal of Aerospace Engineering**, SAGE Publications Sage UK: London, England, p. 0954410017754146, 2018. DOI: <<https://doi.org/10.1177/0954410017754146>>. Citation on page 66.

AVIATION, N. E. R. **N+ 2 Advanced Vehicle Concepts NRA Draft Solicitation Synopsis**. [S.l.], 2012. Citation on page 32.

BAYINDIR, K. Ç.; GÖZÜKÜÇÜK, M. A.; TEKE, A. A comprehensive overview of hybrid electric vehicle: Powertrain configurations, powertrain control techniques and electronic control units. **Energy conversion and Management**, Elsevier, v. 52, n. 2, p. 1305–1313, 2011. DOI: <<https://doi.org/10.1016/j.enconman.2010.09.028>>. Citation on page 45.

BHATTACHARYYA, R. P.; PRITCHETT, A. R.; GERMAN, B. J. Designing air traffic concepts of operation for thin-haul aviation at small airports. In: IEEE. **2017 IEEE/AIAA 36th Digital Avionics Systems Conference (DASC)**. [S.l.], 2017. p. 1–8. DOI: <<https://doi.org/10.1109/DASC.2017.8102000>>. Citation on page 85.

BIBER, K. Estimating propeller slipstream drag on airplane performance. **Journal of Aircraft**, v. 48, n. 6, p. 2172–2174, 2011. DOI: <<https://doi.org/10.2514/1.C031458>>. Citation on page 73.

BIRKE, P.; KELLER, M.; SCHIEMANN, M. Electric battery actual and future battery technology trends. **Electric Motion Prague**, 2010. Citations on pages 39 and 40.

BOGAERT, J. V. Assessment of potential fuel saving benefits of hybrid-electric regional aircraft. 2015. Citation on page 44.

BORER, N. K.; PATTERSON, M. D.; VIKEN, J. K.; MOORE, M. D.; BEVIRT, J.; STOLL, A. M.; GIBSON, A. R. Design and performance of the nasa sceptor distributed electric propulsion flight demonstrator. In: **16th AIAA Aviation Technology, Integration, and Operations Conference**. [S.l.: s.n.], 2016. p. 3920. DOI: <<https://doi.org/10.2514/6.2016-3920>>. Citation on page 67.

BRADLEY, M. K.; DRONEY, C. K. Subsonic ultra green aircraft research: Phase 2. volume 2; hybrid electric design exploration. 2015. Citations on pages 41 and 56.

BRELJE, B. J.; MARTINS, J. R. Electric, hybrid, and turboelectric fixed-wing aircraft: A review of concepts, models, and design approaches. **Progress in Aerospace Sciences**, Elsevier, 2018. Citations on pages 31, 52, and 53.

BRUCE, P. G.; FREUNBERGER, S. A.; HARDWICK, L. J.; TARASCON, J.-M. Li-o 2 and li-s batteries with high energy storage. **Nature materials**, Nature Publishing Group, v. 11, n. 1, p. 19, 2012. DOI: <<https://doi.org/10.1038/nmat3191>>. Citation on page 41.

BRYSON, D. E.; MARKS, C. R.; MILLER, R. M.; RUMPFKEIL, M. P. Multidisciplinary design optimization of quiet, hybrid-electric small unmanned aerial systems. **Journal of Aircraft**, American Institute of Aeronautics and Astronautics, v. 53, n. 6, p. 1959–1963, 2016. DOI: <<https://doi.org/10.2514/1.C033455>>. Citation on page 114.

BUSQUIN, P.; ARGÜELLES, P.; BISCHOFF, M.; DROSTE, B.; EVANS, R. H.; KRÖLL, W.; LAGARDÈRE, J.-L.; LINA, A.; LUMSDEN, J.; RANQUE, D. *et al.* European aeronautics: a vision for 2020—a synopsis. **Air & Space Europe**, v. 3, n. 3, p. 16–18, 2001. DOI: <[https://doi.org/10.1016/S1290-0958\(01\)90042-5](https://doi.org/10.1016/S1290-0958(01)90042-5)>. Citation on page 31.

ch-aviation. **Airbus acquires an ARJ-100 as E-Fan X testbed**. 2018. <<https://www.ch-aviation.com/portal/news/73546-airbus-acquires-an-arj-100-as-e-fan-x-testbed>>, Last accessed on 2019-2-12. Citation on page 55.

CHAN, C. C.; BOUSCAYROL, A.; CHEN, K. Electric, hybrid, and fuel-cell vehicles: Architectures and modeling. **IEEE transactions on vehicular technology**, IEEE, v. 59, n. 2, p. 589–598, 2010. DOI: <<https://doi.org/10.1109/TVT.2009.2033605>>. Citation on page 49.

CHAU, K.; WONG, Y. Overview of power management in hybrid electric vehicles. **Energy conversion and management**, Elsevier, v. 43, n. 15, p. 1953–1968, 2002. DOI: <[https://doi.org/10.1016/S0196-8904\(01\)00148-0](https://doi.org/10.1016/S0196-8904(01)00148-0)>. Citation on page 49.

CINAR, G.; MAVRIS, D. N.; EMENETH, M.; SCHNEEGANS, A.; FEFERMANN, Y. Development of parametric power generation and distribution subsystem models at the conceptual aircraft design stage. In: **55th AIAA Aerospace Sciences Meeting**. [S.l.: s.n.], 2017. p. 1182. DOI: <<https://doi.org/10.2514/6.2017-1182>>. Citation on page 38.

COSTELLO, L. A. State of the art of piloted electric airplanes, nasa's centennial challenge data and fundamental design implications. 2011. Citation on page 54.

CS25, E. Certification specifications and acceptable means of compliance for large aeroplanes. **Amendment**, v. 14, p. 12, 2012. Citation on page 81.

DEB, K.; AGRAWAL, S.; PRATAP, A.; MEYARIVAN, T. A fast elitist non-dominated sorting genetic algorithm for multi-objective optimization: Nsga-ii. In: SPRINGER. **International conference on parallel problem solving from nature**. [S.l.], 2000. p. 849–858. DOI: <https://doi.org/10.1007/3-540-45356-3_83>. Citation on page 103.

DEERE, K. A.; VIKEN, J. K.; VIKEN, S.; CARTER, M. B.; WIESE, M.; FARR, N. Computational analysis of a wing designed for the x-57 distributed electric propulsion aircraft. In: **35th AIAA Applied Aerodynamics Conference**. [S.l.: s.n.], 2017. p. 3923. DOI: <<https://doi.org/10.2514/6.2017-3923>>. Citation on page 111.

DEFENSE, U. D. of. Acquisition of major defense systems. U.S. Government Printing Office, 2009. Citation on page 60.

DONATEO, T.; FICARELLA, A. Designing a hybrid electric powertrain for an unmanned aircraft with a commercial optimization software. **SAE International Journal of Aerospace**, v. 10, n. 2017-01-9000, p. 1–11, 2017. DOI: <<https://doi.org/10.4271/2017-01-9000>>. Citation on page 114.

Encyclopaedia Britannica. **Airship**. 2019. <<https://www.britannica.com/technology/airship#ref265872>>, Last accessed on 2019-2-12. Citation on page 54.

ERLING, U. M. International aviation emissions under international civil aviation organization's global market based measure: Ready for offsetting? **Air and Space Law**, Kluwer Law International, v. 42, n. 1, p. 1–12, 2017. Citation on page 32.

ESDU International PLC. **Thrust and Drag Accounting for Propeller/airframe Interaction. 85017**. ESDU International PLC, 1985. ISBN 0856795232. Available: <<https://www.amazon.com/Thrust-Accounting-Propeller-airframe-Interaction/dp/0856795232?SubscriptionId=AKIAIOBINVZYXZQZ2U3A&tag=chimbori05-20&linkCode=xm2&camp=2025&creative=165953&creativeASIN=0856795232>>. Citation on page 68.

ESHELBY, M. **Aircraft performance: Theory and practice**. [S.l.]: American Institute of Aeronautics and Astronautics, Inc., 2000. DOI: <<https://doi.org/10.2514/4.473982>>. Citation on page 98.

FARHADI, M.; MOHAMMED, O. Energy storage systems for high power applications. In: IEEE. **2015 IEEE Industry Applications Society Annual Meeting**. [S.l.], 2015. p. 1–7. DOI: <<https://doi.org/10.1109/IAS.2015.7356787>>. Citation on page 37.

FEFERMANN, Y.; MAURY, C.; LEVEL, C.; ZARATI, K.; SALANNE, J.-P.; PORNET, C.; THORAVAL, B.; ISIKVEREN, A. T. Hybrid-electric motive power systems for commuter transport applications. In: **Proceedings of the 30th Congress of the International Council of the Aeronautical Sciences, Daejeon, Korea**. [S.l.: s.n.], 2016. p. 25–30. Citation on page 40.

FELDER, J.; KIM, H.; BROWN, G. Turboelectric distributed propulsion engine cycle analysis for hybrid-wing-body aircraft. In: **47th AIAA aerospace sciences meeting including the new horizons forum and aerospace exposition**. [S.l.: s.n.], 2009. p. 1132. DOI: <<https://doi.org/10.2514/6.2009-1132>>. Citations on pages 48 and 67.

FELDER, J. L. Nasa electric propulsion system studies. 2015. Citations on pages 64 and 65.

FINGER, D. F.; BRAUN, C.; BIL, C. An initial sizing methodology for hybrid-electric light aircraft. In: **2018 Aviation Technology, Integration, and Operations Conference**. [S.l.: s.n.], 2018. p. 4229. DOI: <<https://doi.org/10.2514/6.2018-4229>>. Citation on page 34.

FLORIO, F. D. **Airworthiness: An introduction to aircraft certification and operations**. [S.l.]: Butterworth-Heinemann, 2016. Citation on page 61.

- FLYER. **Extra's electric aerobatic 330**. 2016. <<https://www.flyer.co.uk/extras-electric-aerobatic-330/>>, Last accessed on 2019-01-23. Citation on page 43.
- FOLLEN, G. J.; ROSARIO, R. D.; WAHLS, R.; MADAVAN, N. **NASA's Fundamental Aeronautics Subsonic Fixed Wing Project: Generation N+ 3 Technology Portfolio**. [S.l.], 2011. DOI: <<https://doi.org/10.4271/2011-01-2521>>. Citation on page 31.
- FRIEDRICH, C.; ROBERTSON, P. A. Design of hybrid-electric propulsion systems for light aircraft. In: **14th AIAA aviation technology, integration, and operations conference**. [S.l.: s.n.], 2014. p. 3008. DOI: <<https://doi.org/10.2514/6.2014-3008>>. Citation on page 45.
- _____. Hybrid-electric propulsion for automotive and aviation applications. **CEAS Aeronautical Journal**, Springer, v. 6, n. 2, p. 279–290, 2015. DOI: <<https://doi.org/10.1007/s13272-014-0144-x>>. Citation on page 48.
- GALLAGHER, K. G.; GOEBEL, S.; GRESZLER, T.; MATHIAS, M.; OELERICH, W.; EROGLU, D.; SRINIVASAN, V. Quantifying the promise of lithium–air batteries for electric vehicles. **Energy & Environmental Science**, Royal Society of Chemistry, v. 7, n. 5, p. 1555–1563, 2014. DOI: <<https://doi.org/10.1039/c3ee43870h>>. Citation on page 40.
- GERSSSEN-GONDELACH, S. J.; FAAIJ, A. P. Performance of batteries for electric vehicles on short and longer term. **Journal of power sources**, Elsevier, v. 212, p. 111–129, 2012. DOI: <<https://doi.org/10.1016/j.jpowsour.2012.03.085>>. Citations on pages 39 and 41.
- GOHARDANI, A. S.; DOULGERIS, G.; SINGH, R. Challenges of future aircraft propulsion: A review of distributed propulsion technology and its potential application for the all electric commercial aircraft. **Progress in Aerospace Sciences**, Elsevier, v. 47, n. 5, p. 369–391, 2011. DOI: <<https://doi.org/10.1016/j.paerosci.2010.09.001>>. Citation on page 67.
- GRAY, J. S.; MADER, C. A.; KENWAY, G. K.; MARTINS, J. Approach to modeling boundary layer ingestion using a fully coupled propulsion-rans model. In: **58th AIAA/ASCE/AHS/ASC Structures, Structural Dynamics, and Materials Conference**. [S.l.: s.n.], 2017. p. 1753. DOI: <<https://doi.org/10.2514/6.2017-1753>>. Citation on page 110.
- GUYNN, M. D.; BERTON, J. J.; TONG, M. J.; HALLER, W. J. Advanced single-aisle transport propulsion design options revisited. In: **2013 Aviation Technology, Integration, and Operations Conference**. [S.l.: s.n.], 2013. p. 4330. DOI: <<https://doi.org/10.2514/6.2013-4330>>. Citation on page 31.
- HEPPERLE, M. Electric flight - potential and limitations. In: **Energy Efficient Technologies and Concepts of Operation**. [s.n.], 2012. Available: <<https://elib.dlr.de/78726/>>. Citation on page 33.
- HUNG, J.; GONZALEZ, L. F. On parallel hybrid-electric propulsion system for unmanned aerial vehicles. **Progress in Aerospace Sciences**, Elsevier, v. 51, p. 1–17, 2012. DOI: <<https://doi.org/10.1016/j.paerosci.2011.12.001>>. Citation on page 45.
- INSIDEEVs. **NASA Electric X-57 Maxwell Airplane Debuts at AirVenture 2018**. 2018. <<https://insideevs.com/nasa-electric-x-57-maxwell-airplane/>>, Last accessed on 2019-2-12. Citation on page 57.

ISIKVEREN, A. T.; KAISER, S.; PORNET, C.; VRATNY, P. C. Pre-design strategies and sizing techniques for dual-energy aircraft. **Aircraft Engineering and Aerospace Technology: An International Journal**, Emerald Group Publishing Limited, v. 86, n. 6, p. 525–542, 2014. DOI: <<https://doi.org/10.1108/AEAT-08-2014-0122>>. Citations on pages 43, 44, 45, and 66.

ISIKVEREN, A. T.; SEITZ, A.; BIJEWITZ, J.; MIRZOYAN, A.; ISYANOV, A.; GRENON, R.; ATINAULT, O.; GODARD, J.-L.; STÜCKL, S. Distributed propulsion and ultra-high by-pass rotor study at aircraft level. **The Aeronautical Journal**, Cambridge University Press, v. 119, n. 1221, p. 1327–1376, 2015. DOI: <<https://doi.org/10.1017/S0001924000011295>>. Citation on page 50.

JANSEN, R.; DUFFY, K. P.; BROWN, G. Partially turboelectric aircraft drive key performance parameters. In: **53rd AIAA/SAE/ASEE Joint Propulsion Conference**. [S.l.: s.n.], 2017. p. 4702. DOI: <<https://doi.org/10.2514/6.2017-4702>>. Citation on page 111.

JUSTIN, C. Y.; PAYAN, A. P.; BRICENO, S. I.; MAVRIS, D. N. Operational and economic feasibility of electric thin haul transportation. In: **17th AIAA Aviation Technology, Integration, and Operations Conference**. [S.l.: s.n.], 2017. p. 3283. DOI: <<https://doi.org/10.2514/6.2017-3283>>. Citation on page 84.

KUHN, H.; SIZMANN, A. **Fundamental prerequisites for electric flying**. [S.l.]: Deutsche Gesellschaft für Luft-und Raumfahrt-Lilienthal-Oberth eV, 2012. Citations on pages 38, 39, and 40.

MADAVAN, N. K.; ROSARIO, R. D.; JANKOVSKY, A. L. Hybrid-electric and distributed propulsion technologies for large commercial transports: A nasa perspective. 2015. Citation on page 32.

MARCUS, E. A.; VRIES, R. de; KULKARNI, A. R.; VELDHUIS, L. L. Aerodynamic investigation of an over-the-wing propeller for distributed propulsion. In: **56th AIAA Aerospace Sciences Meeting**. [S.l.: s.n.], 2018. p. 2053. DOI: <<https://doi.org/10.2514/6.2018-2053>>. Citation on page 73.

MCKENNA, J. T. **XTI Aims to Fly 60% Scale TriFan 600 Within Year**. 2017. <<http://www.aerospacengineering.net/?p=9752>>, Last accessed on 2019-02-23. Citation on page 113.

MENGISTU, I. H. **Small internal combustion engine testing for a hybrid-electric remotely-piloted aircraft**. [S.l.], 2011. Citation on page 49.

MICHELE, R. **Revealed a new propulsive fuselage hybrid-electric concept**. 2016. <<http://www.aerospacengineering.net/?p=9752>>, Last accessed on 2019-02-23. Citation on page 111.

MILLER, J. M. **Propulsion systems for hybrid vehicles**. [S.l.]: Iet, 2004. DOI: <<https://doi.org/10.1049/PBPO045E>>. Citation on page 49.

MIRANDA, L.; BRENNAN, J. Aerodynamic effects of wingtip-mounted propellers and turbines. In: **4th Applied Aerodynamics Conference**. [S.l.: s.n.], 1986. p. 1802. DOI: <<https://doi.org/10.2514/6.1986-1802>>. Citation on page 112.

MOORE, M. D. Misconceptions of electric aircraft and their emerging aviation markets. In: **52nd Aerospace Sciences Meeting**. [S.l.: s.n.], 2014. p. 0535. DOI: <<https://doi.org/10.2514/6.2014-0535>>. Citations on pages 56 and 111.

NAZAR, L. F.; CUISINIER, M.; PANG, Q. Lithium-sulfur batteries. **MRS Bulletin**, Cambridge University Press, v. 39, n. 5, p. 436–442, 2014. DOI: <https://doi.org/10.1557/mrs.2014.86>. Citation on page 41.

NICOLAI, L. M.; CARICHNER, G. E. **Fundamentals of aircraft and airship design, Volume 1–Aircraft Design**. [S.l.]: American Institute of Aeronautics and Astronautics, 2010. DOI: <https://doi.org/10.2514/4.867538>. Citations on pages 59, 60, and 61.

Oxis Energy. 2019. <https://oxisenergy.com/products/>, Last accessed on 2019-01-20. Citation on page 41.

PATTERSON, M. D. **Conceptual Design of High-Lift Propeller Systems for Small Electric Aircraft**. Phd Thesis (PhD Thesis) — Georgia Institute of Technology, 2016. Citation on page 73.

PATTERSON, M. D.; BORER, N. K. Approach considerations in aircraft with high-lift propeller systems. In: **17th AIAA Aviation Technology, Integration, and Operations Conference**. [S.l.: s.n.], 2017. p. 3782. DOI: <https://doi.org/10.2514/6.2017-3782>. Citations on pages 73 and 78.

PATTERSON, M. D.; DASKILEWICZ, M. J.; GERMAN, B. Simplified aerodynamics models to predict the effects of upstream propellers on wing lift. In: **53rd AIAA Aerospace Sciences Meeting**. [S.l.: s.n.], 2015. p. 1673. DOI: <https://doi.org/10.2514/6.2015-1673>. Citations on pages 71 and 72.

PERULLO, C.; MAVRIS, D. A review of hybrid-electric energy management and its inclusion in vehicle sizing. **Aircraft Engineering and Aerospace Technology: An International Journal**, Emerald Group Publishing Limited, v. 86, n. 6, p. 550–557, 2014. DOI: <https://doi.org/10.1108/AEAT-04-2014-0041>. Citation on page 66.

PETERMAIER, K. Electric propulsion components with high power densities for aviation. In: **2015 Transformational Vertical Flight Workshop, Siemens AG**. [S.l.: s.n.], 2015. Citation on page 42.

Phys.org. **SUGAR Volt: Boeing puts vision to work in hybrid electric aircraft**. 2012. <https://phys.org/news/2012-12-sugar-volt-boeing-vision-hybrid.html>, Last accessed on 2019-2-12. Citation on page 56.

PORNET, C. **Electric drives for propulsion system of transport aircraft**. [S.l.]: John Wiley & Sons, Ltd, 2010. Citation on page 33.

PORNET, C.; GOLOGAN, C.; VRATNY, P. C.; SEITZ, A.; SCHMITZ, O.; ISIKVEREN, A. T.; HORNUNG, M. Methodology for sizing and performance assessment of hybrid energy aircraft. **Journal of Aircraft**, American Institute of Aeronautics and Astronautics, v. 52, n. 1, p. 341–352, 2014. DOI: <https://doi.org/10.2514/1.C032716>. Citation on page 33.

PORNET, C.; ISIKVEREN, A. T. Conceptual design of hybrid-electric transport aircraft. **Progress in Aerospace Sciences**, Elsevier, v. 79, p. 114–135, 2015. DOI: <https://doi.org/10.1016/j.paerosci.2015.09.002>. Citations on pages 43 and 54.

RAYMER, D. P. Aircraft design: a conceptual approach, american institute of aeronautics and astronautics. **Inc., Reston, VA**, v. 21, 1999. Citations on pages 78 and 79.

RITZERT, F.; BOWMAN, R.; STEINGART, D.; HERTZBERG, B. **Structural Batteries for Hybrid Electric Propulsion System**. [S.l.], 2013. Citation on page 40.

ROSKAM, J. **Airplane design**. [S.l.]: DARcorporation, 1985. Citations on pages 72, 76, 93, 94, 95, 96, and 100.

ROSSI, N. Conceptual design of hybrid-electric aircraft. Italy, 2018. Citation on page 93.

SCHÄFER, A.; BARRETT, S. R.; DOYME, K.; DRAY, L.; GNADT, A. R.; SELF, R.; O'SULLIVAN, A.; SYNODINOS, A. P.; TORIJA, A. J. Technological, economic and environmental prospects of all-electric aircraft. **Nature Energy**, 2018. DOI: <<https://doi.org/10.1038/s41560-018-0294-x>>. Citation on page 33.

SCHILTGEN, B. T.; FREEMAN, J. Aeropropulsive interaction and thermal system integration within the eco-150: a turboelectric distributed propulsion airliner with conventional electric machines. In: **16th AIAA Aviation Technology, Integration, and Operations Conference**. [S.l.: s.n.], 2016. p. 4064. DOI: <<https://doi.org/10.2514/6.2016-4064>>. Citation on page 113.

SCIENCES, E. National Academies of; MEDICINE. **Commercial Aircraft Propulsion and Energy Systems Research: Reducing Global Carbon Emissions**. Washington, DC: The National Academies Press, 2016. ISBN 978-0-309-44096-7. Available: <<https://www.nap.edu/catalog/23490/commercial-aircraft-propulsion-and-energy-systems-research-reducing-global-carbon>>. Citations on pages 37, 46, 50, and 64.

Scientific American. **How Lithium Ion Batteries Grounded the Dreamliner**. 2014. <<https://www.scientificamerican.com/article/how-lithium-ion-batteries-grounded-the-dreamliner/>>, Last accessed on 2019-02-23. Citation on page 113.

SHIN, D.; LEE, K.; CHANG, N. Fuel economy analysis of fuel cell and supercapacitor hybrid systems. **International Journal of Hydrogen Energy**, Elsevier, v. 41, n. 3, p. 1381–1390, 2016. DOI: <<https://doi.org/10.1016/j.ijhydene.2015.10.103>>. Citation on page 37.

SHINZATO, T.; ARAKAWA, S.; OYAMA, H.; SAKA, H.; HAYASAKI, T. Development of high-temperature superconducting motor for automobiles. **SEI Technical Review**, v. 75, 2012. Citation on page 43.

Siemens. **Dry Run on the Test Rig**. 2015. <<https://www.siemens.com/press/en/presspicture/?press=/en/presspicture/2015/corporate/2015-03-electromotor/im2015030566coen.htm>>, Last accessed on 2019-01-23. Citation on page 43.

_____. **Technical data for the record electric motor SP260D**. 2016. <<https://www.siemens.com/press/pool/de/events/2016/corporate/2016-12-innovation/inno2016-aerobatic-airplane-e.pdf>>, Last accessed on 2019-01-23. Citation on page 42.

_____. **Extra 330LE electric plane sets new speed world record**. 2017. <<https://www.siemens.com/press/en/presspicture/?press=/en/presspicture/2017/corporate/2017-04-electromotor/im2017040530coen.htm>>, Last accessed on 2019-01-23. Citation on page 43.

SINNIGE, T. **Aerodynamic and Aeroacoustic Interaction Effects for Tip-Mounted Propellers: An Experimental Study**. Phd Thesis (PhD Thesis) — Delft University of Technology, 2018. Citation on page 112.

- THACKERAY, M. M.; WOLVERTON, C.; ISAACS, E. D. Electrical energy storage for transportation—approaching the limits of, and going beyond, lithium-ion batteries. **Energy & Environmental Science**, Royal Society of Chemistry, v. 5, n. 7, p. 7854–7863, 2012. DOI: <<https://doi.org/10.1039/c2ee21892e>>. Citation on page 39.
- THIELMANN, A.; SAUER, A.; ISENMANN, R.; WIETSCHHEL, M. Technology roadmap energy storage for electric mobility 2030. **Fraunhofer ISI**, 2012. Citation on page 41.
- THOMSON, R.; SACHDEVA, N.; NAZUKIN, M.; MARTINEZ, N. Aircraft electrical propulsion the next chapter of aviation. **Roland Berger**, p. 17, 2017. Citation on page 33.
- TODD, R.; WU, D.; GIRIO, J. dos S.; POU CAND, M.; FORSYTH, A. Supercapacitor-based energy management for future aircraft systems. In: IEEE. **2010 Twenty-Fifth Annual IEEE Applied Power Electronics Conference and Exposition (APEC)**. [S.l.], 2010. p. 1306–1312. DOI: <<https://doi.org/10.1109/APEC.2010.5433398>>. Citation on page 37.
- TORENBEEK, E. **Synthesis of subsonic airplane design: an introduction to the preliminary design of subsonic general aviation and transport aircraft, with emphasis on layout, aerodynamic design, propulsion and performance**. [S.l.]: Springer Science & Business Media, 2013. Citations on pages 76 and 78.
- U.S. Energy Information Administration. **U.S. Gulf Coast Kerosene-Type Jet Fuel Spot Price FOB**. 2017. <<https://www.eia.gov/petroleum/>>, Last accessed on 2019-01-15. Citation on page 33.
- VELDHUIS, L. L. M. **Propeller wing aerodynamic interference**. Phd Thesis (PhD Thesis) — Delft University of Technology, The Netherlands, 6 2005. Citations on pages 72 and 73.
- VOSKUIJL, M.; BOGAERT, J. van; RAO, A. G. Analysis and design of hybrid electric regional turboprop aircraft. **CEAS Aeronautical Journal**, Springer, v. 9, n. 1, p. 15–25, 2018. DOI: <<https://doi.org/10.1007/s13272-017-0272-1>>. Citation on page 66.
- VRIES, R. de; BROWN, M. T.; VOS, R. A preliminary sizing method for hybrid-electric aircraft including aero-propulsive interaction effects. In: **2018 Aviation Technology, Integration, and Operations Conference**. [S.l.: s.n.], 2018. p. 4228. DOI: <<https://doi.org/10.2514/6.2018-4228>>. Citations on pages 34, 68, 70, 74, 75, 77, 81, 83, and 84.
- WELSTEAD, J.; FELDER, J. L. Conceptual design of a single-aisle turboelectric commercial transport with fuselage boundary layer ingestion. In: **54th AIAA Aerospace Sciences Meeting**. [S.l.: s.n.], 2016. p. 1027. DOI: <<https://doi.org/10.2514/6.2016-1027>>. Citation on page 110.
- WICK, A. T.; HOOKER, J. R.; ZEUNE, C. H. Integrated aerodynamic benefits of distributed propulsion. In: **53rd AIAA Aerospace Sciences Meeting**. [S.l.: s.n.], 2015. p. 1500. DOI: <<https://doi.org/10.2514/6.2015-1500>>. Citation on page 111.
- YUTKO, B. M.; TITCHENER, N.; COURTIN, C.; LIEU, M.; WIRSING, L.; TYLKO, J.; CHAMBERS, J. T.; ROBERTS, T. W.; CHURCH, C. S. Conceptual design of a d8 commercial aircraft. In: **17th AIAA Aviation Technology, Integration, and Operations Conference**. [S.l.: s.n.], 2017. p. 3590. DOI: <<https://doi.org/10.2514/6.2017-3590>>. Citation on page 110.
- ZAMBONI, J. **A method for the conceptual design of hybrid electric aircraft**. Master's Thesis (Master's Thesis) — Delft University of Technology, 2018. Citations on pages 41, 50, and 51.